UNIVERSITÀ DEGLI STUDI DI MODENA E REGGIO EMILIA

DOTTORATO DI RICERCA IN PHYSICS AND NANOSCIENCES

CICLO XXXI

Tesi per il Conseguimento del Titolo di

Dottore di Ricerca

FIRST PRINCIPLES STUDY OF THE OPTICAL PROPERTIES IN PUSH-PULL MOLECULAR J-AGGREGATES

Candidato: Michele Guerrini

Relatori: Prof. Stefano Corni
Dr. Arrigo Calzolari

Co-relatore: Dr. Daniele Varsano

Coordinatore del dottorato e
Direttore della scuola: Prof. Marco Affronte

DATA Febbraio 2019

“Imagination is more important than knowledge”

A. Einstein

Contents

Abstract

Molecular crystals are physical systems formed by aggregation of molecules in different arrangements. As a result, when excited, they may manifest a collective behavior which is an emergent phenomenon due to the strong inter-molecular electronic interactions. When this happens, the *molecular aggregate* can be treated as one "supermolecule" which manifests optical properties completely different from those of the single molecular units. The latter behavior is a typical feature of the *J-aggregate* molecular crystals which manifest peculiar optical properties such as an intense and narrow absorption band, called *J-band*, which appears at lower energy with respect to the single molecule absorption band. This behavior cannot be explained in term of the optical properties of the single molecules due to its collective nature.

Although the optical properties of J-aggregates have been studied for a long time since their discovery in the 1930s, it is still unclear what kind of microscopic physical mechanisms give origin to the *J-band* and to what extent solid-state effects play a role in the optical properties of these molecular crystals. Most of the attempted first principles descriptions do not take thoroughly into account many-body solid-state effects (e.g., long range interactions, screening effects, etc.) and are based on strong approximations that are not sufficient to correctly predict and reproduce their optical properties. On the other hand, the need to correctly describe these materials is also driven by the recent trend to use J-aggregates in strong coupling experiments to study hybrid excitations due to strong matter-light interaction.

The principal aim and original contribution of this thesis is to give a comprehensive first principles description, based on state-of-the-art methods such as Time-Dependent-Density-Functional-Theory (TDDFT) and Many-Body Perturbation Theory (MBPT), on the optical properties of J-aggregates. In particular, we investigate a specific molecular aggregate composed of organic push-pull dyes manifesting intra-molecular charge transfer and we focus the attention on the analysis of the aggregate J-band.

We adopted two kinds of numerical approaches. In the first one we used TDDFT through which the role of the molecular packing in the enhancement and red-shift of the J-band, along with the effects of the quantum confinement in the optical absorption when the crystal is confined in one or two dimensions have been assessed. By analyzing the induced charge density associated to the J-band, we concluded that:

(i) it is displaced along the crystal principal axis along parallel molecular chains; (ii) the overall red-shift of the *J-band* results from: (1) competing coupling mechanisms such as interactions between monomers in the same chain giving red-shift and weaker interactions between monomers of different chains giving a minor blue shift; (2) renormalization of the single particle energy levels due to molecular aggregation.

In the second part an approach alternative to TDDFT, namely MBPT, based on the GW approximation and the Bethe-Salpeter equation (BSE) methods has been adopted. The latter framework is able to circumvent some of the known shortcomings of TDDFT when using (semi)local functionals, such as the inability to correctly describe exchange and correlation collective many-body effects (e.g., electron-hole screened interaction, charge-transfer mechanisms (CT)) which are non-local by nature. Simulations results showed that the J-band is indeed composed of a rich structure of bound excitonic states which in conventional absorption experiments cannot be resolved due to the broadening effects. The optically active excited state which dominates the *J-band* shows a mixed intra- and intermolecular CT character since the electron is delocalized on the single molecule and on the nearest neighbors. This character comes from the combination between push-pull mechanism and the molecular arrangement which favors electron delocalization along the π-stacking directions of the neighboring molecules. The latter effect significantly depends on the molecular crystalline packing and wavefunctions overlap. BSE results reveal also the presence of pure charge transfer dark excited states within the J-band which could not be detected in conventional experiments.

In the final part of the work we concentrated on the collective mechanisms in the J-band. In particular, we assessed and quantified, within the novel context of molecular plasmonics, to what extent plasmonic collective mechanisms are involved in the *J-band* and demonstrated that this band has not a specific plasmonic character. This result responds to the surrounding question wheatear or not any strong optical absorption band, with some sort of collective character in its microscopic origine, like the *J-band*, share the status of a plasmon.

I cristalli molecolari sono sistemi fisici formati dall'aggregazione di molecole aventi diverse disposizioni spaziali. Di conseguenza, una volta che vengono eccitate in fase aggregata, manifestano tipicamente un comportamento collettivo che rappresenta un fenomeno emergente dovuto alle forti interazioni elettroniche di natura inter-molecolare. Quando ciò accade, *l'aggregato molecolare* può essere considerato come una singola "supermolecola" la quale manifesta proprietà ottiche completamente diverse da quelle delle singole molecole costituenti. Quest'ultimo comportamento è tipico dei cristalli molecolari noti come *J-aggregates*, i quali possiedono caratteristiche proprietà ottiche come una molto intensa e stretta banda di assorbimento, chiamata *J-band*, che compare a più bassa energia rispetto alla banda di assorbimento della singola molecola isolata. Tale comportamento non può essere spiegato in termini delle proprietà ottiche della singola molecola a causa della sua intrinseca natura collettiva.

Sebbene le proprietà ottiche dei J-aggregates sono state studiate da tempo già a partire dalle loro scoperta negli anni '30 del secolo scorso, rimane ancora poco chiaro quali siano i meccanismi microscopici che danno origine alla *J-band* e in quale misura gli effetti di stato solido contribuiscano alle proprietà ottiche di questi cristalli molecolari. Finora, la maggior parte delle descrizioni a principi-primi non tengono in conto in maniera completa ed accurata effetti di stato solido a molti corpi (e.g., interazioni a lungo raggio, effetti di schermo, etc.) e si basano su forti approssimazioni che non sono sufficienti per predire e riprodurre correttamente le proprietà ottiche.

D'altra parte, il bisogno di simulare correttamente questi materiali è spinto anche dalla recente tendenza a impiegarli in esperimenti per studiare nuovi tipi di eccitazioni ibride risultanti dalla forte interazioni fra radiazione e materia.

Il principale obiettivo e originale contributo di questa tesi è quello di fornire una descrizione approfondita e completa a principi primi, usando tecniche allo stato dell'arte quali la teoria del funzionale densità dipendente dal tempo (TDDFT) e la teoria perturbativa a molti corpi (MBPT), sulle proprietà ottiche dei cristalli molecolari J-aggregates. Nello specifico, abbiamo investigato un aggregato composto da molecole organiche di tipo push-pull note per manifestare trasferimento di carica inter-molecolare e abbiamo concentrato l'attenzione sull'analisi della J-band dell'aggregato. Due tipi di approcci numerici sono stati utilizzati. Nel primo, abbiamo usato la TDDFT attraverso cui è stato investigato il ruolo della disposizione molecolare nel determinare il red-shift e l'amplificazione della *J-band* rispetto alla singola molecola; gli effetti del confinamento quantistico sulle proprietà ottiche quando il cristallo molecolare è confinato in una e due dimensioni. Tramite analisi della densità di carica indotta associata al picco principale della *J-band*, si può concludere che: (i) è un'eccitazione in cui la carica è spostata lungo l'asse principale (lungo) del cristallo lungo catene molecolari disposte in senso parallelo;

(ii) il red-shift globale della *J-band* viene fuori da: (1) meccanismi di interazione competitivi: fra molecole nella stessa catena (red-shift) e fra molecole di catene diverse (blue-shift), in cui il primo domina sul secondo; (2) rinormalizzazione dei livelli energetici di singola particella dovuta all'aggregazione molecolare.

Nella seconda parte abbiamo usato un approccio alternativo alla TDDFT, ovvero la MBPT, che si basa sui metodi GW e Bethe-Salpeter. Quest'ultimo schema è capace di aggirare alcuni noti difetti della TDDFT quando si usano funzionali (semi)locali, fra cui l'incapacità di descrivere correttamente gli effetti collettivi di scambio e correlazione (e.g., interazione schermata elettrone-lacuna, meccanismi di trasferimento di carica (CT)) che hanno carattere non locale. I risultati dimostrano che la *J-band* è composta da diversi stati eccitonici legati, i quali, a causa degli effetti di broadening, non sarebbero risolvibili negli esperimenti convenzionali di assorbimento. Lo stato eccitato principale della *J-band* manifesta un carattere misto di CT intra- e inter-molecolare dal momento che l'elettrone non è localizzato su una singola molecola ma anche su quelle più vicine. Questo carattere dipende sia dal fatto che il J-aggregate è composto da molecole push-pull, sia dall'impacchettamento molecolare denso il quale favorisce la delocalizzazione dell'elettrone lungo le direzioni del π-stacking delle molecole più vicine. Quest'ultimo effetto infatti dipende sensibilmente dall'impacchettamento molecolare e dal grado di overlap fra le funzioni d'onda. Oltre al picco principale, è stata anche rilevata la presenza di stati dark (i.e., non otticamente attivi o con bassa forza dell'oscillatore) con carattere di CT totale all'interno della *J-band*. Questi ultimi non possono essere rilevati nei normali esperimenti di assorbimento ottico.

Nella parte finale di questo lavoro ci siamo occupati di quantificare i meccanismi collettivi di tipo plasmonico del J-aggregate. Nello specifico, abbiamo esaminato e quantificato, dal punto di vista di molecolare, il carattere plasmonico della *J-band* e dimostrato che questa banda non ha in pratica alcun carattere plasmonico. Tale risultato risponde alla ricorrente domanda se qualunque banda avente elevato assorbimento ottico e che manifesti un qualche tipo di comportamento collettivo a livello microscopico, come la *J-band*, abbia o meno carattere plasmonico.

List of publications

1. Guerrini, M.; Calzolari, A; Corni, S.
   Solid-State Effects on the Optical Excitation of Push–Pull Molecular J-Aggregates by First-Principles Simulations.
   ACS Omega, 2018, 3 (9), pp 10481–10486

2. Guerrini, M.; Corni, S.; Calzolari, A.; Varsano, D.
   Quantifying the plasmonic character of optical excitations in a molecular J-aggregate.
   Submitted (2018)

3. Guerrini, M.; Cocchi, C.; Calzolari, A.; Varsano, D.; Corni, S.
   Interplay between intra- and inter-molecular charge transfer in the optical excitations of organic push-pull J-aggregates
   Submitted (2018)

Chapter I – Introduction

1.1 J-aggregates: overview and state of the art

J-aggregates are fascinating fluorescent nanomaterials formed by highly ordered assemblies of molecular units with spectroscopic properties dramatically different from the constituting organic molecules taken on its own. Discovered in the 1930s independently by Jelley[1,2] (J-aggregates after *Jelley*) and Scheibe[3], they represent one of the most important milestones in dye chemistry as well as the birth of supramolecular chemistry. Some of the most characteristic properties of these molecular crystals are very narrow red-shifted absorption and emission bands, strongly increased absorbance with respect to the constituting molecules together with the decrease of radiative lifetime and highly polarized emission.

All these intriguing optical properties and the countless prospects for applications (e.g. photovoltaics, biological sensing, color film photography, imaging, dye lasers, light absorbers in optoelectronics and non-linear optics, quantum information technology just to cite few) have stimulated over the years many scientists both from the theoretical and from the experimental points of view. Historically, the first J-aggregates to be studied were composed of cyanine dyes (i.e., *pseudoisocyanine* or PIC) in solutions and the observation of their very narrow light absorption and emission bands suggested high level of molecular ordering. Experiments showed in fact that the direction of their absorption dipole is parallel to the aggregate axis and from this result it was concluded that the monomers in J-aggregates are aligned parallel (or slightly inclined) to the aggregate direction. It was noticed also by J. Frank and E. Teller[4] the similarity of their excited states with excitons proposed by Y. Frenkel for molecular crystals. Later on, based on the molecular exciton theory of Davydov, M. Kasha developed a model of excitonic coupled dimers that, despite its simplicity, can describe the basic properties of molecular aggregates.

Through the years of rich developments of theory and applications, J-aggregates have been widely studied and characterized in the literature. We shall give here a brief general review about J-aggregates characterization from the experimental and the theoretical points of view.

In the past 80 years since their discovery, there has been a great number of technical analyses about dimensions, shapes, and morphologies of J-aggregate molecular crystals. From the experimental point of view, J-aggregates are prepared and formed in solutions (usually water) and real crystals are not observed in the form of 3D solid-state structures. Rather, they tend to be observed in low-dimensional structures[5–7]. At the mesoscale, they manifest a complex morphological and structural variability, so that various structures have been observed at different dyes concentrations and solution conditions[5]. For cyanine dyes, for example, using optical microscopy, TEM and AFM measurements, several morphological groups have been revealed such as extended two-dimensional rods, strings, sheets, giant tubes, fibrils, quasi one-dimensional stripes, twisted ribbons[5–17]. In particular, as reported experimentally[16,18] for cyanine dye aggregates, monolayers are typically about 3-400 nm long and few nm deep. Moreover, molecules tend to aggregate and be packed in a herringbone, brickwork, or in ladder/staircase structures, with molecular planes oriented normally to the monolayer plane (Figure 1(a)). There are also morphological studies[13,15], performed by using fluorescence optical microscopy (FOM) and AFM measurements, of formation of tubular TC J-aggregates from self-folding of narrow and wide monolayer strips (Figure 1(b)).

In parallel, lots of theoretical analytical models have been put forward to explain the J-aggregates characteristic narrow red shifted absorption band (*J-band*). One of the best accepted quantum mechanical descriptions, taking into account also vibronic effects (i.e., electron-phonon coupling), is the so-called Frenkel-Hölstein model[19–22], which has been widely used to describe photo-physical properties of J-aggregates[23,24] and conjugated polymers[25,26]. Albeit its popularity, this model is not practical for aggregates of more than ~20 monomer units[21,22]. Nevertheless, if one focuses on the *J-band* optical absorption, there is no vibronic coupling[27,28] since the electronic coupling between molecules is much bigger than the characteristic vibrational energy[28] of monomers and the model can be simplified assuming the adiabatic (Born-Oppenheimer) approximation. The latter is called Frenkel model and, assuming weak overlap between molecular wave-functions and no electron-phonon coupling, describes the whole aggregate excited state as an electronic excitation delocalized over several molecular sites[21,29] in which each molecule stays charge neutral. The Frenkel model has been used extensively for the description of excitonic energy transfer in mono-molecular chains[21,30,31]. In other related works[27,32] one can also find a general theoretical description of J-aggregates, taking into account also the monomers vibrational degrees

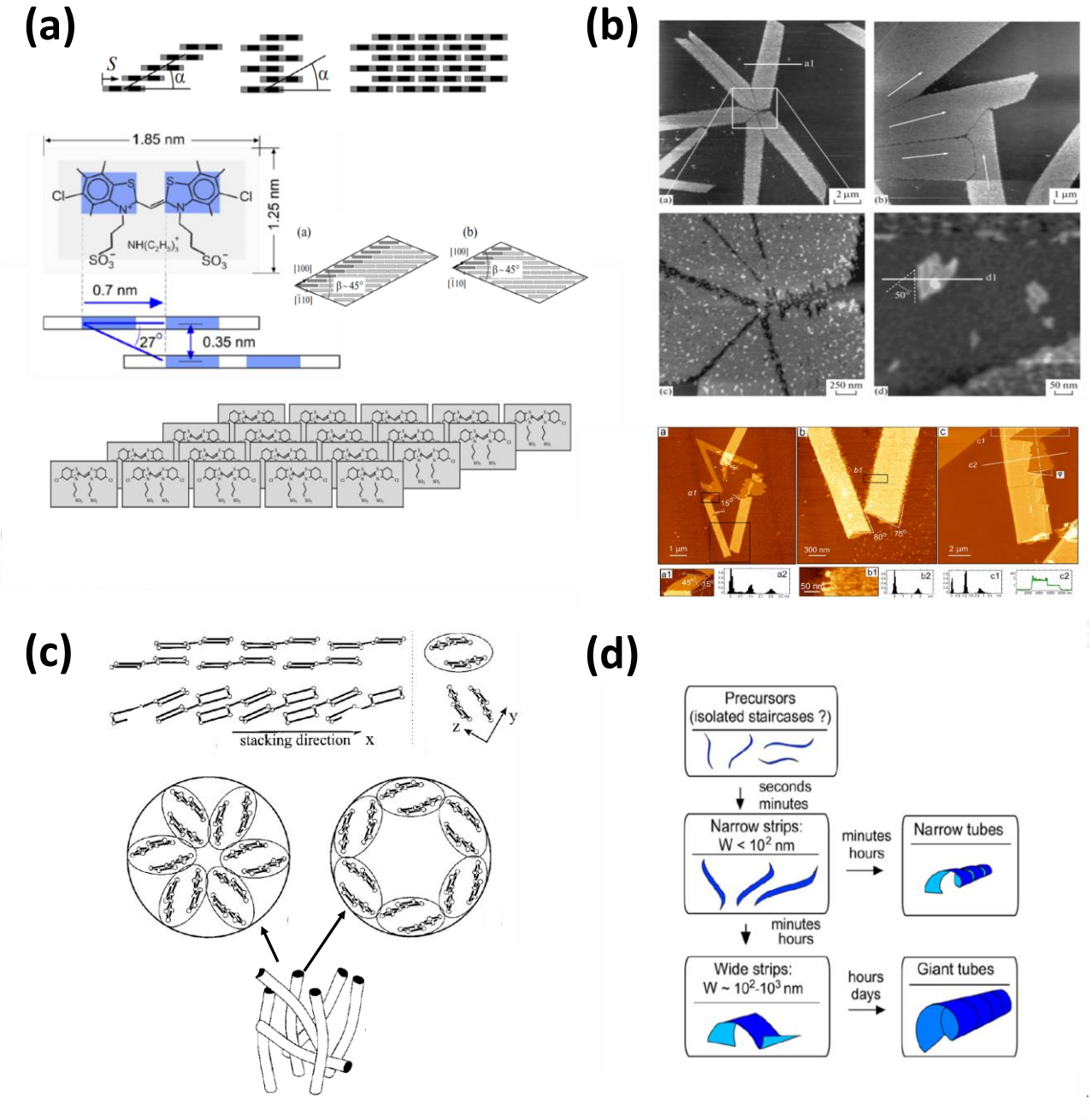

Figure 1- Structure and morphologies of J-aggregates. Panel a: (upside part) typical molecular arrangements in J-aggregate molecular crystals (from right to left: brickwork, ladder and staircase type; (downside part) model of brickwork molecular packing of tubular crystal (TC) pseudoisocyanine (PIC) J-aggregate in an asymmetrical monolayer with an AFM measured height of 1nm. TC molecules are symbolically represented by rectangles with edgewise orientations, a side surface area of 1.7 x 1.0 nm^2. The orientation of the transition dipole moments is along the long axes of TC molecules (i.e. long rectangle sides). Panel (b): AFM topography images of TC J-aggregate during adsorption on mica surface. Panel (c): (up-left part) threadlike arrangement of the PIC molecules derived from X-ray analysis of PIC chloride single crystals. The single stack was often used as a structural model for a one-dimensional PIC J-aggregate; (upside-right part) top view of the stacks along the x-axis. Taking van der Waals radii into account, one stack can be modeled by a thread with an elliptical cross section;(downside part) two possible quasi one-dimensional models for the PIC J-aggregate: a star-like and a tubular arrangement of six stack within a cylinder of 2.3 nm diameter. Panel (d): scheme of morphological transformations in TC J-aggregates. Figures adapted from Reference[33].

of freedom, to predict the red shifted peak position from the knowledge of monomers lineshape function (i.e., absorption spectrum) and of the electronic inter-molecular interaction strength within the aggregate. In particular this model has been proved useful to estimate the molecular packing configurations from measured absorption spectra. A complete and comprehensive theoretical description of the proposed mechanisms to explain the physical nature of the *J-band* is discussed in a review by *Egorov et al.* [29] ; a comprehensive theoretical explanation about the origin of the narrowing of the J-band was presented by *A. Eisfeld et al.*[28] . A more general view on the formation and the spectroscopic properties of dye J-aggregates can be find in a review by *Würthner et al.*[34]. *Spano and Silva*[35] provided detailed analysis of H- and J- aggregates with a focus on applications for organic semiconductors. In the review of *J.L. Brick at al.*[36] there is a thorough and comprehensive description of the basic research and applications of fluorescent cyanine dye J-aggregates with a focus on the relation between optical properties and dye structures. Finally, a detailed and interesting study of the entanglement dynamics in one-dimensional J-aggregate systems is reported in Reference[37].

1.2 Optical properties of J-aggregates

The major characteristic features of J-aggregates are the strong shift of their absorption and emission spectra to lower energies (i.e., longer wavelength) with respect to the spectra of the constituting monomers, together with a dramatic amplification and narrowing of the red-shifted peak (Figure 2). The formation of J-aggregates proceeds via supramolecular self-organization, normally via π-π dispersive interactions between highly polarizable groups of atoms together with electrostatic interactions between opposite charges. Once molecules are aggregated, their transition dipole moments are aligned (almost) parallel to the line joining their centers through a *head-to-tail* or *shifted-plates* arrangement that demonstrate high optical anisotropy[38–41]. In this configuration, the J-aggregate demonstrates the properties of a molecular ensemble acting as one unit with strongly increased dipole moment[34]. As we will describe in more detail hereafter, the observed spectroscopic changes are the result of excitonic coupling between individual molecules forming the aggregate.

In other cases, in some conditions the dyes can assemble into quite different H-aggregates (*H* is referred to *hypsochromic* shift, i.e. energy blue-shift) that are characterized by *side-by-side* arrangements[17]. Compared to the isolated monomer units, the visible excited states in H-aggregates are shifted to shorter wavelengths but the corresponding fluorescence spectra (which can be very low in intensity) are shifted to longer wavelengths[17]. Such division into H- and J-aggregates is a simplification so that in general *H*- and *J-bands* or several *J-bands* can be observed simultaneously. In Figure 2 are reported schematically the spectral changes on formation of J and H aggregates.

The basic spectroscopic characteristics of J-aggregates are very unique. They demonstrate very narrow J-bands in absorption spectra and manifest dramatic red-shift. Vibrational component in their broadening is not observed, so these bands are almost symmetric[42]. Another characteristic is the strong absorbance in comparison with the isolated monomers[43]. Due to strong coupling between the molecular transition dipoles, two-photon absorption cross-section can also achieve very high values much exceeding that of monomers[39].

The fluorescent properties of J-aggregates are also unique. Their fluorescence spectra match the absorption spectra and are of equally narrow width, they demonstrate nearly resonant behavior and display very small (~200 cm^{-1} and smaller) Stokes shifts and insensitivity to the environment[34]. The strong increase in the oscillator strength is coupled with the increase in radiative rates, therefore the fluorescence lifetimes are much shorter than in the monomers and are observed on picosecond time scales[44]. The latter effect is usually called *superradiance*[45]. J-aggregates demonstrate also high optical anisotropy resulting in polarized fluorescent emission[13,38] and absorption parallel to the aggregate axis. In Table 1 we have put a list of the most essential spectroscopic properties of J-aggregates. In Figure 3 is showed the dramatic transformation of PIC absorption spectrum as it forms a J-aggregates: we can see how its formation is a dynamic and concentration-dependent process.

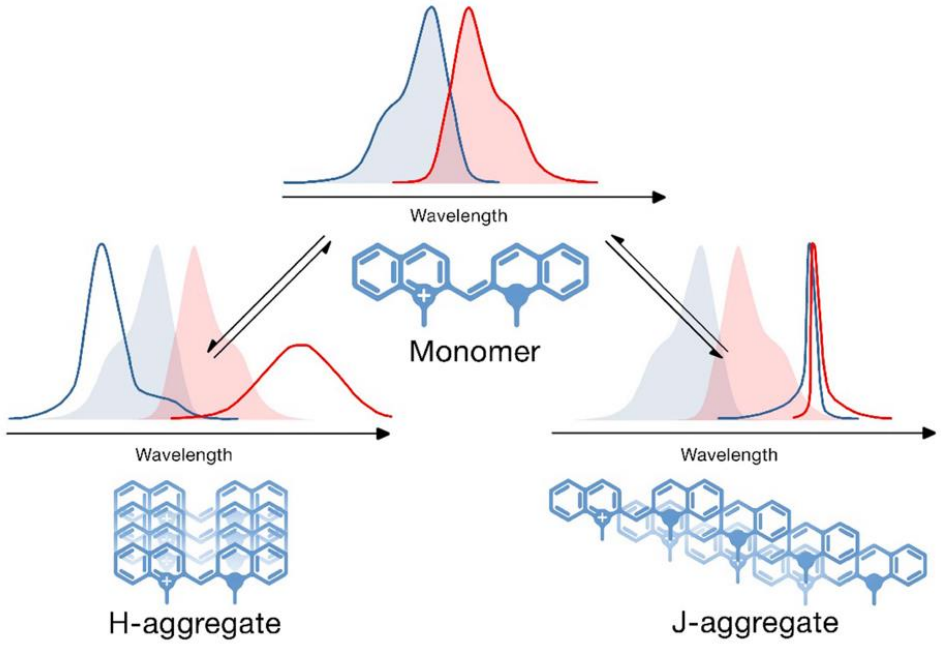

Figure 2 – Schematic representation of the changes in absorption (blue) and fluorescence (red) spectra on the formation of H- and J-aggregates from organic dye monomers (image taken from J. L. Bricks et al.[36], IOP Publishing 2018)

1.2.1 Molecular excitons in J-aggregates

The excitonic collective nature of electronic transitions in J-aggregates is responsible for their optical properties[36]. These aggregates represent the case where the resonant excitation transfer interaction between constituting molecules is much stronger than the interaction with the environment (e.g. with the molecular vibrations).

Due to this strong inter-molecular electronic coupling, the excitation is no longer localized on a single monomer but it demonstrates *coherent exciton motion* along the molecular chain as a wave packet[46].

By definition, excitons are collective charge neutral excitations in the form of electron-hole pairs that appear in solids and molecular systems upon electronic excitaton[46]. In J-aggregates one typically deals with Frenkel or strongly bound excitons[47] where each electron-hole pair stays localized on the same molecule, while the excitation passes from one molecular site to another and so it can be delocalized across many chromophores[48].

The optical properties of J-aggregates can be conceived within the framework of *molecular exciton theory* that was firstly developed by Davydov to describe the energetically delocalized states in molecular crystals[49]. According to this treatment, the excitation achieved in a single molecule of a periodic molecular assembly is transferred from molecule to molecule within a period which is much shorter than the characteristic molecular vibrational time of the monomer units in the assembly.

TABLE I. some of the most essential spectroscopic properties of J-aggregates of organic dyes

Absorption
• Very narrow J-band in absorption
• Dramatic shift of J-band to the red with respect to the monomers spectra
• Absence of vibrational component in J-band
• Strongly increased absorbance concentrated within very narrow absorption band
• Strongly increased tow-photon cross-section, in comparison with constituting monomer units

Fluorescence
• The spectra match the absorption spectra and have very narrow width
• Stokes shifts very small (~200 cm^{-1}) and negligible
• Fluorescence lifetimes much shorter than monomers as a result of *superradiance*
• Spectra insensitive to the environment

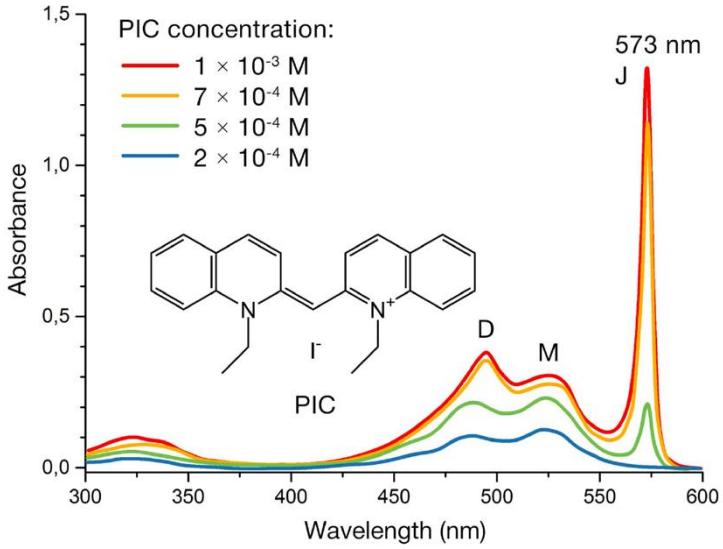

Figure 3 – Chemical structure and absorption spectra of pseudoisocyanine dye (PIC) as the classic example of J-aggregate. The concentration-dependent formation of J-aggregates is evident from the appearance and growth of the narrow band at ~573 nm with the increase of dye concentration in 0.2M NaCl acqueous solution. Note that on the growth of the J-band, the spectral features of monomer (M) and H-type dimer (D) do not disappear. (Reprinted from Reference[39]. Elsevier publishing 2006)

In this case the electron-hole pairs remain localized within the same molecule, while the entire excitation is coherently delocalized over many monomers in the form of *excitation waves*[46]. From superpositions of these excitation waves, *excitation packets* can be formed, which describe the coherent motion of (molecular-localized) excitations[50]. In this way the excitation can migrate over hundreds of monomer units[51,52]. This is an essential difference from the Förster-type excitation energy transfer, in which the chromophores retain their identity and their oscillating dipoles interact at a distance[36].

1.2.2 Kasha's dipole model

The first model linking the molecular packing geometry and the photophysical properties of molecular aggregates of organic dyes was done by M. Kasha[53,54]. Based on exciton theory he studied the effect of relative orientation of two molecules approximated as point dipoles, so that their transition dipoles are aligned along the long axis of the molecules (Figure 4). Upon excitation of the dimer, the model demonstrates the splitting (*Davydov splitting*) of the single molecule excited state energy level into two levels due to the Coulomb coupling between the two monomers. The angle between the transition dipoles and the molecular axis of the aggregate as well as the mutual orientation between transition dipoles determine the amount of energy level splitting and whether an optical transition is allowed to a lower or to a higher excited-state level[53] with respect to the monomer one.

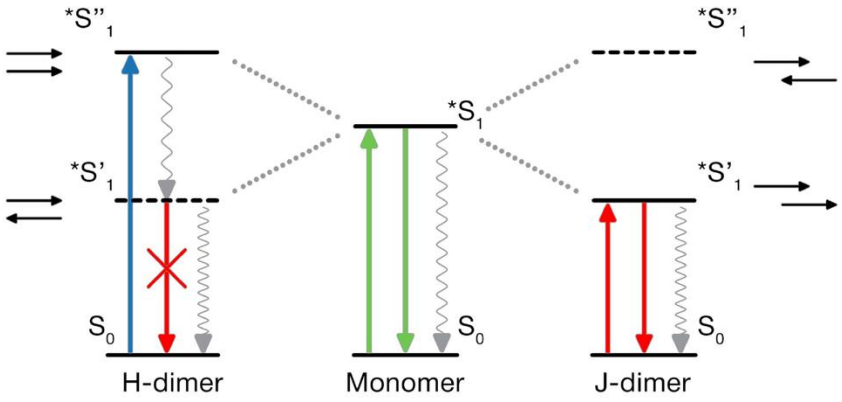

Figure 4 – Illustration of molecular exciton model suggested by Kasha for the variation of energy in electronic transitions of molecular dimers. The H-type dimers formed by side-to-side association demonstrate strongly increased energy separation between absorbing and emitting states and have low fluorescence, due to their very low lowest excited state transition dipole. In contrast, in J-type dimer the transition dipoles are in line. They exhibit a strong decrease in transition energy and an increase in the transition dipole moment enhancing the probability of light absorption together with red-shift in absorption and emission. (Image taken from J. L. Bricks et al.[36]*, IOP Publishing 2018)*

In the former case there is a red-shift and one explains the J-aggregate behavior, while in the latter where there is blue-shift one talks about H-aggregate behavior. The Kasha model predicts also the *emissive* properties of dye aggregates.

In H-type dimers with a *side-by-side* alignment, for example, the radiative decay is suppressed (the transition is symmetry-forbidden), while in J-type dimers that are *head-to-tail* (partially) aligned it is enhanced compared to the uncoupled molecules.

In addition to that, in J-aggregates, the transitions only to the lowest energy excited state level are allowed and, as a consequence, they possess negligible Stokes shift with high fluorescence quantum yield[36]. Thus, the simple Kasha's model considering two point dipoles allows the explanation of the most essential features of molecular aggregates – the strongly blue-shifted (red-shifted) absorption spectra of H-(J-) aggregates. These two extreme cases provide the basis for understanding the absorption and emission behavior in systems with more complicated morphologies where both mechanisms are present and compete each other. If the Coulomb electronic couplings J_0 between neighboring molecules are positive (i.e. repulsive interaction) one has predominantly H-arrangements and the optically allowed state is on top of the band; for J-aggregates these couplings are negative (i.e. attractive), so that the excited energy level is found at the bottom, leading to red-shift with respect to the monomer (see Figure 5). We will see in more detail this behavior in Chapter 4 where the couplings J_0 are expressed in terms of interaction between monomers transition densities. The basic idea of Kasha

that the sign of electronic coupling in dimer, positive for *H* and negative for *J*, distinguishes the two basic aggregate forms was explored by many researchers.

Kuhn and co-workers extended the Kasha model by introducing *physical dipoles* in description of Coulombic interactions in the dimer[55,56] that allowed a better understanding the 'staircase' formation of aggregated structures. It was predicted also that the impact of exciton-vibrational coupling should be strong for H-aggregates and negligible for J-aggregates[24], so that in J-aggregates both the absorption and emission bands represent the 0-0 vibronic transitions[35] (Figure 5(a)).

In development of this model it was accounted that at small intermolecular distances, in addition to the long-range Coulomb coupling, a significant wave function overlap between neighboring molecular orbitals may be essential[57]. Such effective short-range exciton coupling due to wave function overlap facilitates the charge-transfer that can also induce J- or H-aggregate behavior. However, unlike Coulomb coupling, the short-range coupling must be extremely sensitive to small transverse displacements between neighboring chromophores.

1.2.3 J-band narrowing

The explanation of the extreme vibrational narrowing of the J-band, i.e., the abnormally narrow, high intensity, red-shifted optical absorption band arising in J-aggregate molecular crystals, has attracted the attention of many researchers[43] and it still remains disputable[28,29,58]. The common accepted explanation is based on the Frenkel's statistical exciton model[29,59,60] which assumes assumes that the electronic excitation is transferred so fast between molecules that it averages out the (quasi)static disorder (disorder is associated to coupling of electronic degrees of freedom with molecular vibrations) in electronic transition energies of molecules in the J-aggregate[59] . In this way the narrow *J-band* is due to the strong electronic coupling between molecules and weak electronic coupling with intra-molecular vibrations.

The electronic excitations within the J-band to a large extent are decoupled from vibrational modes[61] and, in contrast to H-aggregates, the 0–0 transition becomes dominant in absorption and emission[35]. Since vibrational modes are not involved and there are no energy losses on molecular relaxations, the absorption origin is also the emission origin, and therefore the Stokes shift may become negligible. The absorption and fluorescence bands of J-aggregates are also much narrower because of motional and exchange-derived narrowing that dynamically average the energies over their inhomogeneous distribution[42]. The origin of very narrow band widths may be also connected with the narrow distribution of excitons delocalization lengths *Nc* and of the short excited-state lifetimes.

Recently a new theory of formation of the J-band has been proposed by *Egorov et al.*[29] which is based on charge transfer[62,63] and dozy chaos[62] but it is only at its first steps[29,62,63] and its validity is not commonly accepted.

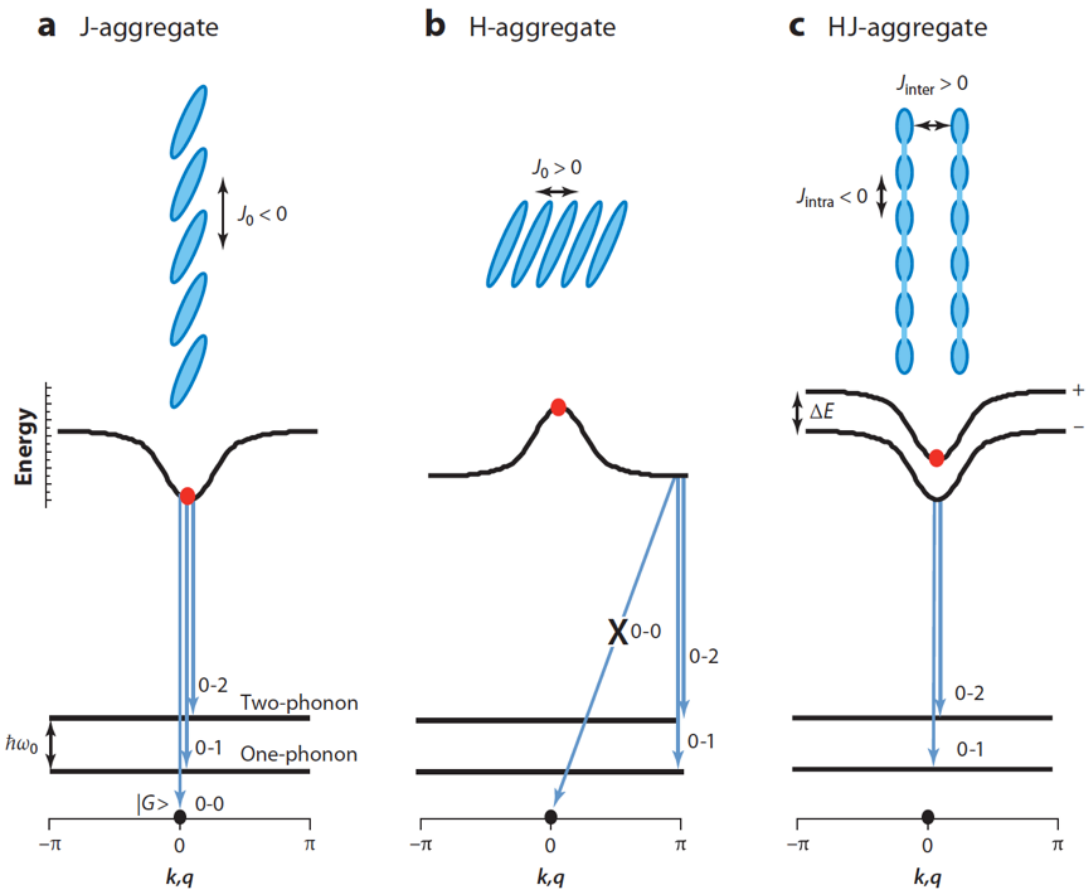

*Figure 5 – (**a**,**b**) Molecular orientations within conventional J- and H-aggregates. The sign of the nearest-neighbor coupling J_0 is determined by the through-space Coulombic coupling. Generally, head-to-tail orientations lead to $J_0 < 0$ and J-aggregation, whereas side-by-side orientations lead to $J_0 > 0$ and H-aggregation. (**c**) In polymer HJ-aggregates, Coulombic interchain coupling is positive ($J_{inter} > 0$), whereas the effective intrachain coupling between adjacent repeated units is negative ($J_{intra} < 0$) owing to through-bond interactions. Also shown is the energy dispersion, E(k), corresponding to the lowest vibronic band in each aggregate (higher bands are omitted for clarity). The band curvature at k = 0 is positive (negative) in J- (H-) aggregates. The red dot indicates the (k = 0) exciton that is optically allowed from the ground state, $|G\rangle$ (black dot). The energies of the one- and two-phonon states within the electronic ground state are also indicated. Arrows indicate emission pathways at low temperatures, such that emission originates primarily from the lowest-energy exciton. In J-aggregates (**a**), 0-0 emission is strongly allowed, leading to superradiance. In contrast, in H-aggregates (**c**), rapid intraband relaxation subsequent to absorption populates the lowest-energy k = π exciton, which cannot radiatively couple to $|G\rangle$, thereby preventing 0-0 emission (assuming no disorder). In the HJ-polymer dimer (**c**), the J-like intrachain band in each polymer is split into symmetric (+) and antisymmetric (−) bands by interchain interactions. Owing to selection rules, only the k = 0 symmetric state can radiatively couple to $|G\rangle$. (image taken from F.C. Spano et al.[35])*

1.2.4 Superradiance

Molecular aggregates are also characterized by the so called *superradiance*, which is a cooperative spontaneous emission manifested by ultrafast radiative decays[45]. This effect has a simple classical interpretation: when a collection of dipoles oscillates in phase, their amplitudes add up coherently to form a large effective dipole. Since the extension of the exciton and hence the size of the dipole moment is restricted to a finite number *Nc* of coupled molecules constituting the macrodipole, the radiative lifetime $\tau_0(J)$ of these coupled structures should be strongly decreased being inversely proportional to *Nc*[28,60].

1.2.5 Enhanced light-matter interaction: J-aggregates in nano plasmonics

In the last few years J-aggregates have been extensively employed together with metallic nanosystems to study the field enhancement resulting from strong light-matter coupling phenomena[36]. In fact the possibility to control and enhance the radiative properties of these nanomaterials by their near-field coupling to optical fields generated by plasmonic metal nanostructures has attracted many researchers[64].

Strong molecular-scale electromagnetic fields can increase the fluorescence by enhancing locally the light absorbance and by modifying the radiative rate. Such field enhancement can be provided by depositing J-aggregates directly on top of plasmonic gold[65,66] and silver[67,68] nanoparticles.

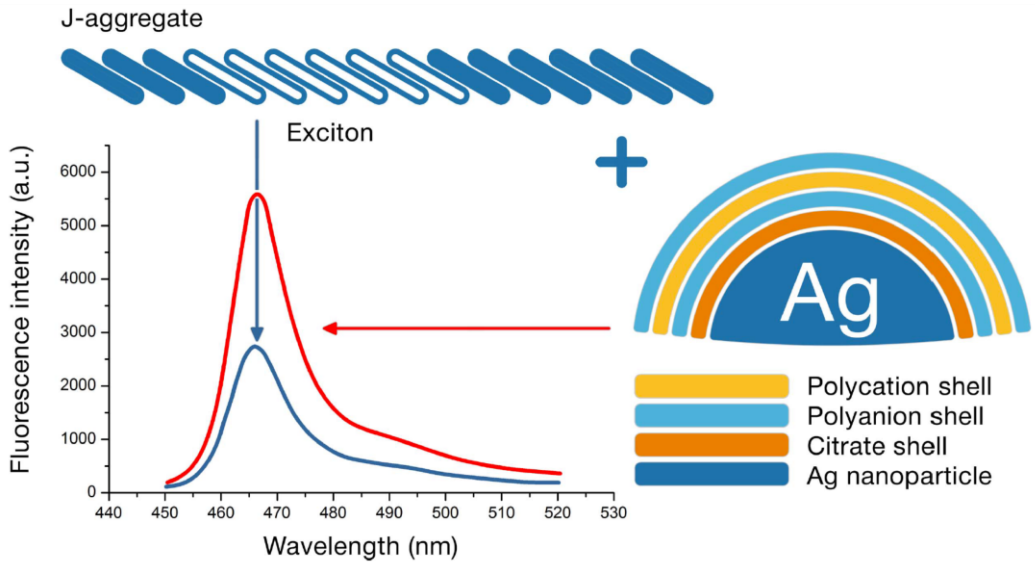

Figure 6 - Plasmonic enhancement effect observed on interaction of J-aggregate of thiacyanine dye with plasmonic Ag nanoparticles in water solution[69]. To control the distance between J-aggregates and silver nanoparticles the latter was covered by a polymer shell of variable thickness using the layer-by-layer assembly method. (Reprinted from Ref.[69]. Copyright (2014) American Chemical Society.)

The noble metal nanoparticles generate localized surface plasmons that provide strong modulation of the light absorption and scattering showing the features of coherent coupling between the localized plasmons of the metallic nanoparticle and the excitons of the molecular J-aggregate[70]. Such coherent coupling was demonstrated in experiments with gold and silver tunable plasmonic nanoparticles covered with inert molecular layers of variable width[69,71] (Figure 6). While providing high local fields and large enhancement factors, such excitonic–plasmonic constructs demonstrate high sensitivity to the nanoscale geometry of their structures and the effects of distance. The enhancement effect also depends on the J-aggregate structure: the strongest effect is expected from J-aggregates with large exciton coherence length[69].

Much stronger plasmon–exciton coupling is observed with noble metal nanorods[72–74], nanostars[75], nanodisks[76] and nanoprisms[77] that generate stronger electromagnetic

field at the sharp edges of these nanostructures. These hybrid states that combine plasmonic and excitonic effects opened new ways in designing nanocomposites materials[78].

In spite of the rapidly growing number of publications addressed to the coupling between J-aggregates and metallic nanoparticles, there are still a lot of questions about the plasmon–exciton interaction between them. Most of the present studies are focused on light absorption and scattering effects[79–81] and the studies of fluorescence emission are rare. Still, the questions about the influence of adsorption and aggregation of dye molecules on the surface of plasmonic nano-particles on the decay of excited states and the photoinduced degradation are remaining for detailed investigations and understanding[36].

1.3 Motivations and goals

In this thesis we investigate the optical properties of a molecular J-aggregate[1,52] composed of push-pull organic dyes, representative of a broad range of molecular crystals with enhanced light-matter interaction, by means of state-of-the-art first principles approaches, namely *Time-Dependent-Density-Functional-Theory*[82,83] (TDDFT) which is based on a density functional formalism, and *Many-Body perturbation theory*[83–85] (MBPT), which relies on a Green function formalism. The overall motivation of this work is to be able to capture all the details of the electronic excitations involved in the optical response of a realistically complex molecular aggregate.

The need to investigate by first principles these molecular systems is driven by several reasons:

(1) Still there has never been attempted any realistic *ab initio* simulation of J-aggregate molecular crystals which takes thoroughly into account long-range and intermolecular many-body solid-state effects. So far, all the theoretical models are based on strong assumptions – such as assuming a simple one-dimensional crystal, weak intermolecular interactions, no ground state variation of the molecules when

they aggregate, small electronic excitations, weak overlap between molecular wave-functions[22,29,86] without properly taking into account also exchange and correlation effects[29]– and on the a-priori knowledge of the molecular properties[29]. To date, the most realistic and accurate first principles simulations have described not really extended systems, but rather small clusters with just a few tens of molecules[87,88] (~20), while J-aggregate experimental samples are typically composed of hundreds or thousands of molecular units[6,7,9,15,16]. These simplified models revealed not sufficient to correctly describe and predict the optical properties of J-aggregates and fundamentally lack of a comprehensive and quantitative description of the inter-molecular interactions (e.g. van der Waals) that become crucial in condensed (i.e., aggregated) systems. Solid-state approaches, which take thoroughly into account many-body effects (e.g. screening, long range interactions, etc.) to characterize both the electronic and the optical properties, have never been proposed. Thus, a first-principles description of realistic extended J-aggregates would shed light on how the complex inter-molecular interactions play a role on their peculiar optical response.

(2) The renewed experimental interests about J-aggregate molecular systems employed for ultra-strong and coherent light-matter interaction[73,75–78,80,89,90], useful to probe objects at the nanoscale. In particular, J-aggregates are employed together with plasmonic metallic nanosystems to study hybrid nanostructures in the strong coupling regime[31,65–68,70,71,90–93], (e.g., the coupling between organic J-aggregates with metallic nano-systems such as nanoparticles, nanorods, nano-disks, etc.) which forms surface-plasmon exciton hybrid states (called plexcitons[68,71,94]) that soon could pave the way towards a new generation of nano-composite materials and active plasmonic devices operating at room temperature[78]. In relation with these experimental interests, *ab-initio first-principles* numerical methods offer the non-negligible advantage to retrieve physical information that could not be possible to access in conventional experiments, e.g., the possibility to resolve all the excited states, even the dark ones, and to get qualitative and quantitative insights into the character of the excitations[82,83,95,96].

(3) The interest in *ab-initio* simulation of low-dimensional J-aggregate molecular crystals (1D like-polymer chains and 2D like-monolayer films) in order to see what are the major effects of the quantum confinement on their optical response with respect to a bulk phase molecular crystal.

(4) The renewed interest in investigating the microscopic physical origin of the red-shifted *J-band*. Even though lots of theoretical models have been proposed over the years in order to explain the red-shift of the *J-band*[29], it is still not so clear what is its microscopic physical origin, i.e. what kind of collective excitations are involved that are responsible for the intense optical absorption and the very narrowing of that band. A thorough first principles study shall get physical insights about the microscopic nature and character of the *J-band*.

Chapter II – investigating J-aggregates from first principles: TDDFT approach

In this chapter we shall present the main results and findings of the Time-Dependent-Density-Functional-Theory (TDDFT) first principles simulations performed on a molecular J-aggregate composed of push-pull organic dyes[97]. Simulations have been performed by using the Quantum Espresso[98,99] suite of codes.

Within the TDDFT framework, we have focused more on a qualitative description of the optical properties of the molecular J-aggregate by describing the principal microscopic physical mechanism which underlies the formation of the red-shifted band (*J-band*). We investigated three main aspects: (1) the role played by the different molecular arrangements within the bulk crystal on its optical response; (2) the microscopic nature of the *J-band* by means of induced charge density analysis; (3) the effects of the quantum confinement when moving from the bulk crystal to low dimensional crystal structures where a two-dimensional monolayer film and a one-dimensional polymer chain, extracted from the bulk crystal, have been simulated. The main findings are:

(1) the optical behavior of the bulk crystal, due to the complex inter molecular couplings, cannot be deduced considering its isolated parts such as dimers or even an extended chain extracted from it.

(2) The *J-band* is associated to a collective excitation in which the induced charge density in each molecular unit is displaced along the crystal long axis and in which all the molecular transition dipoles are coherently aligned. The latter explains the enhancement of the J-aggregate red-shifted peak. The red-shift of the *J-band* results from competing coupling mechanisms such as couplings between molecules within the same chain (intra-chain) which cause red-shift and couplings between molecules of different chains (inter-chain) which cause blue-shift. The former is the dominant mechanism and explains the observed red-shift of the *J-band.*

(3) The confinement of the crystal in one dimension (i.e., 2D J-aggregate) perpendicular to the long axis does not affect the J-band peak but it generates new excitations at higher energy that, due to

surface effects, reflect the broken symmetry of the bulk crystal. Confinement in two dimensions (i.e., 1D J-aggregate) causes a stronger red-shift of the J-band with respect of the bulk since there are no more interchain couplings which causes the blue-shift.

The following results will be included in the form of a published paper together with the supporting information in Appendix A which contains the material complementary to the main text.

ACS OMEGA

Article

Cite This: ACS Omega 2018, 3, 10481−10486

http://pubs.acs.org/journal/acsodf

Solid-State Effects on the Optical Excitation of Push−Pull Molecular J-Aggregates by First-Principles Simulations

Michele Guerrini,[†,‡] Arrigo Calzolari,[‡] and Stefano Corni*[,‡,§]

[†]Dipartimento FIM, Università di Modena e Reggio Emilia, 41125 Modena, Italy

[‡]CNR Nano Istituto Nanoscienze, Centro S3, 41125 Modena, Italy

[§]Dipartimento di Scienze Chimiche, Università di Padova, 35131 Padova, Italy

Supporting Information

ABSTRACT: J-aggregates are a class of low-dimensional molecular crystals which display enhanced interaction with light. These systems show interesting optical properties as an intense and narrow red-shifted absorption peak (J-band) with respect to the spectrum of the corresponding monomer. The need to theoretically investigate optical excitations in J-aggregates is twofold: a thorough first-principles description is still missing and a renewed interest is rising recently in understanding the nature of the J-band, in particular regarding the collective mechanisms involved in its formation. In this work, we investigate the electronic and optical properties of a J-aggregate molecular crystal made of ordered arrangements of organic push−pull chromophores. By using a time-dependent density functional theory approach, we assess the role of the molecular packing in the enhancement and red shift of the J-band along with the effects of confinement in the optical absorption, when moving from bulk to low-dimensional crystal structures. We simulate the optical absorption of different configurations (i.e., monomer, dimers, a polymer chain, and a monolayer sheet) extracted from the bulk crystal. By analyzing the induced charge density associated with the J-band, we conclude that it is a longitudinal excitation, delocalized along parallel linear chains and that its overall red shift results from competing coupling mechanisms, some giving red shift and others giving blue shift, which derive from both coupling between transition densities and renormalization of the single-particle energy levels.

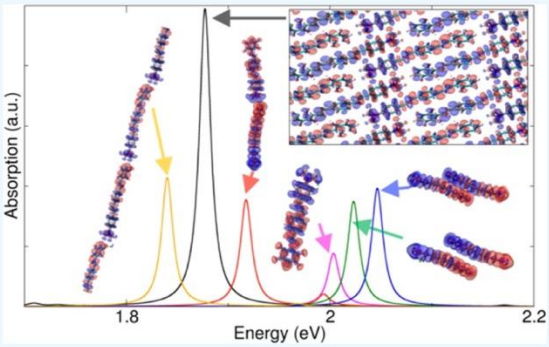

INTRODUCTION

J-aggregates[1] are a general class of low-dimensional molecular dye crystals, which display coherent interaction with light. These systems have interesting optical properties such as an intense and narrow (i.e., long radiative lifetime) red-shifted absorption peak (called J-band) not present in the spectrum of the single monomer unit they are composed of, that enhances both emissive and nonlinear optical properties.[2] Furthermore, because of the intermolecular mechanisms (i.e., van der Waals, $\pi-\pi$ stacking, hydrogen bonding, etc.), they have the ability to delocalize and migrate electronic excitations at long distances.[3,4] The position, intensity, and width of the red-shifted peak is strongly related to the molecular arrangements and their mutual interactions.[4−6]

Since their discovery in 1936 by Jelley,[1] J-aggregates have been widely studied and characterized in the literature, with a number of technical analyses about their dimensions, shapes, and morphologies. From the experimental point of view, they are prepared and formed in solutions (e.g., water) and extended three-dimensional (3D) crystals are not usually observed. Rather, they often assemble in low-dimensional structures. At the mesoscale, J-aggregates manifest a complex morphological and structural variability, so that various shapes have been observed at different dye concentrations and solution conditions.[2,5−9] Moreover, these molecules tend to aggregate in herringbone, brickwork, ladder/staircase structures, with molecular planes normally oriented to the monolayer plane. A detailed discussion about the links between J-aggregates morphologies and optical properties is in ref 10.

In parallel, several theoretical models have been put forward to explain the characteristic narrowing and enhancement of red-shifted band of J-aggregates.[11−17] Because vibronic effects play no relevant role in the J-band,[18] these models are often simplified by assuming the adiabatic Born−Oppenheimer approximation and weak overlap between molecular wavefunctions, as well as small excitations.[11] This description has been extensively used to reproduce the excitonic energy transfer in monomolecular chains.[19,20] In other related works,[18,21] the position of the red-shifted peak is predicted from the knowledge of the monomer absorption spectrum and the interaction strength between the monomers. The latter model has been proved useful in particular to estimate the

Received: June 26, 2018
Accepted: August 17, 2018
Published: September 4, 2018

DOI: 10.1021/acsomega.8b01457
ACS Omega 2018, 3, 10481−10486

molecular packing arrangements from measured absorption spectra.

Despite the huge amount of experimental data, on the theoretical side some crucial problems remain unsolved: to date, the most accurate simulations have described not really extended systems but rather small clusters,[22] with just a few tens of monomers (~20), whereas experimental samples are composed of hundreds or thousands of units. Solid-state approaches, which take thoroughly into account long-range and many-body effects, have never been proposed. Thus, a *first-principles* description of extended low-dimensional J-aggregates, such as films and (quasi) one-dimensional (1D) chains, would shed light on the complex interplay between the intermolecular coupling and the resulting optical response. The goal is to provide a microscopic rational of how the various molecular arrangements that coexist in a realistic J-aggregate crystal, as well as the quantum confinement along a given direction, contribute to the overall red shift of the peak. This may also help to identify guidelines for the design of J-aggregate with specific optical properties.

This is particularly relevant in view of the renewed experimental interests about these systems, which exhibit an ultrastrong and coherent light−matter interaction, useful to probe objects at the nanoscale. For this reason, J-aggregates have been recently employed together with plasmonic antennas to study hybrid nanostructures in the strong-coupling regime.[23−27] For example, the coupling between organic J-aggregates with metallic nanosystems (e.g., nanoparticles, nanorods, nanodisks, etc.) forms surface-plasmon exciton hybrid states (plexcitons) that could pave the way toward active plasmonic devices operating at room temperature.[28−33]

In this work, we investigate a J-aggregate molecular crystal composed of 4-(*N*,*N*-dimethyl-amino)-4′-(2,3,5,6-tetrafluorostyryl)-stilbene.[34]

This molecule is also a push−pull organic dye (Figure 1): it is a π-conjugated system that possesses an intrinsic electric dipole because of the electron donating (push) amine group and the electron withdrawing (pull) F substituents and manifests an intramolecular charge-transfer (ICT) behavior when optically excited.[35−37] The latter is a key property to polarize the molecular crystal because it permits to transfer energy from one molecule to the other and to delocalize the excitation throughout the whole aggregate. The unusual combination of J-aggregate coupling and push−pull character makes this a unique system with fascinating optical properties. Moreover, the choice of this molecule is also motivated by the availability of the X-ray crystal structure (encompassing several kinds of relative molecular arrangements) and optical spectra characterization,[34] and the computational convenience of its being charge neutral (no counterions to simulate) but still electrostatically not trivial due to its ground state dipole moment.

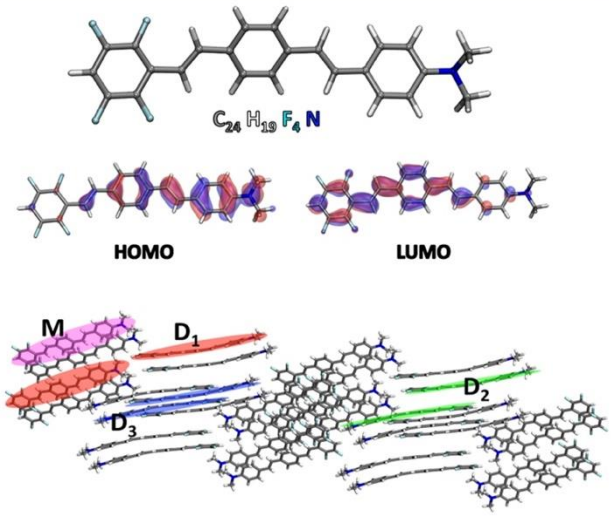

Figure 1. (Top) Push−pull dye molecule investigated in this work. Its DFT frontier orbitals are also shown. (Bottom) 3D view of a section of the X-ray structure of the bulk crystal.[34] Here, we have highlighted in different colors the single monomer and the dimer configurations that have been simulated in the present work.

RESULTS AND DISCUSSIONS

In this section, we present and discuss the results of first-principles time-dependent density functional theory (TDDFT) simulations of a J-aggregate bulk molecular crystal and of two low-dimensional structures, specifically a linear chain and a monolayer film, extracted from it. In particular, we focused on the J-bands and on the associated induced charge densities, to describe the microscopic physical mechanisms involved in the observed red shift. The bulk aggregate is composed of the push−pull organic dye in Figure 1. Because of the presence of the amino substituent on one side and the fluorine atoms on the other, this dye has an intrinsic dipole that polarizes the frontier orbitals, see, for example, highest occupied molecular orbital and lowest unoccupied molecular orbital shown in Figure 1. This is a well-known property of push−pull molecules that imparts an ICT when optically excited.

This property is important to excite the molecular crystal because it permits to delocalize the excitation throughout the whole aggregate. When moving from the isolated molecule to the bulk aggregate (Figure 2), we observe both an enhancement and a red shift of the J-band, in agreement with the experimental evidence.[34] Quantitatively speaking, the experimental red shift turns out to be somewhat larger than what predicted here (0.3 eV vs 0.1 eV), but within the expected accuracy of the calculation. The absolute position of the TDDFT peak is red-shifted (by 0.7 eV) compared with the experiment, as expected for Perdew−Burke−Ernzerhof (PBE) (more in Methods). We do not observe the narrowing of J-band reported in the experiments for extended aggregates because in our simulations the width of the peak has been externally fixed.

To dissect the origin of the red shift, we have first considered three dimer arrangements: a longitudinal (D_1) and two stacked dimers (D_2, D_3), whose atomic positions have been extracted from the experimental X-ray structure of the bulk crystal (Figure 1). In Figure 2, the peak D_{11} is red-shifted with respect to the monomer, whereas D_2 and D_3 are blue-shifted. These different behaviors can be understood if we analyze the imaginary part of the induced charge density associated with each peak (from now on with the term induced density we will refer to the imaginary part of the induced charge density). In the frequency domain, the imaginary part of the induced charge density represents the portion of the charge that is dephased by $\pi/2$ with respect to the incident electric field and quantifies the optical absorption.[38,39] Thus, assuming a simple dipolar model of the induced densities, the first absorption peak (D_{11} in Figure 2) of the longitudinal dimer

DOI: 10.1021/acsomega.8b01457
ACS Omega 2018, 3, 10481−10486

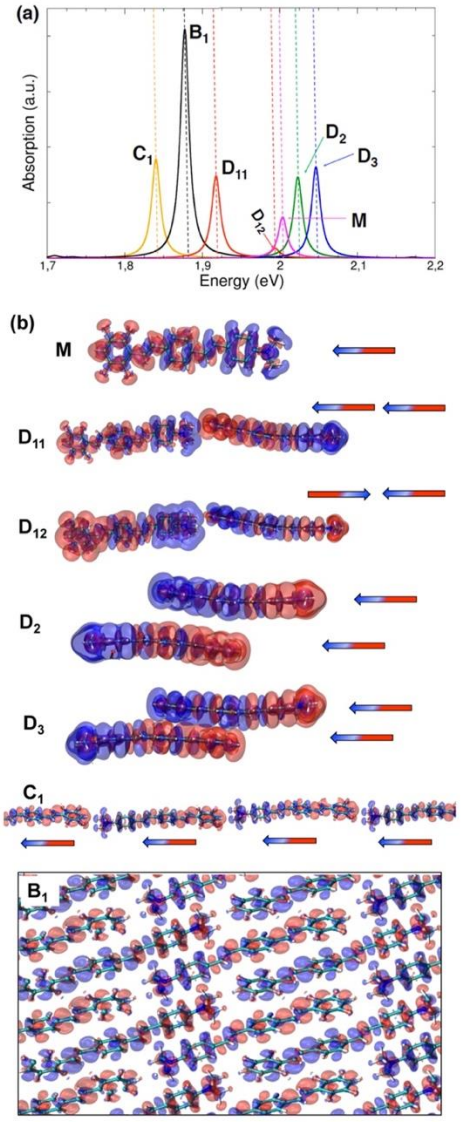

Figure 2. (a) TDDFT optical absorption spectra of bulk crystal (black), monomer (magenta), dimers (red, green, blue), and linear chain (ochre) arrangements taken into account. (b) Induced charge density isosurfaces associated with the different absorption peaks selected in the spectra shown in panel (a). The accompanying arrows represent dipole toy models to get a simplified representation of the interaction between the induced charge densities.

(D_1) is associated with two interacting dipoles in a head−tail configuration.

The origin of the resulting red shift with respect to the isolated monomer is twofold: (i) the coherent Coulomb coupling between the induced charge densities of the two monomers and (ii) the renormalization of single particle energy levels and consequently of the single particle transition energies participating to the total excitation (see Table S.II in section S1 of the Supporting Information). This is due to the ground state Coulomb interaction when monomers are sufficiently close (i.e., in aggregate configuration). In rough terms, the dipole moment of a molecule produces an electric field that acts on those nearby and modifies ground-state properties including single-particle energy levels. These mechanisms contribute to the lowering of the total excitation energy (red shift).

Along the same lines, the induced charge densities of peaks D_2 and D_3 can be modeled as two stacked and horizontal interacting dipoles. In this case, because of the different orientations (i.e., vertically stacked with a slight lateral shift, see section 2 of the Supporting Information for additional pictorial views) of both induced and static dipoles in each monomer, their interaction causes an overall increase in the total excitation energy. In this configurations, the increase of the total excitation energy can be ascribed to the $\pi-\pi$ interactions. In general, the closer the two dimers are in a vertical stacked arrangement, the higher the blue shift is (see peak D_5 in Figure S3 in section 1 of the Supporting Information).

Because the spectra of the isolated dimer configurations extracted from the bulk crystal alone cannot explain the formation of the J-band, we have considered another arrangement that is the periodic version of dimer D_1 (red Figure 1): a polymer chain that represents the limit of the bulk crystal if confined in two directions, that is, a 1D J-aggregate. This configuration was revealed to have a J-band even more red-shifted with respect to the bulk. Again, analyzing the overall induced charge density (peak C_1 in Figure 2), the red shift can be explained, as before, in terms of intra-chain Coulomb couplings. Because in this case the number of aligned monomers is greater than in D_1, both red shift and peak intensity are enhanced. If we consider now the 3D bulk crystal, we observe that the induced charge density of peak B_1 in Figure 2 describes an excitation delocalized along parallel chains and with the same crystal symmetry of peak C_1 in Figure 2. The corresponding peak is slightly blue-shifted with respect to the linear chain. This is due to the stacking interactions in the bulk (peaks D_2, D_3) that cause an increase of the excitation energy (i.e., H-aggregate behavior[18,21]).

In addition to the 1D chain, we considered also a two-dimensional (2D) J-aggregate. This 2D film has been obtained from the bulk crystal extracting a monolayer confined along a direction perpendicular to the long axis (see Figure 3 and

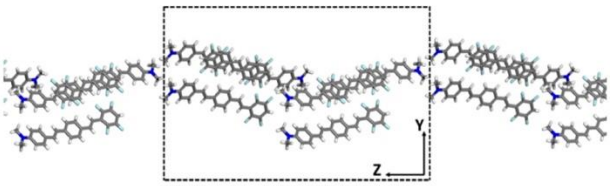

Figure 3. Side view of the monolayer film extracted from bulk crystal and confined in one dimension (Y axis) perpendicular to the long axis (Z axis) of the molecular crystal (dashed lines denote the unit cell boundaries).

appendix B of the Supporting Information). Absorption spectra of bulk and monolayer crystals have been reported in Figure 4, whereas the induced charge densities of their J-bands have been plotted in Figure 5.

From 3D bulk to 2D layer, the energy of the J-band changes by a tiny amount. This can be understood by inspecting the corresponding induced charge densities: the confinement of the film does not influence the bulk J-band which is predominantly a longitudinally excitation oriented along the principal crystal axis. Nevertheless, because of the quantum confinement, new peaks at higher energy emerge in the absorption spectrum of the film. In particular, peak F_3 in Figure

DOI: 10.1021/acsomega.8b01457
ACS Omega 2018, 3, 10481−10486

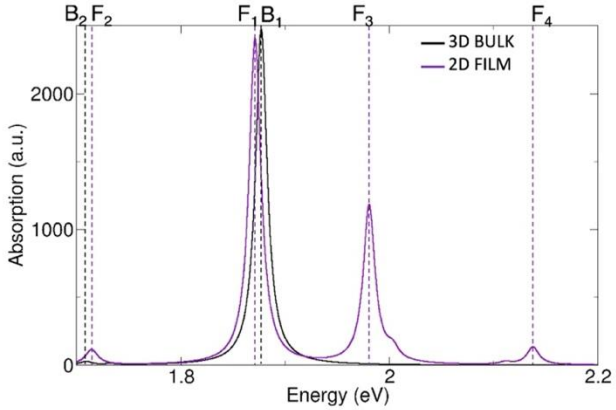

Figure 4. TDDFT optical absorption spectra of J-aggregate bulk crystal and monolayer film extracted from it. B1−2 are peaks of bulk crystal, whereas F1−4 are those of the monolayer film.

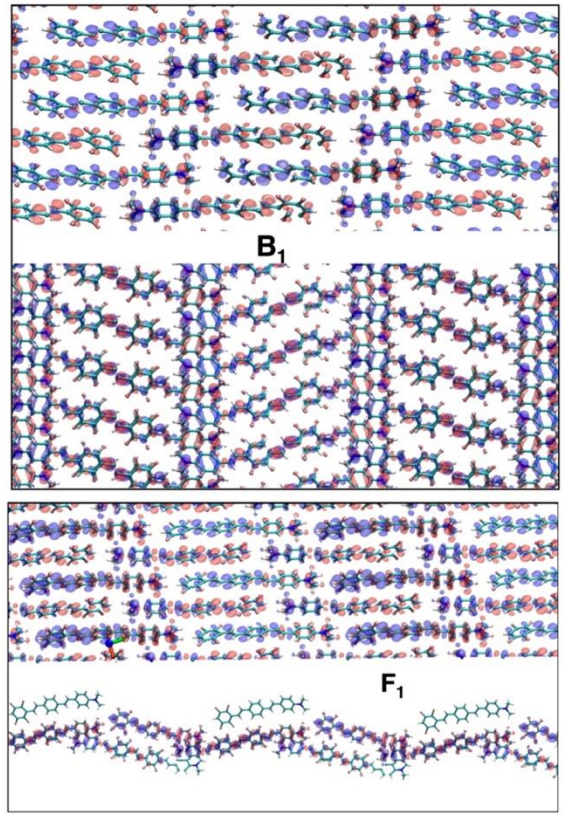

Figure 5. Induced charge densities of the main absorption peaks of Figure 4. (Top panel) Induced charge density of peak B_1 of bulk crystal; (bottom panel) induced charge density of peak F_1 of monolayer film crystal. For each induced charge density, we have plotted two different side views, one is along the plane where both bulk and film are extended and the other along the plane where the film is confined.

4 has an induced density (see Figure S1c in the Supporting Information) whose spatial distribution reflects the broken symmetry of the crystal along the confinement direction. Finally, a small satellite peak (F_2) appears at low energy in the spectrum of the film. This peak is present in the spectrum of the bulk crystal as well (B_2).

By analyzing the induced charge densities of those peaks (see Figure S1a,b in the Supporting Information), we see that because they do not sum up to zero separately in each monomer (i.e., some of the monomers undergo a depletion, others an increase of charge), these small peaks are expected to have a charge-transfer (CT) character. However, because experiments do not detect any other peak at energies lower than the J-band, we conclude that the simulated CT states are misplaced by the limitations of the adopted semilocal xc functional (PBE), which notoriously underestimates CT excited states.[40]

To conclude, our findings presented in this work allow us to answer most of the questions raised in the introduction:

(1) The behavior of the bulk crystal cannot be deduced considering only its isolated components (i.e., monomer and dimers). Instead, the nature of its optical properties is supramolecular, such that the only way to account for all of the many-molecules related effects is to simulate the extended system.

(2) The microscopic nature of the J-band is analyzed by means of the imaginary part of the induced charge density. The typical red-shifted peak (i.e., J-band) of a J-aggregate can be explained in terms of competitions between stacked and longitudinal molecular arrangements. The coherent Coulomb coupling between the induced charge densities of the longitudinal arrangements (i.e., linear chains) contributes to the red shift, whereas out-of-plane stacking interactions contribute to the blue shift. The latter is weaker than the former, and the overall result is the red shift that characterizes the J-band. In addition, the enhancement of the J-band is discussed in terms of a coherent alignment (along the principal crystal axis) of the transition dipole moments of each monomer in the aggregate, resulting in an overall amplified oscillator strength that gives the enhancement of the intensity of the main peak.

(3) We compared the 3D bulk crystal with two kinds of low dimensional J-aggregate crystals: a monolayer 2D film, confined in one dimension, perpendicular to the principal crystal axis; and a linear 1D chain, confined along two dimensions. These systems allowed us to investigate the major effects of quantum confinement in the extended J-aggregate: in the case of the 2D film, the confinement does not break the symmetry of the J-band, but it generates new excitations at higher energies that, due to surface effects, reflect the broken symmetry of the 3D crystal. In the linear 1D chain case, where the bulk is confined in all but the principal crystal axis, the observed red shift of the J-band is even stronger with respect to that of the bulk. This effect is due to the absence of the stacking interaction that contributes to the blue shift of the main absorption peak.

METHODS

The geometries of the push−pull molecular dye and unit cell of the bulk J-aggregate (Figure 1) have been taken from the experimental X-ray structure available in the CCDC no. 961738 (for more details see also the Supporting Information of ref 34) with no further relaxations. These are the only external data that have been used.

All of the supramolecular interactions (i.e., van der Waals, $\pi-\pi$, hydrogen bonds, etc.) that contribute to determine the

DOI: 10.1021/acsomega.8b01457
ACS Omega 2018, 3, 10481−10486

ground-state geometry of the aggregate are implicitly taken into account within the X-ray structure. For the evaluation of the absorption spectra and of the induced charge densities, we have used the Quantum Espresso[41] (QE) suite of codes, based on (time dependent) DFT. In particular, for each system, we have first evaluated the DFT ground state by using the PBE[42] generalized gradient exchange−correlation functional and ultrasoft pseudo-potentials from the PS library.[43] Single-particle wavefunctions (charge density) are expanded in planewaves up to an energy cutoff of 50 Ry (500 Ry).

Only Γ point has been considered for Brillouin zone sampling in the reciprocal space.

The dynamic polarizabilities and the absorption spectra have been simulated by using the turbo-TDDFT code[39,44] of QE, which employs a Liouville−Lanczos superoperator approach for linearized TDDFT.[38] The broadening parameter for each peak has been fixed to 70 meV. The spectra in Figure 2 are normalized following the Thomas−Reiche−Kuhn sum rule in order that the integral over all the frequency range adds up to the total number of electrons per unit cell. For this reason, because in the unit cell of the bulk there are four molecules, its principal peak B_1 is about four times that of the monomer (i.e., M) and about two times the peaks of composite molecules (i.e., D_{11}−D_2−D_3) and linear chain (i.e., C_1) which contain two molecules per unit cell (see section S2 of the Supporting Information). This explains also why the intensity of peak C_1 is about half that of B_1. This same reasoning applies to the Figure 4 where the unit cell of the 2D film has a total of six molecules and its absorption spectrum has a larger underlying area with respect to the bulk one.

We exploited the turbo-TDDFT code also for the calculation of the induced charge densities shown in Figure 2b. For each energy, the code returns three different complex-induced charge densities, one for each independent (orthogonal) polarization of the external exciting electric field, see also ref 45 where the same approach has been used. Here, we focus on optical absorption, so we analyze specifically the imaginary parts of the induced densities.

To obtain a unique induced density for each excitation of the system, we evaluated the one that gives the maximum optical absorption. This happens when external electric field and transition dipole moment are maximally coupled and point in the same direction. To achieve that, we have properly linearly combined the three induced charge densities calculated before (see section S3 of the Supporting Information for a clearer explanation).

To simulate the bulk crystal with QE, we have used a monoclinic unit cell containing four monomers with a total of 192 atoms. The isolated structures (monomer and dimers) obtained from the bulk experimental X-ray data were simulated by exploiting periodically repeated supercells, containing the molecular systems in the central position, separated by adjacent replica with ∼10 Å of vacuum in all spatial directions.

For the low-dimensional structures (polymer chain and monolayer film J-aggregates), we applied the same procedure only for the direction(s) along which the system is confined. The monolayer film unit cell has been obtained by extracting a bidimensional layer from the bulk crystal. With the aid of Materials Studio,[46] we have constructed a supercell and then isolated from it a monoclinic unit cell containing six monomer units (288 atoms) and with ∼10 Å of vacuum along the confinement direction (see section S2 of the Supporting Information for crystal structures and computational details).

■ ASSOCIATED CONTENT

Supporting Information

The Supporting Information is available free of charge on the ACS Publications website at DOI: 10.1021/acsomega.8b01457.

Details of absorption peaks of Figures 2 and 4 and the induced charge densities of the extra peaks B_2, F_2−F_4 in Figure 4; additional information about principal transitions involved in the energy peaks of Figure 2 for monomer and dimer configurations and two additional spectra associated with other two dimer configurations extracted from the bulk crystal with the induced charge densities associated with their principal peaks; additional absorption plot referred to the single monomer where we compared PBE and B3LYP xc-functionals; details about crystal structure characterization and computational details of simulated molecular systems; and post-processing procedure we adopted to obtain the induced charge densities associated with each absorption peak (PDF)

■ AUTHOR INFORMATION

Corresponding Author

*E-mail: stefano.corni@unipd.it.

ORCID

Arrigo Calzolari: 0000-0002-0244-7717

Stefano Corni: 0000-0001-6707-108X

Notes

The authors declare no competing financial interest.

■ ACKNOWLEDGMENTS

The authors thank Prof. Caterina Cocchi of Physics department at Humboldt Universitat Zu-Berlin and Dr. Luca Bursi of Physics and Astronomy department at Rice University Houston (TX) for the useful discussions and the critical reading of the manuscript. This work was partially funded by the European Union under the ERC grant TAME-Plasmons (ERC-CoG-681285).

■ REFERENCES

(1) Jelley, E. E. Spectral Absorption and Fluorescence of Dyes in the Molecular State. *Nature* **1936**, *138*, 1009−1010.

(2) von Berlepsch, H.; Böttcher, C.; Dähne, L. Structure of J-Aggregates of Pseudoisocyanine Dye in Aqueous Solution. *J. Phys. Chem. B* **2000**, *104*, 8792−8799.

(3) Würthner, F.; Kaiser, T. E.; Saha-Möller, C. R. J-aggregates: from serendipitous discovery to supramolecular engineering of functional dye materials. *Angew. Chem., Int. Ed.* **2011**, *50*, 3376−3410.

(4) Egorov, V. V.; Alfimov, M. V. Theory of the J-band: From the Frenkel exciton to charge transfer. *Phys.-Usp.* **2007**, *50*, 985.

(5) Eisfeld, A.; Briggs, J. S. The J-band of organic dyes: lineshape and coherence length. *Chem. Phys.* **2002**, *281*, 61−70.

(6) Eisfeld, A.; Briggs, J. S. The J- and H-bands of organic dye aggregates. *Chem. Phys.* **2006**, *324*, 376−384.

(7) Haverkort, F.; Stradomska, A.; Knoester, J. First-Principles Simulations of the Initial Phase of Self-Aggregation of a Cyanine Dye: Structure and Optical Spectra. *J. Phys. Chem. B* **2014**, *118*, 8877−8890.

(8) Prokhorov, V. V.; Pozin, S. I.; Lypenko, D. A.; Perelygina, O. M.; Mal'tsev, E. I.; Vannikov, A. V. Molecular Arrangements in Two-Dimensional J-Aggregate Monolayers of Cyanine Dyes. *Macroheterocycles* **2012**, *5*, 371−376.

DOI: 10.1021/acsomega.8b01457
ACS Omega 2018, 3, 10481−10486

(9) Prokhorov, V. V.; Pozin, S. I.; Lypenko, D. A.; Perelygina, O. M.; Mal'tsev, E. I.; Vannikov, A. V. AFM Height Measurements of Molecular Layers of a Carbocyanine Dye. *World J. Nano Sci. Eng.* **2011**, *01*, 67−72.
(10) Yao, H.; Kitamura, S.-i.; Kimura, K. Morphology transformation of mesoscopic supramolecular J-aggregates in solution. *Phys. Chem. Chem. Phys.* **2001**, *3*, 4560−4565.
(11) Yao, H. 5 Morphology trasnformations in solutions: dynamic supramolecular aggregates. *Annu. Rep. Prog. Chem., Sect. C: Phys. Chem.* **2004**, *100*, 99−148.
(12) Prokhorov, V. V.; Pozin, S. I.; Perelygina, O. M.; Zolotarevskii, V. I.; Mal'tsev, E. I.; Vannikov, A. V. Polymorphism of 2D monolayer J-aggregates of cyanine dyes. *Inorg. Mater. Appl. Res.* **2017**, *8*, 494−501.
(13) von Berlepsch, H.; Kirstein, S.; Hania, R.; Pugžlys, A.; Böttcher, C. Modification of the Nanoscale Structure of the J-Aggregate of a Sulfonate-Substitued Amphiphilic Carbocyanine Dye through Incorporation of Surface-Active Additives. *J. Phys. Chem. B* **2007**, *111*, 1701−1711.
(14) Kirstein, S.; Daehne, S. J-aggregates of Amphiphilic Cyanine Dyes: Self-Organization of Artificial Light Harvesting Complexes. *Int. J. Photoenergy* **2006**, *2006*, 1−21.
(15) Barford, W.; Marcus, M. Theory of optical transitions in conjugated polymers. I. Ideal systems. *J. Chem. Phys.* **2014**, *141*, 164101.
(16) Marcus, M.; Tozer, O. R.; Barford, W. Theory of optical transitions in conjugated polymers. II. Real systems. *J. Chem. Phys.* **2014**, *141*, 164102.
(17) Spano, F. C.; Yamagata, H. Vibronic Coupling in J-Aggregates and Beyond: A Direct Means of Determining the Exciton Coherence Length from the Photoluminescence Spectrum. *J. Phys. Chem. B* **2011**, *115*, 5133−5143.
(18) Spano, F. C. The Spectral Signatures of Frenkel Polarons in H- and J-Aggregates. *Acc. Chem. Res.* **2010**, *43*, 429−439.
(19) Yamagata, H.; Hestand, N. J.; Spano, F. C.; Köhler, A.; Scharsich, C.; Hoffmann, S. T.; Bässler, H. The red-phase of poly[2-methoxy-5-(2-ethylhexyloxy)-1,4-phenylenevinylene] (MEH-PPV): A disordered HJ-aggregate. *J. Chem. Phys.* **2013**, *139*, 114903.
(20) Yamagata, H.; Spano, F. C. Strong Photophysical Similarities between Conjugated Polymers and J-aggregates. *J. Phys. Chem. Lett.* **2014**, *5*, 622−632.
(21) Paquin, F.; Yamagata, H.; Hestand, N. J.; Sakowicz, M.; Bérubé, N.; Côté, M.; Reynolds, L. X.; Haque, S. A.; Stingelin, N.; Spano, F. C.; Silva, C. Two-dimensional spatial coherence of excitons in semicrystalline polymeric semiconductors: Effects of molecular weight. *Phys. Rev. B: Condens. Matter Mater. Phys.* **2013**, *88*, 155202.
(22) Engelhard, S.; Faisal, F. H. M. Quantum mechanical study of time-dependent energy transfer between perturbers in a Scheibe aggregate. *J. Chem. Phys.* **1999**, *110*, 3596−3605.
(23) Bartnik, E. A.; Blinowska, K. J. Efficient energy transfer in Langmuir-Blodgett monolayers by optimized quantum capture. *Phys. Lett. A* **1989**, *134*, 448−450.
(24) Tame, M. S.; McEnery, K. R.; Özdemir, Ş. K.; Lee, J.; Maier, S. A.; Kim, M. S. Quantum plasmonics. *Nat. Phys.* **2013**, *9*, 329−340.
(25) Pirotta, S.; Patrini, M.; Liscidini, M.; Galli, M.; Dacarro, G.; Canazza, G.; Guizzetti, G.; Comoretto, D.; Bajoni, D. Strong coupling between excitons in organic semiconductors and Bloch surface waves. *Appl. Phys. Lett.* **2014**, *104*, 051111.
(26) Wang, H.; Toma, A.; Wang, H.-Y.; Bozzola, A.; Miele, E.; Haddadpour, A.; Veronis, G.; De Angelis, F.; Wang, L.; Chen, Q.-D.; Xu, H.-L.; Sun, H.-B.; Zaccaria, R. P. The role of Rabi splitting tuning in the dynamics of strongly coupled J-aggregates and surface plasmon polaritons in nanohole arrays. *Nanoscale* **2016**, *8*, 13445−13453.
(27) Todisco, F.; D'Agostino, S.; Esposito, M.; Fernández-Domínguez, A. I.; De Giorgi, M.; Ballarini, D.; Dominici, L.; Tarantini, I.; Cuscuná, M.; Della Sala, F.; Gigli, G.; Sanvitto, D. Exciton-Plasmon Coupling Enhancement via Metal Oxidation. *ACS Nano* **2015**, *9*, 9691−9699.
(28) Zengin, G.; Johansson, G.; et al. Approaching the strong coupling limit in single plasmonic nanorods interacting with J-aggregates. *Sci. Rep.* **2013**, *3*, 3074.
(29) Ferdele, S.; Jose, B.; Foster, R.; Keyes, T. E.; Rice, J. H. Strong coupling in porphyrin J-aggregate excitons and plasmons in nano-void arrays. *Opt. Mater.* **2017**, *72*, 680−684.
(30) DeLacy, B. G.; Miller, O. D.; Hsu, C. W.; Zander, Z.; et al. Coherent Plasmon-Exciton Coupling in Silver Platelet-J-aggregate Nanocomposites. *Nano Lett.* **2015**, *15*, 2588−2593.
(31) Li, J.; Ueno, K.; Uehara, H.; Guo, J.; et al. Dual Strong Couplings Between TPPS J-Aggregates and Aluminum Plasmonic States. *J. Phys. Chem. Lett.* **2016**, *7*, 2786−2791.
(32) Sugawara, Y.; Kelf, T. A.; Baumberg, J. J.; et al. Strong Coupling between Localized Plasmons and Organic Excitons in Metal Nanovoids. *Phys. Rev. Lett.* **2006**, *97*, 266808.
(33) Lekeufack, D. D.; Brioude, A.; Coleman, A. W.; Miele, P.; et al. Core-shell gold J-aggregate nanoparticles for highly efficient strong coupling applications. *Appl. Phys. Lett.* **2010**, *96*, 253107.
(34) Botta, C.; Cariati, E.; Cavallo, G.; Dichiarante, V.; Forni, A.; Metrangolo, P.; Pilati, T.; Resnati, G.; Righetto, S.; Terraneo, G.; Tordin, E. Fluorine-induced J-aggregation enhances emissive properties of a new NLO push-pull chromophore. *J. Mater. Chem. C* **2014**, *2*, 5275−5279.
(35) Zhu, H.; Wang, X.; Ma, R.; Kuang, Z.; Guo, Q.; Xia, A. Intramolecular Charge Transfer and Solvation of Photoactive Molecules with Conjugated Push-Pull Structures. *ChemPhysChem* **2016**, *17*, 3245−3251.
(36) Panja, S. K.; Dwivedi, N.; Saha, S. Tuning the intramolecular charge transfer (ICT) process in push-pull systems: effect of nitro groups. *RSC Adv.* **2016**, *6*, 105786−105794.
(37) Bureš, F. Fundamental aspects of property tuning in push-pull molecules. *RSC Adv.* **2014**, *4*, 58826.
(38) Rocca, D.; Gebauer, R.; Saad, Y.; Baroni, S. Turbo charging time-dependent density-functional theory with Lanczos chains. *J. Chem. Phys.* **2008**, *128*, 154105.
(39) Malcıoğlu, O. B.; Gebauer, R.; Rocca, D.; Baroni, S. turboTDDFT − A code for the simulation of molecular spectra using the Liouville-Lanczos approach to time-dependent density-functional perturbation theory. *Comput. Phys. Commun.* **2011**, *182*, 1744−1754.
(40) Dreuw, A.; Head-Gordon, M. Single-Reference ab initio Methods for the Calculation of Excited States of Large Molecules. *Chem. Rev.* **2005**, *105*, 4009−4037.
(41) Giannozzi, P.; Baroni, S.; Bonini, N.; Calandra, M.; Cavazzoni, C.; et al. QUANTUM ESPRESSO: a modular and open source software project for quantum simulations of materials. *J. Phys.: Condens. Matter* **2009**, *21*, 395502.
(42) Perdew, J. P.; Burke, K.; Ernzerhof, M. Generalized Gradient Approximation Made Simple. *Phys. Rev. Lett.* **1996**, *77*, 3865−3868.
(43) https://dalcorso.github.io/pslibrary/, 2018.
(44) Ge, X.; Binnie, S. J.; Rocca, D.; Gebauer, R.; Baroni, S. turboTDDFT 2.0-Hybrid functionals and new algorithms within time-dependent density-functional perturbation theory. *Comput. Phys. Commun.* **2014**, *185*, 2080−2089.
(45) Bursi, L.; Calzolari, A.; Corni, S.; Molinari, E. Light-induced field enhancement in nanoscale systems from first-principles: the case of polyacenes. *ACS Photonics* **2014**, *1*, 1049−1058.
(46) http://accelrys.com/products/collaborative-science/biovia-materials-studio/, 2018.

DOI: 10.1021/acsomega.8b01457
ACS Omega 2018, 3, 10481−10486

Appendix A - Supporting Information for: Solid-state effects on the optical excitation of push-pull molecular J-aggregates by first principles simulations

2.2 Appendix A1 - Response charge densities and optical spectra

The complete analysis of the response charge density and of the optical spectra for the systems discussed in the main text is collected in Figure A1 and A2, respectively. Red-blue colors in Fig. A1 indicates the positive-negative sign of the response charge densities.

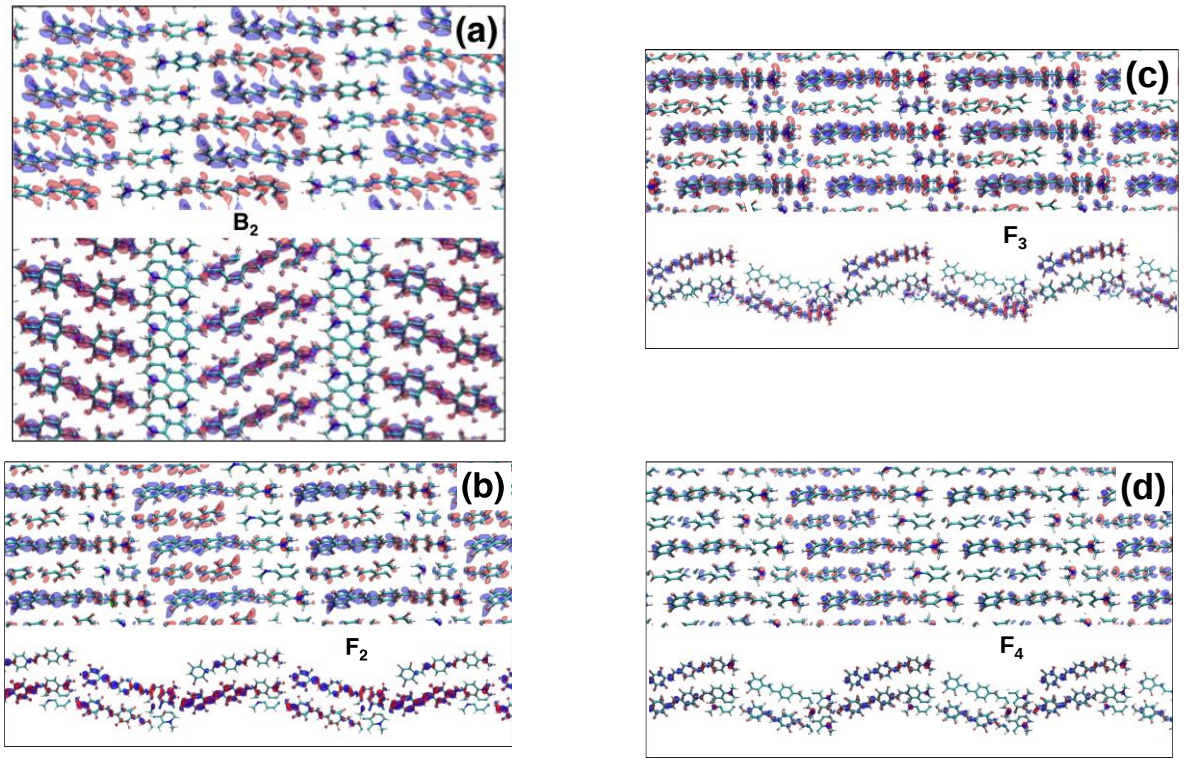

Figure A1 – (a) Imaginary part of induced charge density peak B2 of 3D bulk crystal. (b-d) Imaginary parts of induced charge densities of peaks F2-F4 of 2D film crystal. For each induced charge density we have plotted two different side-views, one along the plane where both 3D bulk and 2D film are extended and the other along the plane where the film is confined. All induced charge density isosurfaces are fixed at 0.1 Bohr $^{-3}$.

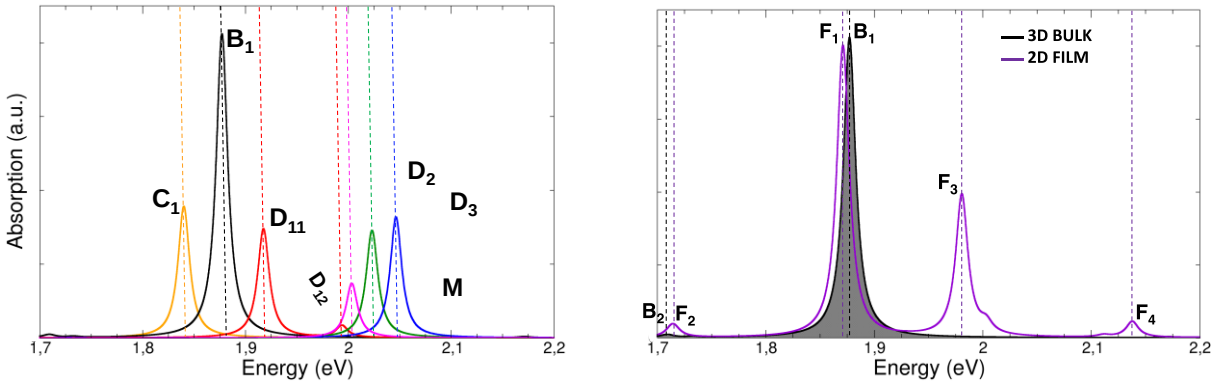

Figure A2 – Absorption optical spectra of 3D bulk (black), 2D film (violet), 1D chain (ochre), dimers (red, blue, green) and monomer (magenta) extracted from the 3D bulk crystal.

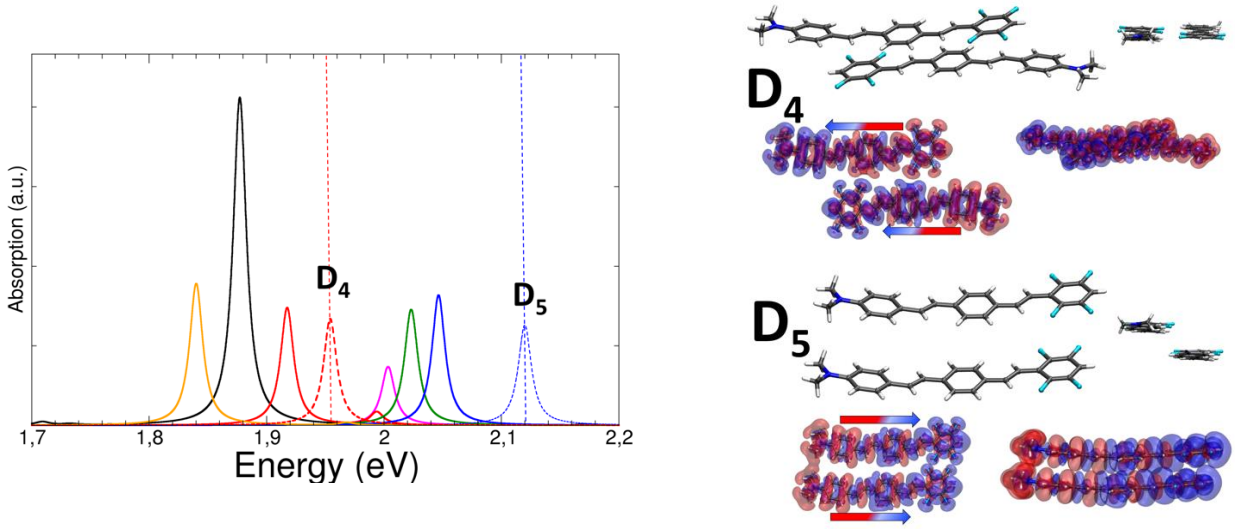

Figure A3 – (Left) Absorption optical spectra of other two dimer configurations extracted from the bulk crystal. The new spectra have been plotted in dashed lines. (Right) Spatial arrangements of new dimers with the associated induced charge densities associated to the absorption peaks D4 and D5. The values of the isosurface plots have been fixed to 0.05 Bohr $^{-3}$.

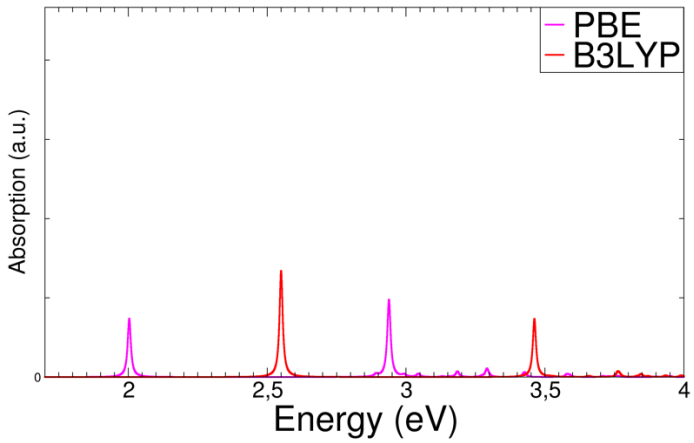

Figure A4 – Comparison of absorption optical spectra of single push-pull monomer using two different xf-functionals: PBE and B3LYP. The hybrid functional gives a blue-shift with respect to the semi-local PBE of ~0.55 eV for the first two principal peaks

TABLE A.1

	Peak energy (eV)		Oscillator strength		Homo – Lumo gap (eV)
Monomer	M 2		1.537		1.667
Dimer 1	D_{11} 1.918	D_{12} 1.994	3.153	0.331	1.442
Dimer 2	D_2 2.023		2.981		1.693
Dimer 3	D_3 2.047		3.282		1.635
1D chain	C_1 1.841	C_2 1.968	3.95	0.0725	1.636
2D film	F_1 1.87	F_2 1.71	7.821	0.24	1.5
	F_3 1.98	F_4 2.138	3.912	0.27	
3D bulk	B_1 1.887	B_2 1.71	7.96	0.08	1.567

TABLE A.2

	Peak energy	Transitions (occ →vir)	Tran. amplitude
Monomer	2 eV (M)	H → L (1.66 eV) H-1 → L (2.607 eV) H → L + 1 (2.637 eV)	0.96 -0.19 0.21
Dimer 1	1.918 eV (D_{11})	H-2 → L (2.394 eV) H-1 → L (1.605 eV) H → L+1 (1.642 eV) H-1 → L+2 (2.598 eV)	-0.15 -0.84 -0.48 -0.18
	1.994 eV (D_{12})	H-3 → L (2.577 eV) H-2 → L+1 (2.594 eV) H-1 → L (1.605 eV) H-1 → L+2 (2.598 eV) H → L+1 (1.642 eV) H → L+3 (2.623 eV)	-0.123 -0.181 -0.464 -0.122 0.828 -0.2
Dimer 2	2.023 eV (D_2)	H-1 → L (1.694 eV) H-1 → L+1 (1.698 eV) H → L+1 (1.697 eV) H-2 → L (2.615 eV) H-1 → L+2 (2.654 eV) H → L (1.693 eV)	0.84 0.34 -0.26 -0.17 -0.17 -0.14
Dimer 3	2.047 eV (D_3)	H-1 → L (1.703 eV) H → L+1 (1.754 eV) H-3 → L (2.706 eV) H-2 → L+1 (2.57 eV) H-1 → L+2 (2.698 eV) H → L+3 (2.646 eV)	0.59 -0.76 -0.17 -0.128 0.13 0.13

2.3 Appendix A2 – Structural and crystal characterizations

We report here the unit cells of 3D bulk, 2D film and 1D chain, dimers and monomer extracted from the bulk crystal.

3D bulk

Primitive cell parameters:

- Lattice type : *monoclinic*
- Crystal lengths (Å) : X = 7,59 Y = 5,87 Z = 41,51
- Angles (degrees) : α (XY) = 90,00° β (ZX) = 94,30° γ (YZ) = 90,00°

Computational parameters:

- Number of atoms = 192
- Number of electrons = 592
- Kinetic energy cut-off = 50 Ry
- Charge density cut-off = 500 Ry
- Exchange-correlation = PBE

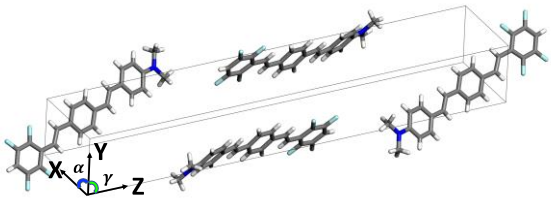

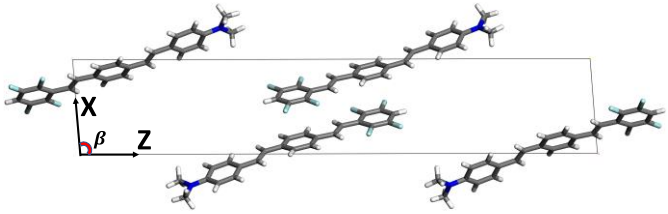

2D film

Primitive cell parameters:

- Lattice type : *monoclinic*
- Crystal lengths (Å) : X = 7,59 Y = 26,64 Z = 43,12
- Angles (degrees) : α (XY) = 90,00° β (ZX) = 73,74° γ (YZ) = 90,00°

Computational parameters:

- Number of atoms= 288
- Number of electrons= 888
- Kinetic energy cut-off = 50 Ry
- Charge density cut-off = 500 Ry
- Exchange-correlation = PBE

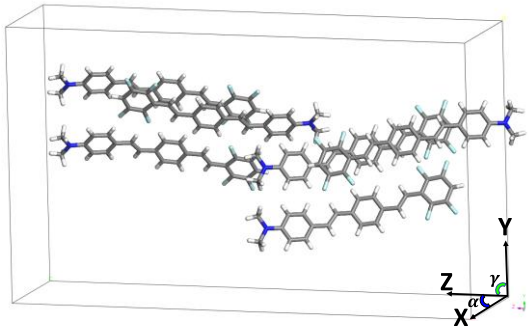

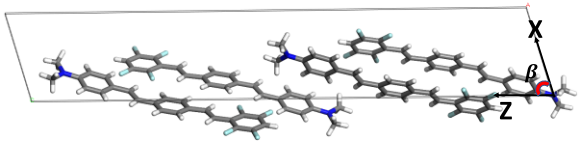

1D chain

Primitive cell parameters:

- Lattice type : *orthorombic*
- Crystal lengths (Å) : X = 16,90 Y = 16,90 Z = 43,12
- Angles (degrees) : α (XY) = 90,00° β (ZX) = 90,00° γ (YZ) = 90,00°

Computational parameters:

- Number of atoms= 96
- Number of electrons= 296
- Kinetic energy cut-off = 50 Ry
- Charge density cut-off = 500 Ry
- Exchange-correlation = PBE

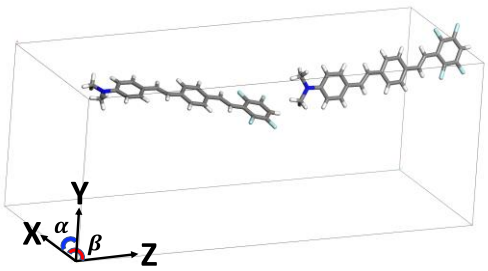

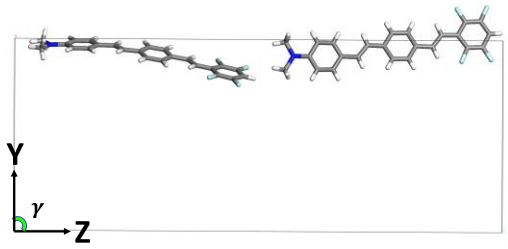

Dimer 1

Primitive cell parameters:

- Lattice type : *orthorombic*
- Crystal lengths (Å) : X = 31,75 Y = 24,77 Z = 56,22
- Angles (degrees) : α (XY) = 90,00° β (ZX) = 90,00° γ (YZ) = 90,00°

Computational parameters:

- Number of atoms= 96
- Number of electrons= 296
- Kinetic energy cut-off = 50 Ry
- Charge density cut-off = 500 Ry
- Exchange-correlation = PBE

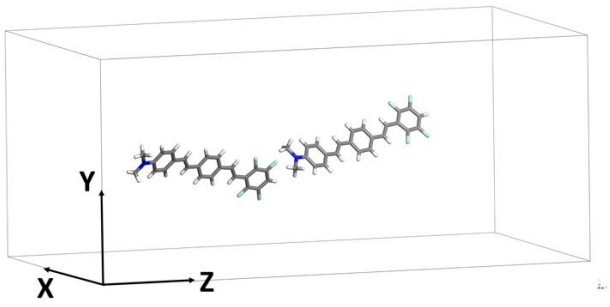

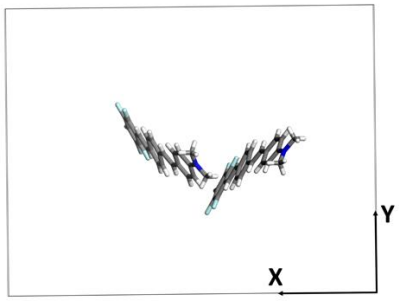

Dimer 2

Primitive cell parameters:

- Lattice type : *orthorombic*
- Crystal lengths (Å) : X = 26,02 Y = 22,33 Z = 36,75
- Angles (degrees) : α (XY) = 90,00° β (ZX) = 90,00° γ (YZ) = 90,00°

Computational parameters:

- Number of atoms= 96
- Number of electrons= 296
- Kinetic energy cut-off = 50 Ry
- Charge density cut-off = 500 Ry
- Exchange-correlation = PBE

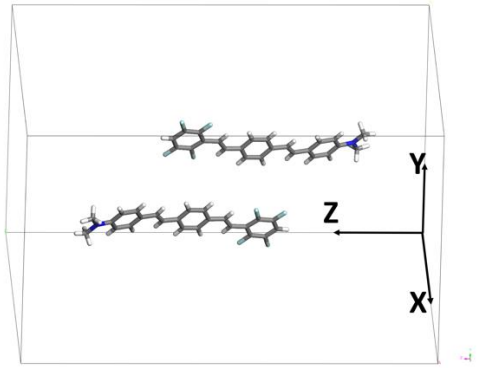

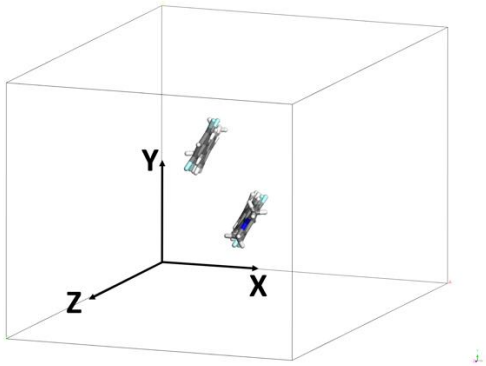

Dimer 3

Primitive cell parameters:

- Lattice type : *orthorombic*
- Crystal lengths (Å) : X = 36,75 Y = 17,83 Z = 36,75
- Angles (degrees) : α (XY) = 90,00° β (ZX) = 90,00° γ (YZ) = 90,00°

Computational parameters:

- Number of atoms= 96
- Number of electrons= 296
- Kinetic energy cut-off = 50 Ry
- Charge density cut-off = 500 Ry
- Exchange-correlation = PBE

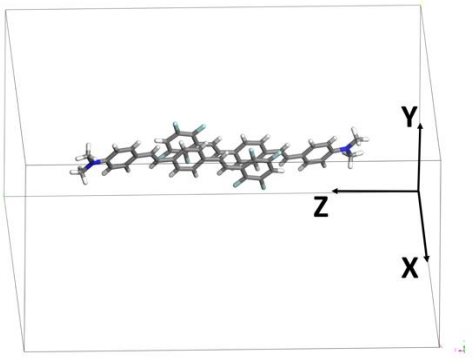

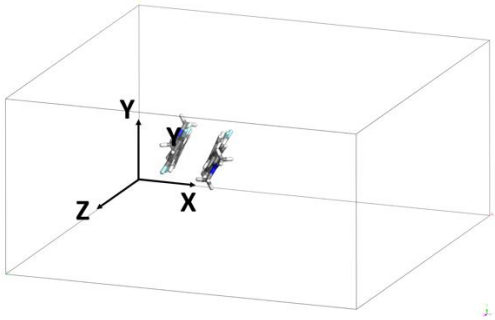

Monomer

Primitive cell parameters:

- Lattice type : *orthorombic*
- Crystal lengths (Å) : X = 27,52 Y = 27,52 Z = 40,18
- Angles (degrees) : α (XY) = 90,00° β (ZX) = 90,00° γ (YZ) = 90,00°

Computational parameters:

- Number of atoms= 48
- Number of electrons= 148
- Kinetic energy cut-off = 50 Ry
- Charge density cut-off = 500 Ry
- Exchange-correlation = PBE

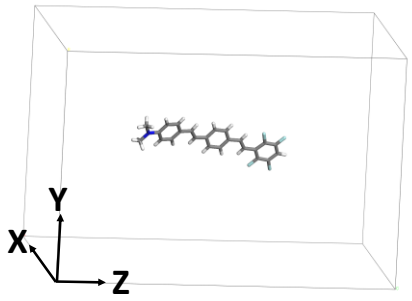

2.4 Appendix A3– Evaluation of the response charge density

In this section we will explain the post-processing procedure we have used in order to get the induced charge densities for each peak. Firstly, we have performed three independent excitations with three (orthogonal) electric field linear polarizations of frequency ω

$$E^i_{ext,P}(\omega) = E_0(\omega)\delta^i_P \tag{A.1}$$

where index *P=x,y,z* fixes direction of external electric field polarization, index *i* refers to electric field *i*-th component and δ^i_j is delta Kronecker symbol. Since we are in dipolar regime, we have assumed uniform electric field. Using linear response theory in space-frequency domain, for each specific polarization direction *P*, one gets a different induced charge density, namely

$$n_P(\boldsymbol{r},\omega) = \int \varphi_{ext,P}(\boldsymbol{r}',\omega)\chi(\boldsymbol{r},\boldsymbol{r}',\omega)d\boldsymbol{r}' = -\int r'_i E^i_{ext,P}(\omega)\chi(\boldsymbol{r},\boldsymbol{r}',\omega)d\boldsymbol{r}' = -E_0(\omega)\int r'_P\chi(\boldsymbol{r},\boldsymbol{r}',\omega)d\boldsymbol{r}' \tag{A.2}$$

where repeated indices are implicitly summed and χ is the polarizability causal response function.
Since we want to plot a unique induced charge density, we decided to evaluate the one which gives the maximum absorption for a certain peak or, in other words, the one whose transition dipole moment is oriented along the direction of the external field. In order to do that, we have applied a simple post-processing procedure by linearly combining the three induced charge densities obtained in (A.2). From the knowledge of the induced charge density (A.2) one can evaluate the induced dipole moment for a certain field polarization *P* in the following way

$$d_{i,P}(\omega) = \int n_P(\boldsymbol{r},\omega)r_i d\boldsymbol{r} = -\int r_i r_j \chi(\boldsymbol{r},\boldsymbol{r}',\omega)E^j_{ext,P}(\omega)d\boldsymbol{r}'d\boldsymbol{r} = \alpha_{ij}(\omega)E^j_{ext,P}(\omega) \tag{A.3}$$

$$\alpha_{ij}(\omega) = -\int r_i r'_j \chi(\boldsymbol{r},\boldsymbol{r}',\omega)d\boldsymbol{r}'d\boldsymbol{r} \tag{A.4}$$

where (A.4) is the so called dynamic polarizability tensor. Since the induced dipole (A.3) is a functional of the induced charge density, its magnitude and orientation depend on the external field polarization also. By diagonalizing (A.4), one can get the special directions along which the induced dipole has the same orientation of the external applied field. These special directions are the eigenvectors of the polarizability tensor and are an intrinsic property of the system. The spectral decomposition of the polarizability tensor (A.4) is

$$\alpha_{ij}(\omega) = -\sum_\xi d^\xi_i \left(d^\xi_j\right)^* \left[\frac{1}{\omega-\omega_\xi+i\eta} - \frac{1}{\omega+\omega_\xi+i\eta}\right] \tag{A.5}$$

where index ξ refer to an electronic many-body excited state of the system, ω_ξ is the excitation energy from ground state to excited state ξ and d^ξ_i is the i-th component of the transition dipole moment from ground state to excited state ξ. We can give a more compact representation of expression (A.5) by using a matrix notation

$$\bar{\bar{\alpha}}(\omega) = W\Lambda W^{-1} = \sum_\xi \boldsymbol{w}^\xi \left(\boldsymbol{w}^\xi\right)^\dagger \lambda_\xi(\omega) \tag{A.6}$$

$$w_i^{\xi} = \frac{\langle \xi | \hat{\Psi}^{\dagger}(\boldsymbol{r}) \hat{r}_i \hat{\Psi}(\boldsymbol{r}) | 0 \rangle}{\sqrt{\sum_{i=x,y,z} \left| \langle \xi | \hat{\Psi}^{\dagger}(\boldsymbol{r}) \hat{r}_i \hat{\Psi}(\boldsymbol{r}) | 0 \rangle \right|^2}} = \frac{d_i^{\xi}}{\|d^{\xi}\|^2} \tag{A.7}$$

$$\lambda_{\xi}(\omega) = \|d^{\xi}\|^2 \left[\frac{1}{\omega - \omega_{\xi} + i\eta} - \frac{1}{\omega + \omega_{\xi} + i\eta} \right] \tag{A.8}$$

where Wmatrix contains column by column the normalized eigenvectors $\boldsymbol{w}^{\xi}$with components (A.7), which gives the normalized direction of the transition dipole moment associate to excited state ξ, while diagonal matrix Λ contains the associated eigenvalue λ_{ξ} that is frequency dependent. If one assumes that the excitation energies are well separated, when in proximity of a certain peak of energy ω_{ξ} there is a dominant pole in (A.5) and the response is dominated by the imaginary part of the polarizability tensor evaluated at the energy $\omega = \omega_{\xi}$. Each peak has associated a normalized eigenvector (A.8) whose components are the weights we can use to combine our induced charge densities in (A.2) in order to get the one which gives the maximum absorption at the selected peak at frequency ω_{ξ}. At the end we obtain our final density as

$$n(\boldsymbol{r}, \omega_{\xi}) = w_x^{\xi} n_x(\boldsymbol{r}, \omega_{\xi}) + w_y^{\xi} n_y(\boldsymbol{r}, \omega_{\xi}) + w_z^{\xi} n_z(\boldsymbol{r}, \omega_{\xi}) \tag{A.9}$$

TABLE A.3

Peak (ξ)	weights w_i^{ξ}
M	(0.335, -0.187, 0.923)
D_{11}	(0.341, -0.06, 0.938)
D_{12}	(0.319, 0.293, 0.887)
D_2	(0.344, 0.173, 0.923)
D_3	(0.386, 0.186, 0.904)
C_1	(-0.011, 0.037, 0.999)
C_2	(0, 0.035, 0.999)
B_1	(0.276, 0, 0.961)
B_2	(0.278, 0, 0.954)
F_1	(0.255, 0.967, 0.014)
F_2	(0.34, 0.929, -0.003)
F_3	(0.259, 0.965, -0.03)
F_4	(0.313, 0.946, -0.042)

Chapter III – Investigating J-aggregates by first-principles: MBPT approach

In this chapter we shall present the results of Many-Body-Perturbation-Theory (MBPT) first-principles simulations on the push-pull J-aggregate molecular system studied in the previous chapter by a TDDFT approach. Simulations have been carried out by Yambo[96] and MOLGW[100] codes. This latter work has been done in collaboration with Prof. Caterina Cocchi of Department of Physics at Humboldt University in Berlin, where I spent three months as a Ph.D. visiting student, with Dr. Daniele Varsano of CNR Nanoscience Institute in Modena, as well as with my personal advisors cited before. The study has been also supported by an HPC-Europa 3 and a DAAD project grants which I have benefited from.

As second step of this work we explicitly focused on the investigation and characterization of the excitonic properties of the J-band, which – as described in the first Chapter – are particular relevant for applications. In order to pursue this issue, we considered alternative simulation approaches (with respect to the already mentioned TDDFT), that allowed us to have a direct insight into the correlated two-particle nature of optical excitations. In particular, we adopted the so called many-body-perturbation-theory (MBPT) approach that has been motivated by the need to use a higher level of methodology and accuracy to assess the microscopic character of the excitations forming the J-band and to go beyond the TDDFT qualitative description we presented in the previous part. The latter, since we adopted a semi-local exchange-correlation (xc) functional[82] (PBE[101]), has a low accuracy in describing electron-hole correlation (i.e, exchange and correlation effects) and notoriously misses a correct description of long range and non-local solid-state effects[102–105] (i.e., van der Waals, charge transfer effects, etc.).

In the following section we shall discuss the main results of the MBPT simulations with a thorough and detailed analysis on the collective character of the optical excitations of the push-pull J-aggregate. In particular, we address the role of the molecular packing and of the interplay between intra- and inter-molecular interactions in influencing the electronic and optical properties of the systems, including the

intensity and character of the excitations within the J-band. These questions are particularly relevant in the broad context of optical properties of organic crystals, where already in case of non-polar molecules, there is a persistent debate regarding the nature of the excitations. To do so, we perform a first-principles study, based on density-functional theory (DFT) and MBPT, on the J-aggregate and, for comparison, on its molecular constituent. With the analysis of the quasi-particle electronic structure and optical absorption spectra including excitonic effect, we characterize the excited states with unprecedented insight, that contributes to the understanding the nature of collective excitations in molecular crystals.

The MBPT computational framework is implemented by codes such as Yambo[96] and MOLGW[100]. We used the former, which is a plane wave code, to simulate the extended molecular J-aggregate and the latter, based on localized basis sets, to simulate the isolated push-pull monomer extracted from the bulk crystal.

The main findings are: (1) *J-band* is indeed composed of a rich structure of excited states where the most intense excitation giving rise to the strong absorption peak is associated to a mixed intra- and inter-molecular charge transfer exciton. The latter comes out from the combination between push-pull behavior (intra-molecular CT) of the single molecules and the particular dense molecular packing (inter-molecular CT) that favors the electron delocalization around the neighboring molecules. Simulations reveal also the presence of dark electronic excitations within the *J-band* manifesting a complete charge-transfer behavior where electrons are completely transferred on the neighboring molecules. With the latter result we show that the MBPT approach is indeed able to correctly detect excited states which, being dark, could not be in conventional absorption experiments.

(2) The complex mechanisms ruling the optical properties of these molecular aggregates cannot be unveiled based solely on simple models, but require a higher level of theory. With the explicit inclusion of electron-hole correlation one is capable to give a better description of collective effects and to provide a robust and insightful characterization of the excitations of the system.

In the following we put the results in the form of a drafted paper that we submitted for publication in scientific international journal.

3.1 Interplay between intra- and inter-molecular charge transfer in the optical excitations of organic push-pull J-aggregates

Michele Guerrini[1,2,3], Caterina Cocchi[3], Arrigo Calzolari[2], Daniele Varsano[2] and Stefano Corni[2,4]

[1]*Dipartimento FIM, Università di Modena e Reggio Emilia, Italy*

[2]*CNR Nano Istituto Nanoscienze, Centro S3, Modena, Italy*

[3]*Department of Physics and IRIS Adlershof, Humboldt Universität zu-Berlin, Berlin, Germany*

[4]*Dipartimento di Scienze Chimiche, Università di Padova, Italy*

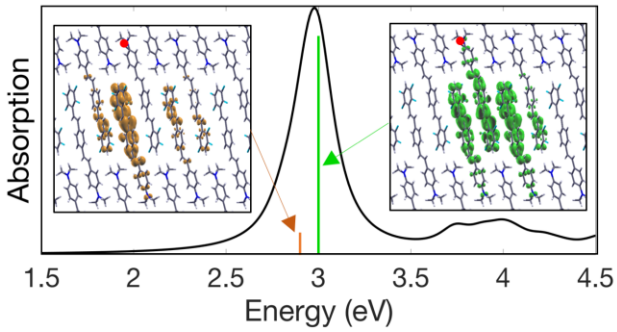

ABSTRACT – In a first-principles study based on density-functional theory and many-body perturbation theory, we address the interplay between intra- and inter-molecular interactions in a J-aggregate formed by push-pull organic dyes by investigating its electronic and optical properties. We find that the most intense excitation dominating the spectral onset of the aggregate, i.e., the J-band, exhibits a combination of intra-molecular charge transfer, coming from the push-pull character of the constituting dyes, and of inter-molecular charge-transfer, due to the dense molecular packing. We also show the presence within the J-band, of a pure inter-molecular charge-transfer excitation which is expected to play a relevant role in the emission properties of the J-aggregate. Our results shed light into the microscopic character of optical excitations of J-aggregates and offer new perspectives to further understand the nature of collective excitations in organic semiconductors.

KEYWORDS – *excitons, organic semiconductors, push-pull dye, density-functional theory, many-body perturbation theory*

INTRODUCTION

J-aggregates are a special class of molecular crystals with enhanced light-matter interaction properties[1–5]. Their optical spectra are dominated by a very strong and narrow peak at the onset – the so-called J-band –, which appears at lower energy with respect to the isolated molecular constituents[6–10]. This peculiar feature emerges as a collective effect of the monomers in the aggregated phase and is typically explained in terms of coherent inter-molecular dipole coupling[6,8,9,11,12]. The microscopic nature and the fundamental mechanisms which give rise to the J-band are still debated[6]. The situation is even more complex in case of J-aggregates formed by polar molecules like push-pull organic dyes. In this case intra-molecular charge transfer adds up to the aforementioned inter-molecular interactions that are responsible for the formation of the J-band. An example of this kind of system is the J-aggregate formed by the organic chromophore 4-(N,N-dimethyl-amino)-4-(2,3,5,6-tetra-fluorostyryl)-stilbene ($C_{24}H_{19}F_4N$) which has been recently proposed and synthesized by Botta et al.[13] Some of the authors of this work recently investigated this J-aggregate by means of time-dependent density-functional theory (TDDFT) showing that its optical behavior cannot be deduced by considering only its isolated components due to the intrinsically supramolecular nature of its optical response[14]. On the other hand, the character of the excitations forming the J-band and the interplay between inter- and intra-molecular interactions still needs to be addressed. This issue is relevant in the broader context of electronic-structure characterization of molecular crystals. Even in case of non-polar molecules, the discussion regarding the nature of optical excitations in organic semiconductors[15–19] is still on-going. Both localized Frenkel excitons and delocalized intermolecular excitations can appear at the spectral onset of organic semiconductors: Their relative energetic position has been rationalized in terms of intermolecular interactions and wave-function overlap[19]. Identifying the character of the lowest-energy excitations in molecular crystals is particularly relevant to interpret phenomena like multiple exciton generation and singlet fission that have been recently observed in these systems[20–32] and that promise a breakthrough in view of opto-electronic applications Addressing this question from a theoretical perspective requires a high-level methodology that incorporates a reliable description of the electronic structure and excitations including electron-electron and electron-hole (e-h) correlation effects.

Many-body perturbation theory (MBPT), based on the *GW* approximation and the solution of the Bethe-Salpeter equation, is the state-of-the-art approach to investigate optical excitations in crystalline materials. In the last two decades it has been successfully applied also to molecular systems, providing unprecedented understanding on the character of the excitations therein[15–19,33–39]. Many of these studies are focused on oligoacenes[15,16,19,35] which have drawn particular attention since the last years of the past

century for their appealing opto-electronic and transport properties[40–47]. The first-principles works cited above have revealed that the low-energy excitations in these materials exhibit remarkable excitonic character, with binding energies of the order of a few hundred of meV and an intermixed Frenkel-like and intermolecular *charge-transfer* (CT) character. Intermolecular interactions generally play a decisive role in the optical properties of a variety of molecular aggregates[48,49]. For example, in azobenzene-functionalized self-assembled monolayers intermolecular interactions impact strongly on light-absorption and excitonic coupling, and hence critically influence the photo-isomerization process[50–53]. In these systems, intermolecular coupling and packing effects have been shown to be crucial also in core excitations[54].

In this work, we adopt the formalism of MBPT to investigate the nature of the excitations in a J-aggregate formed by $C_{24}H_{19}F_4N$ dyes (Fig. 1), devoting specific attention to the interplay between intra- and inter-molecular charge transfer. MBPT calculations are carried on top of density-functional theory (DFT) on the J-aggregate and, for comparison, also on its isolated molecular unit. With the analysis of the quasi-particle electronic structure and the optical absorption spectra including excitonic effects, we characterize the excited states of this J-aggregate with unprecedented insight. Specifically, we focus on two excited states with different character appearing within the J-band: the first one gives rise to the main peak of the J-band and manifests a mixed intra- and inter-molecular charge transfer nature;

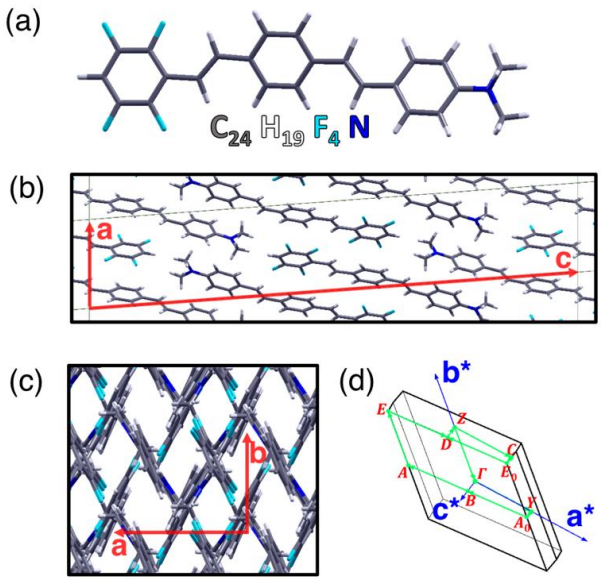

Figure 1 – (a) Push-pull organic dye 4-(N,N-dimethyl-amino)-4-(2,3,5,6-tetra-fluorostyryl)-stilbene ($C_{24}H_{19}F_4N$) and its J-aggregate viewed (b) from the a-c plane and (c) from the a-b plane, with the lattice vectors marked in red; crystallographic structure from CCDC No. 961738 and *Ref[13]. (d) Brillouin Zone associated to the unit cell of the J-aggregate with the reciprocal lattice vectors indicated in blue, the high-symmetry points highlighted in red and the path chosen for the band-structure plot marked in green.*

the second one is a very weak excited state possessing a dominant inter-molecular CT behavior. This analysis demonstrates how the interplay between intra and inter-molecular charge transfer determines the optical properties in a molecular J-aggregate and contributes to the more general understanding of the nature of collective excitations in molecular crystals.

METHODS

THEORETICAL BACKGROUND – This study is based on DFT[55,56] and MBPT (the *GW* approximation and the Bethe-Salpeter equation)[57–59]. The workflow adopted to calculate electronic and optical properties proceeds through three steps: First, a DFT calculation is performed to compute KS single-particle energies and wavefunctions as a basis in the successive steps; Next, the quasiparticle (QP) correction to the KS energies is calculated through a single-shot GW calculation[57,58,60] and finally the Bethe-Salpeter equation (BSE) is solved to obtain optical absorption spectra together with excitonic eigenfunctions and eigenenergies[57]. This approach ensures state-of-the-art accuracy methods in the calculation of excited-state properties and, concomitantly, quantitative insight into the character of the excitations.

In solving the Bethe-Salpeter equation we adopt the Tamm-Dancoff approximation[57] consisting in diagonalizing an effective excitonic Hamiltonian:+

$$\widehat{H}_{ex} = \sum_{c\boldsymbol{k}} \epsilon_{c\boldsymbol{k}} a^{\dagger}_{c\boldsymbol{k}} a_{c\boldsymbol{k}} - \sum_{c\boldsymbol{k}} \epsilon_{v\boldsymbol{k}} b^{\dagger}_{v\boldsymbol{k}} b_{v\boldsymbol{k}} + \sum_{\substack{vc\boldsymbol{k} \\ v'c'\boldsymbol{k}'}} \left(2\bar{v}^{vc\boldsymbol{k}}_{v'c'\boldsymbol{k}'} - W^{vc\boldsymbol{k}}_{v'c'\boldsymbol{k}'}\right) a^{\dagger}_{c\boldsymbol{k}} b^{\dagger}_{v\boldsymbol{k}} b_{v'\boldsymbol{k}'} a_{c'\boldsymbol{k}'} \qquad (1)$$

where the index v (c) indicates valence (conduction) bands, $\boldsymbol{k}$ and $\boldsymbol{k}'$ are wave-vectors in the first BZ, and $a^{\dagger}$ (a) and $b^{\dagger}$ (b) are creation (annihilation) operators for electrons and holes, respectively. The quasi-particle energies $\epsilon_{c\boldsymbol{k}}$ and $\epsilon_{v\boldsymbol{k}}$ are obtained from the *GW* step. The matrix elements of $\bar{v}$, which is the short-range unscreened Coulomb interaction and of W , the statically screened Coulomb interaction, represent the exchange and direct part of the BSE Hamiltonian of Eq. (1) and are expressed as $\bar{v}^{vc\boldsymbol{k}}_{v'c'\boldsymbol{k}'} = \langle ck, v'k'|\bar{v}|vk, c'k'\rangle$ and $W^{vc\boldsymbol{k}}_{v'c'\boldsymbol{k}'} = \langle ck, v'k'|W|c'k', vk\rangle$, respectively. The latter takes into account the screened electron-hole interaction (i.e. excitonic effects), while the former is responsible for crystal local-field effects (the factor 2 derives from spin summation in the singlet channel). Note that the potential $\bar{v}$ is a modified Coulomb interaction defined as the bare Coulomb interaction without the long range contribution (i.e., $\lim_{\boldsymbol{q}\to 0} \bar{v}_{G=0}(\boldsymbol{q}) = 0$ in reciprocal space)[61]. As a measure of local field collective effects for a certain excited eigenstate $|\lambda\rangle$ of the excitonic Hamiltonian (1) with excitation energy E^{λ}, we define the e-h *exchange energy* $E^{\lambda}_{x} = \sum_{\substack{vck \\ v'c'k'}} A^{\lambda}_{vc\boldsymbol{k}} \left(A^{\lambda}_{v'c'\boldsymbol{k}'}\right)^{*} \bar{v}^{vc\boldsymbol{k}}_{v'c'\boldsymbol{k}'}$, where $A^{\lambda}_{vc\boldsymbol{k}}$ are the BSE coefficients of

eigenstate $|\lambda\rangle$. When the total excitation energy E^{λ} is below the QP gap, i.e., $E^{\lambda} - E_{GW}^{gap} < 0$, the excited state $|\lambda\rangle$ is considered as a bound exciton with a binding energy defined as $E_b = E_{GW}^{gap} - E^{\lambda}$ which physically represents the energy required to separate a bound electron-hole (e-h) pair into a free electron and a free hole.

COMPUTATIONAL DETAILS – The monomer unit has been extracted from the bulk J-aggregate molecular crystal structure and subsequently relaxed to its equilibrium structure with the Gaussian package[62] using *cam-b3lyp*[63] xc-functional until the forces were smaller than 10^{-6} Hartree/Bohr. For this purpose, a localized Gaussian basis *cc-pVTZ* adopting the frozen core approximation was employed. To investigate the electronic and optical properties of the gas-phase push-pull dye we adopted the MOLGW[64] code implementing DFT and MBPT using localized basis orbitals. These DFT calculations were carried out using *cam-b3lyp*[63]. Single-shot G_0W_0 calculations were performed to compute the QP correction and the BSE was solved in the Tamm-Dancoff approximation (TDA) over a transition space of 50 occupied and 100 unoccupied orbitals.

The J-aggregate crystal structure has been taken from Ref.[13] (*CCDC No.* 961738) without any further structural relaxation. DFT calculations were performed with the Quantum Espresso package[65] using the semi-local PBE[66] xc functional and treating core electrons with a norm conserving pseudo-potential[67]. *GW* and BSE calculations are subsequently performed by using the Yambo[68] code. QP corrections were calculated adopting the *Godby-Needs* plasmon pole model[69] to approximate the frequency dependency of the inverse dielectric function. Since the GW QP corrections revealed to be constant for all the KS states around the gap, in building the BSE Hamiltonian (Eq. 1) we have applied a scissor operator with stretching correction for all the energies within the irreducible BZ (scissor $E_{g,GW} - E_{g,DFT} = 1.73$ eV and stretching factors $S_v = 1.258$, $S_c = 1.216$ for occupied and unoccupied states, respectively). The absorption spectrum of the bulk crystal is obtained by averaging the spectra computed for three orthogonal electric field polarizations (i.e., along a, b axes and along the component of c axis perpendicular to the a-b plane). The BSE Hamiltonian of the J-aggregate has been evaluated and diagonalized within the TDA using an e-h basis composed of 27 occupied and 34 unoccupied states and (5x3x2) *k*-point grid to sample the BZ. All the absorption spectra obtained with Yambo and MOLGW have been plotted with a fixed linewidth of 0.2 eV.

RESULTS AND DISCUSSION

We start our analysis by inspecting the electronic structure of the isolated push-pull dye [Figure 1(a)] and of its J-aggregate [Figure 1(b)–(d)]. In Figure 2(a) the quasi-particle (QP) energy levels of the isolated

organic dye are shown, together with the isosurface plots of the frontier molecular orbitals (MOs). The dimethylamino (push) and the fluorinated ring (pull) groups at the opposite ends of the π-conjugated chromophore induces a strong polarization on the frontier orbitals and an intrinsic dipole. The highest-occupied one (HOMO) and the lowest-unoccupied one (LUMO) are mostly localized on the electron-donating (push) and the electron-withdrawing (pull) side of the molecule, respectively. The QP bandstructure shown in Figure 2(b) exhibits a direct gap of 3.2 eV at the *Y* point, which is more than twice as large as the corresponding DFT (PBE) value of 1.48 eV and is half the QP gap of the isolated molecule which is 6.4 eV in Figure 2(a). The QP correction manifests itself as an almost rigid shift of 1.7 eV for all the conduction bands. This behavior is consistent with that of other organic crystals like pentacene and polythiophene polymers[18,70]. As expected for molecular crystals[15,16,39,71], the band dispersion is very limited and quite anisotropic: bands are almost flat along those directions where inter-molecular interactions are negligible and the wavefunction overlap is hence minimized. Conversely, along the π-stacking directions (*e.g.*, along the Γ-Y path in the BZ), inter-molecular interactions are enhanced. As a result, bands are slightly more dispersive and band splitting is observed.

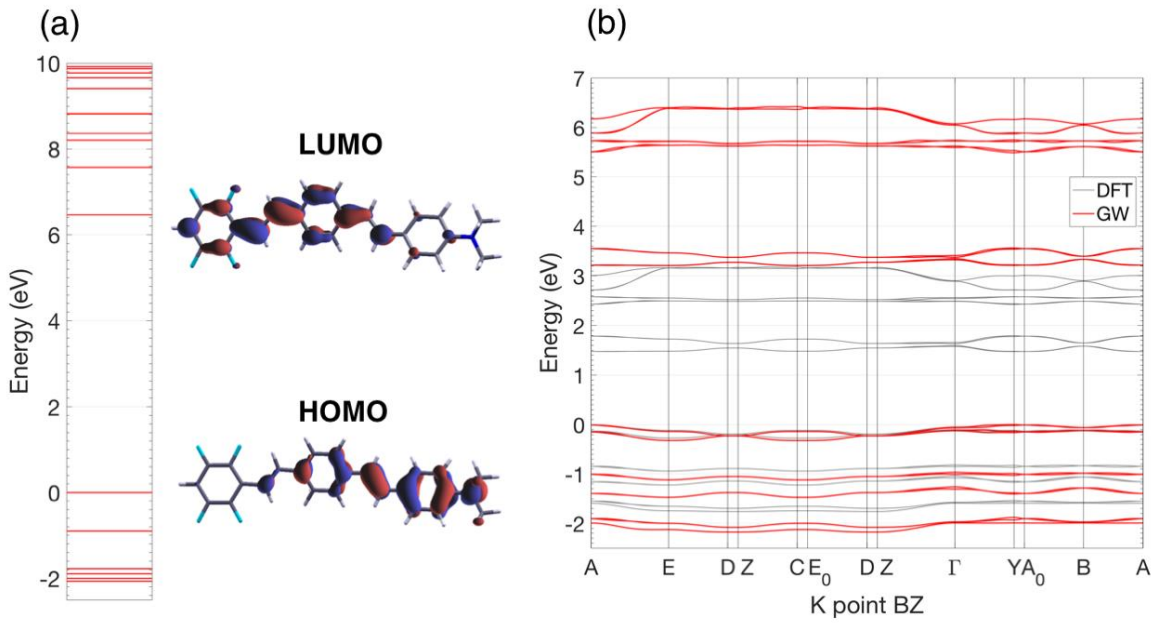

Figure 2 – (a) GW energy levels (HOMO level set to zero) and frontier molecular orbitals of the isolated push-pull dye. The isovalues are fixed at 0.04 Bohr$^{-3/2}$. (b) Band structure of the J-aggregate computed from DFT (gray) and GW (red). The Fermi energy is set to zero at the GW valence band maximum.

Due to the presence of four inequivalent molecules in the unit cell, the bands close to the gap, which exhibit π-π* character, are almost degenerate. In Figure 3 the square moduli of the wave functions at the

valence-band maximum (VBM) and at the conduction-band minimum (CBm) at the high-symmetry point Y are reported. The localized character of the frontier MOs found in the isolated push pull dye is preserved also in the J-aggregate: The Kohn-Sham (KS) states corresponding to the VBM and the CBm are mostly localized on the push and the pull end of each monomer, respectively. Figure 4 displays the optical absorption spectra of the isolated push-pull dye in gas phase (panel a) and of its J-aggregate (panel b). In each of these plots, the vertical bars mark the excited-state energies corresponding to the solution of the Bethe-Salpeter equation (BSE). In Tables 1 and 2, we report the information about the most relevant excitations analyzed below for the monomer and for the J-aggregate, respectively. The red-shift of the principal peak in the spectrum of the J-aggregate with respect to the one of the single molecule amounts to ∼0.73 eV. This result is in better agreement with the measured value of ∼0.54 eV[13], compared to the outcomes of TDDFT calculations with a semi-local xc-functional[14].

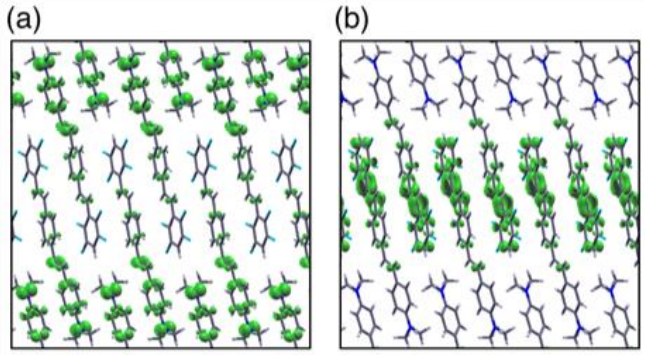

Figure 3 – Isosurfaces of the squared modulus of the KS wave-functions of the (a) valence band maximum and (b) conduction band minimum of the J-aggregate computed at the high-symmetry point Y. Isovalues fixed at 0.001 Bohr^{-3}.

The BSE results reveal also the rich excitonic structure in the J-band, which turns out to be composed of several transitions. Most of the excitations comprised within the J-band appear below the QP gap at 3.2 eV. Their binding energies do not exceed 0.4 eV, in line with the values reported for conjugated polymers[17,72–75] and slightly smaller than those of crystalline pentacene (0.5 eV)[16,19], picene (0.7 eV)[19] and antracene (0.8 eV)[15].

In the following, we focus on two representative excited states within the J-band: the most intense one, labeled J, appears at 3 eV and a very weak one, J_{CT} , at 2.89 eV. Both excitations are analyzed in Figure 5 in terms of excitonic wave-functions and transition densities. The character of the intense excitation J is very similar to the one of the first intense transition in the isolated push-pull molecule, which gives rise to the sharp peak M dominating the spectrum in Figure 4(a). This excitation stems mainly from the HOMO-LUMO transition, and, as such, bears intra-molecular CT character.

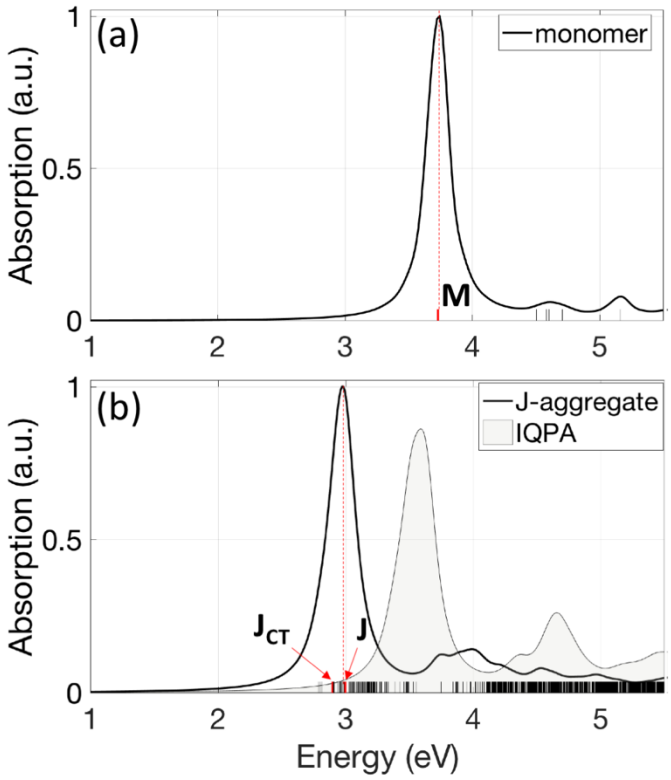

Figure 4 – Absorption spectra of (a) the push-pull dye in the gas phase and (b) the J-aggregate. In both spectra all the calculated excited states (both bright and dark) are marked by short vertical bars. The J and J_{CT} analyzed excitations are highlighted in red . The BSE spectra are normalized with respect to their maximum value. In panel (b) the absorption spectrum calculated from the independent quasi particle approximation (IQPA) is also shown (gray shaded area).

In Table II the composition of the *J* excitation is reported, showing that it is mainly formed by transitions between (quasi-)degenerate bands at the valence-band top and conduction-band bottom, which carry π and π* character like the HOMO and the LUMO of the isolated dye [see Figures 2(a) and 3]. The exciton joint probability density (with fixed hole position) of excited state *J* reveals its intermixed intramolecular charge transfer as well as intermolecular charge transfer between nearest-neighboring molecules. Having fixed the position of the hole on the *push* side (i.e., the dimethylamino group) of one molecule in the unit cell, the electron is found on the *pull* part (i.e., the fluorinated ring) of the same molecule and of its nearest neighbors. By inspecting Figure 5(a), the electron distribution is also delocalized around neighboring molecules along the π-stacking direction (i.e., the a-b plane) where the dispersion is more pronounced because of enhanced wave-function overlap. The intermolecular character of this excitation is therefore due to the π-interactions in the molecular packing

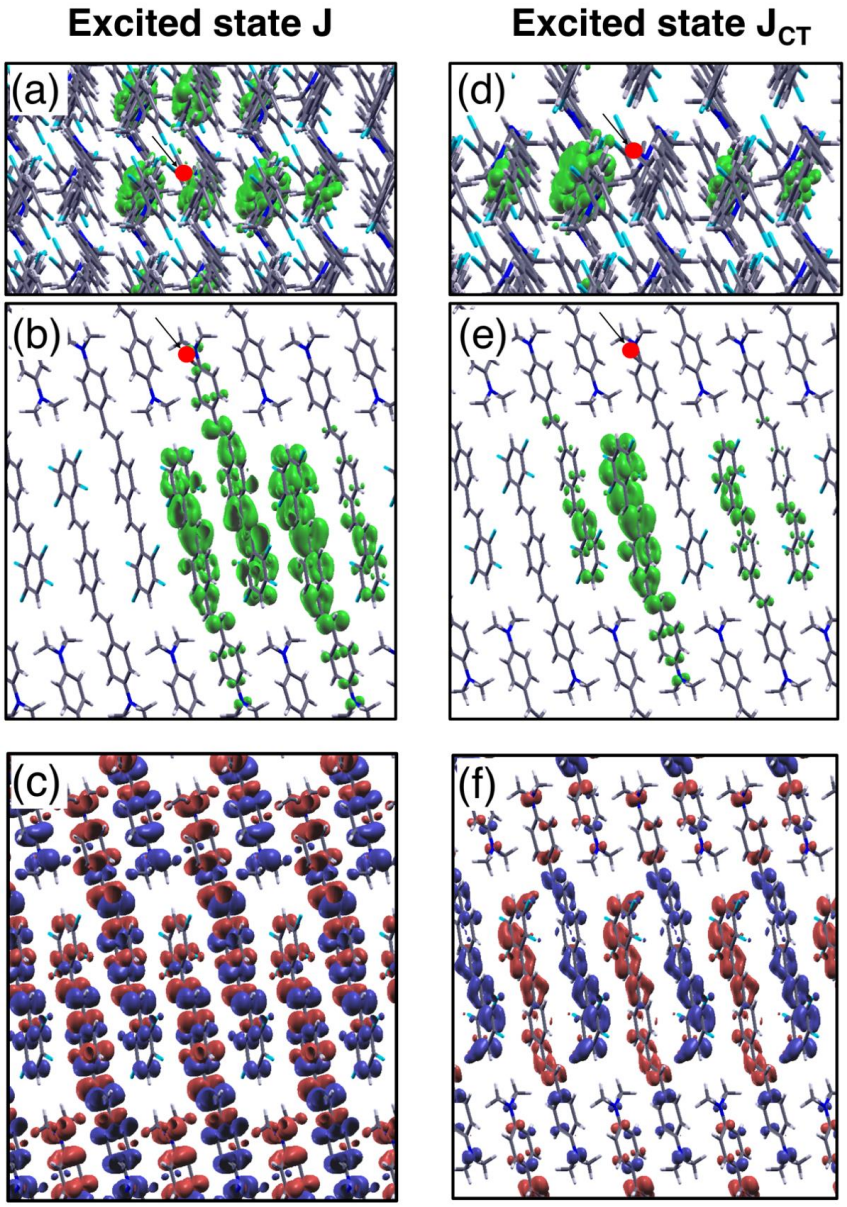

Figure 5 – (Panels a,b,d,e) exciton joint probability density with fixed hole position (red dot), defined as $|\Psi_\lambda(r_e,\bar{r}_h)|^2 = \left|\langle\lambda\left|\Psi^\dagger(r_e)\Psi(\bar{r}_h)\right|0\rangle\right|^2 = \left|\sum_{cvk} A^\lambda_{vck}\varphi_{ck}(r_e)\varphi^*_{vk}(\bar{r}_h)\right|^2$, *where* $\Psi_\lambda(r_e,\bar{r}_h)$ *exciton two-body wavefunction,* $\bar{r}_h$ *(*r_e*) hole (electron) position,* A^λ_{vck} *the BSE coefficients for the excited states* $\lambda = J, J_{CT}$ *of the J-aggregate,* φ_{vk} *(*φ_{ck}*) occupied (unoccupied) KS electronic states with wavevector* ***k*** *in the BZ; views from the a-b plane (panels a, d) and from a-c plane (panels b, e). The exciton plot gives the probability to find the electron at position* r_e *with the hole fixed at* $\bar{r}_h$*. (Panels c, f) transition density, defined as* $\rho_\lambda(r) = \langle\lambda\left|\Psi^\dagger(r)\Psi(r)\right|0\rangle = \sum_{cvk} A^\lambda_{vck}\varphi_{ck}(r)\varphi^*_{vk}(r)$*, for the excited states* $\lambda = J, J_{CT}$ *of the J-aggregate; views from the a-c plane. The transition density provides information about the charge spatial displacement associated to the specific excited state λ. Isosurfaces of exciton wavefunctions (transition densities) fixed at 0.05 Bohr*$^{-3}$ *(*10^{-4} *Bohr*$^{-3}$*).*

direction, in analogy with the excitons of organic crystals formed by non-polar molecules[16,17,76,77]. On the other hand, the intramolecular CT nature of the J excitation is inherited from the polarized character of contributing electronic states, in analogy with the MOs of the push-pull molecules constituting the J-aggregate. The transition density of J shown in Figure 5(c) offers complementary information to the exciton wave-function in terms of the spatial distribution of the excitation and the orientation of the transition dipole moment. With the molecular transition dipoles coherently aligned and in phase with respect to each other, the intense excitation J is associated to an induced charge density mainly displaced along the long crystal axis within the a-c plane [see Figure 1(b)]. It is worth noting that the transition density shown in Figure 5(c) does not completely integrate to zero within a single monomer unit, as positive and negative displaced charges are not present in equal amount. This fact is compatible with the partial intermolecular CT mechanism highlighted above in the analysis of the exciton wave-function. This result has similarities with that obtained for pentacene molecular crystals[16,19] where exciton delocalization on neighboring molecules also appears. However, as opposed to pentacene, the J-aggregate considered here is composed of polar push-pull molecules: the intrinsic dipole strongly polarizes the frontier MOs and thus reduces the spatial overlap between electron and hole. At slightly lower energy compared to J, the weaker excitation J_{CT} appears in the spectrum in Figure 4(b) with a completely different nature. As shown in Figures 5(d)-(f) by the exciton wave-function and the transition density, this excitation has a pure intermolecular CT character, with the electron and the hole localized on different neighboring molecules. The slightly larger binding energy of J_{CT} (E_b= 0.32 eV) compared to J (E_b= 0.21 eV) is consistent with its enhanced spatial localization [Figure 5(d)-(e)], while the reduced wave-function overlap between the hole and the electron components is consistent with the very weak oscillator. Such a CT excitation is associated to lower electron-hole recombination rates and enhanced electron-hole dissociation probability compared to excitons with more pronounced intramolecular character[78]. The transition density associated to J_{CT} [Figure 5(c)] confirms and complements this picture: neighboring monomers are almost completely depleted of positive and negative charge, respectively, meaning that intermolecular CT is the dominant mechanism here. It is worth mentioning that the character and the microscopic features of excited states such as J_{CT} cannot be captured by simple models based on transition dipoles coupling (e.g., the Kasha's model[11]) but need an advanced first-principles description as provided in this work.

The intra- and intermolecular character of singlet excitations in organic crystals is determined by a competition between the e-h exchange interaction, which is responsible for the local field effects, and the screened e-h attraction[19]. While the exchange interaction is quite sensitive to the spatial overlap between occupied and unoccupied electronic states involved in the transition, the direct e-h attraction can be non-vanishing even upon negligible spatial overlap between occupied and unoccupied states[19]. Here,

Table 1. *Energy and composition of the first excited state of the push-pull monomer $C_{24}H_{19}F_4N$, including the associated transition energy and weight given by the square of the BSE coefficient.*

Excited state energy (eV)	**Occupied level**	**Unoccupied level**	$\epsilon_c^{QP} - \epsilon_v^{QP}$ **(eV)**	**Weight** $\left\|A_{cv}^{\lambda}\right\|^2$
E^M= 3.73	HOMO	LUMO	6.46	0.768

Table 2. *Energy and composition of the J and J_{CT} excitations of the J-aggregate, including the associated transition energy, the associated k-point in the Brillouin Zone expressed in reciprocal crystal units (rcu), and the weight given by the square of the BSE coefficient. Only weights larger than 2% are reported.*

Excited state energy (eV)	**Occupied band**	**Unoccupied band**	**k-point (rcu)**	$\epsilon_{ck}^{QP} - \epsilon_{vk}^{QP}$ **(eV)**	**Weight** $\left\|A_{cvk}^{\lambda}\right\|^2 \times$ **10**
E^J= 3	VBM-2	CBm+1	(0.4, 0, -0.5)	3.34	0.59
	VBM -2	CBm +1	(-0.4, 0, 0.5)	3.34	0.56
	VBM -3	CBm	(0.4, 0, 0)	3.35	0.54
	VBM -3	CBm	(-0.4, 0, 0)	3.35	0.52
	VBM -2	CBm +1	(0.4, 0, 0)	3.33	0.29
	VBM -3	CBm	(0.4, 0, -0.5)	3.34	0.29
	VBM -3	CBm	(-0.4, 0, 0.5)	3.34	0.26
	VBM -2	CBm+1	(-0.4, 0, 0)	3.33	0.26
E^{JCT} = 2.89	VBM	CBm +1	(-0.2, 0, 0.5)	3.29	0.47
	VBM	CBm +1	(-0.2, 0, 0)	3.28	0.41
	VBM	CBm +1	(0.2, 0, -0.5)	3.29	0.40
	VBM -1	CBm	(-0.2, 0, 0)	3.31	0.37
	VBM	CBm +1	(0.2, 0, 0)	3.28	0.36
	VBM -1	CBm	(0.2, 0, 0)	3.31	0.32
	VBM -1	CBm	(-0.2, 0, 0.5)	3.29	0.26
	VBM -1	CBm	(-0.4, 0, 0.5)	3.23	0.24
	VBM	CBm +1	(-0.4, 0, 0)	3.22	0.23
	VBM -1	CBm	(0.2, 0, -0.5)	3.29	0.23

due to the push-pull character of the constituting dyes, the gap states of the J-aggregate are quite polarized and hence do not overlap much [see Figures 2(a) and 3], as opposed, for instance, to pentacene[19]. Hence, we should expect a reduced influence from the local fields to the low-lying excited states of the J-aggregate. To quantify the contribution of the local fields on a given excited state $|\lambda\rangle$ we use the e-h

exchange energy E_x^λ and its ratio with respect to the total excitation energy $\tilde{E}_x^\lambda = E_x^\lambda / E^\lambda$ (see Method section). In the isolated monomer E_x^M =0.68 eV ($\tilde{E}_x^M = 0.182$), while in the J-aggregate $E_x^J = 0.07$ eV ($\tilde{E}_x^J = 0.023$) and $E_x^{J_{CT}} = 0.01$ eV ($\tilde{E}_x^{J_{CT}} = 0.003$). From these values it is apparent that local fields contribute ~20% in the first excitation of the isolated monomer while they are almost negligible in the J-aggregate (2% for J and 0.3% for J_{CT}). The predominant intermolecular CT character of J_{CT} is therefore related to the weaker e-h exchange interaction with respect to J, where in the latter the spatial overlap between the electron and the hole is larger [see also Figure 5(a)-(b)]. The intermolecular charge transfer that characterizes both J and J_{CT} is favored by the close molecular packing of the aggregate, which promotes electron delocalization between neighboring molecules.

CONCLUSIONS

To summarize, in the framework of MBPT, we have investigated the electronic and optical properties of a J-aggregate formed by the push-pull organic dye $C_{24}H_{19}F_4N$, specifically addressing the interplay between intra- and inter-molecular interactions. We have found that the intense J-band dominating the absorption onset is formed by a number of excitations stemming from transitions between the highest-occupied and the lowest-unoccupied bands. The most intense of these excitations exhibits a combination of inter- and intra-molecular charge transfer, resulting from the competing effects of dense molecular packing and the push-pull nature of the constituting molecules. The other excitations within the J-band have very weak intensity. Among them, J_{CT} has pronounced intermolecular charge-transfer character. Being at lower energy compared to the most intense excitation in the J-band, this state is expected to play a relevant role in the emission properties of the J-aggregate. We have also demonstrated that in push-pull molecular aggregates the contribution of the local fields within is small, due to the polar nature of the constituting molecules which in turn reduces the spatial overlap between electron and hole.

Our analysis demonstrates that the complex mechanisms ruling the optical properties of organic crystalline aggregates cannot be unveiled based solely on simple models, but require a high level of theory that is able to quantitatively address all the facets of the problem. Many-body perturbation theory is capable to thoroughly capture the collective effects and to provide a robust insight on the excitations of the system. As such, our results offer unprecedented insight into the nature of the excitations of J-aggregates formed by push-pull chromophores and contribute to the further understanding of these materials that are relevant for opto-electronic applications.

ACKNOWLEDGMENTS

We acknowledge financial support from DAAD. The work has been performed under the Project HPC-EUROPA3 (INFRAIA-2016-1-730897), with the support of the EC Research Innovation Action under the H2020 Programme; in particular we gratefully acknowledges the support of department of Physics and IRIS Adlershof, Humboldt Universität zu-Berlin and the computer resources and technical support provided by HLRS. C.C. appreciates funding from Deutsche Forschungsgemeinschaft (DFG, German Research Foundation) - Projektnummer 182087777 - SFB 951 and HE 5866/2-1. This work was also partially funded by the European Union under the ERC grant TAME Plasmons (ERC-CoG-681285). DV acknowledges financial support from the EU Centre of Excellence "MaX - Materials Design at the Exascale" (Horizon 2020 EINFRA-5, Grant No. 676598). Computational resources were partly provided by PRACE on the Marconi machine at CINECA.

REFERENCES

(1) Bricks, J. L.; Slominskii, Y. L.; Panas, I. D.; Demchenko, A. P. Fluorescent J-Aggregates of Cyanine Dyes: Basic Research and Applications Review. *Methods Appl. Fluoresc.* **2017**, *6* (1), 2001.

(2) Melnikau, D.; Savateeva, D.; Susha, A. S.; Rogach, A. L.; Rakovich, Y. P. Strong Plasmon-Exciton Coupling in a Hybrid System of Gold Nanostars and J-Aggregates. *Nanoscale Res. Lett.* **2013**, 8 (1), 134.

(3) Ferdele, S.; Jose, B.; Foster, R.; Keyes, T. E.; Rice, J. H. Strong Coupling in Porphyrin J-Aggregate Excitons and Plasmons in Nano-Void Arrays. *Opt. Mater.* **2017**, *72*, 680–684.

(4) Wurtz, G. A.; Evans, P. R.; Hendren, W.; Atkinson, R.; Dickson, W.; Pollard, R. J.; Zayats, A. V; Harrison, W.; Bower, C. Molecular Plasmonics with Tunable Exciton−Plasmon Coupling Strength in J-Aggregate Hybridized Au Nanorod Assemblies. *Nano Lett.* **2007**, *7* (5), 1297–1303.

(5) Fofang, N. T.; Park, T.-H.; Neumann, O.; Mirin, N. A.; Nordlander, P.; Halas, N. J. Plexcitonic Nanoparticles: Plasmon−Exciton Coupling in Nanoshell−J-Aggregate Complexes. *Nano Lett.* **2008**, *8* (10), 3481–3487.

(6) Egorov, V. V. Theory of the J-Band: From the Frenkel Exciton to Charge Transfer. *Phys. Procedia* **2009**, *2* (2), 223–326.

(7) Jelley, E. E. Spectral Absorption and Fluorescence of Dyes in the Molecular State. *Nature* **1936**, *138*, 1009-1010.

(8) Eisfeld, A.; Briggs, J. S. The J-Band of Organic Dyes: Lineshape and Coherence Length. *Chem. Phys.* **2002**, *281* (1), 61–70.

(9) Eisfeld, A.; Briggs, J. S. The J- and H-Bands of Organic Dye Aggregates. *Chem. Phys.* **2006**, *324* (2–3), 376–384.

(10) Walczak, P. B.; Eisfeld, A.; Briggs, J. S. Exchange Narrowing of the J Band of Molecular Dye

Aggregates. *J. Chem. Phys.* **2008**, *128* (4), 1–12.

(11) Kasha, M. Energy Transfer Mechanisms and the Molecular Exciton Model for Molecular Aggregates. *Radiat. Res.* **1963**, *20* (1), 55–70.

(12) Kasha, M.; Rawls, H. R.; Ashraf El-Bayoumi, M. The Exciton Model in Molecular Spectroscopy. *Pure Appl. Chem.* **1965**, *11* (3–4), 371–392.

(13) Botta, C.; Cariati, E.; Cavallo, G.; Dichiarante, V.; Forni, A.; Metrangolo, P.; Pilati, T.; Resnati, G.; Righetto, S.; Terraneo, G.; et al. Fluorine-Induced J-Aggregation Enhances Emissive Properties of a New NLO Push-Pull Chromophore. *J. Mater. Chem. C* **2014**, *2* (27), 5275–5279.

(14) Guerrini, M.; Calzolari, A.; Corni, S. Solid-State Effects on the Optical Excitation of Push–Pull Molecular J-Aggregates by First-Principles Simulations. *ACS Omega* **2018**, *3* (9), 10481–10486.

(15) Hummer, K.; Puschnig, P.; Ambrosch-Draxl, C. Lowest Optical Excitations in Molecular Crystals: Bound Excitons versus Free Electron-Hole Pairs in Anthracene. *Phys. Rev. Lett.* **2004**, *92* (14), 1–4.

(16) Cocchi, C.; Breuer, T.; Witte, G.; Draxl, C. Polarized Absorbance and Davydov Splitting in Bulk and Thin-Film Pentacene Polymorphs. *Phys. Chem. Chem. Phys.* **2018**. DOI: 10.1039/C8CP06384B

(17) Ruini, A.; Caldas, M. J.; Bussi, G.; Molinari, E. Solid State Effects on Exciton States and Optical Properties of PPV. *Phys. Rev. Lett.* **2002**, *88* (20), 4.

(18) Tiago, M. L.; Northrup, J. E.; Louie, S. G. *Ab Initio* Calculation of the Electronic and Optical Properties of Solid Pentacene. *Phys. Rev. B* **2003**, *67* (11), 5212.

(19) Cudazzo, P.; Gatti, M.; Rubio, A. Excitons in Molecular Crystals from First-Principles Many-Body Perturbation Theory: Picene versus Pentacene. *Phys. Rev. B - Condens. Matter Mater. Phys.* **2012**, *86* (19), 1–8.

(20) Broch, K.; Dieterle, J.; Branchi, F.; Hestand, N. J.; Olivier, Y.; Tamura, H.; Cruz, C.; Nichols, V. M.; Hinderhofer, A.; Beljonne, D.; et al. Robust Singlet Fission in Pentacene Thin Films with Tuned Charge Transfer Interactions. *Nat. Commun.* **2018**, *9* (1), 954.

(21) Zeng, T.; Hoffmann, R.; Ananth, N. The Low-Lying Electronic States of Pentacene and Their Roles in Singlet Fission. *J. Am. Chem. Soc.* **2014**, *136* (15), 5755–5764.

(22) Refaely-Abramson, S.; da Jornada, F. H.; Louie, S. G.; Neaton, J. B. Origins of Singlet Fission in Solid Pentacene from an Ab Initio Green's Function Approach. *Phys. Rev. Lett.* **2017**, *119* (26), 7401.

(23) Coto, P. B.; Sharifzadeh, S.; Neaton, J. B.; Thoss, M. Low-Lying Electronic Excited States of Pentacene Oligomers: A Comparative Electronic Structure Study in the Context of Singlet Fission. *J. Chem. Theory Comput.* **2015**, *11* (1), 147–156.

(24) Beljonne, D.; Yamagata, H.; Brédas, J. L.; Spano, F. C.; Olivier, Y. Charge-Transfer Excitations Steer the Davydov Splitting and Mediate Singlet Exciton Fission in Pentacene. *Phys. Rev. Lett.* **2013**, *110* (22), 6402.

(25) Kolata, K.; Breuer, T.; Witte, G.; Chatterjee, S. Molecular Packing Determines Singlet Exciton Fission in Organic Semiconductors. *ACS Nano* **2014**, *8* (7), 7377–7383.

(26) Berkelbach, T. C.; Hybertsen, M. S.; Reichman, D. R. Microscopic Theory of Singlet Exciton Fission. III.

Crystalline Pentacene. *J. Chem. Phys.* **2014**, *141* (7), 4705.

(27) Berkelbach, T. C.; Hybertsen, M. S.; Reichman, D. R. Microscopic Theory of Singlet Exciton Fission. II. Application to Pentacene Dimers and the Role of Superexchange. *J. Chem. Phys.* **2013**, *138* (11), 4103.

(28) Sharifzadeh, S.; Darancet, P.; Kronik, L.; Neaton, J. B. Low-Energy Charge-Transfer Excitons in Organic Solids from First-Principles: The Case of Pentacene. *J. Phys. Chem. Lett.* **2013**, *4* (13), 2197–2201.

(29) Wilson, M. W. B.; Rao, A.; Ehrler, B.; Friend, R. H. Singlet Exciton Fission in Polycrystalline Pentacene: From Photophysics toward Devices. *Acc. Chem. Res.* **2013**, *46* (6), 1330–1338.

(30) Wilson, M. W. B.; Rao, A.; Clark, J.; Kumar, R. S. S.; Brida, D.; Cerullo, G.; Friend, R. H. Ultrafast Dynamics of Exciton Fission in Polycrystalline Pentacene. *J. Am. Chem. Soc.* **2011**, *133* (31), 11830–11833.

(31) Zimmerman, P. M.; Bell, F.; Casanova, D.; Head-Gordon, M. Mechanism for Singlet Fission in Pentacene and Tetracene: From Single Exciton to Two Triplets. *J. Am. Chem. Soc.* **2011**, *133* (49), 19944–19952.

(32) Zimmerman, P. M.; Zhang, Z.; Musgrave, C. B. Singlet Fission in Pentacene through Multi-Exciton Quantum States. *Nat. Chem.* **2010**, 2 (8), 648-652.

(33) Schuster, R.; Knupfer, M.; Berger, H. Exciton Band Structure of Pentacene Molecular Solids: Breakdown of the Frenkel Exciton Model. *Phys. Rev. Lett.* **2007**, *98* (3), 98–101.

(34) Cudazzo, P.; Sottile, F.; Rubio, A.; Gatti, M. Exciton Dispersion in Molecular Solids.*J. Phys. Condens. Matter* **2015**, 27 (11), 3204.

(35) Hummer, K.; Ambrosch-Draxl, C. Oligoacene Exciton Binding Energies: Their Dependence on Molecular Size. *Phys. Rev. B - Condens. Matter Mater. Phys.* **2005**, *71* (8), 1–4.

(36) Bussi, G.; Ruini, A.; Molinari, E.; Caldas, M. J.; Puschnig, P.; Ambrosch-Draxl, C. Interchain Interaction and Davydov Splitting in Polythiophene Crystals: An Ab Initio Approach. *Appl. Phys. Lett.* **2002**, *80* (22), 4118–4120.

(37) Rangel, T.; Berland, K.; Sharifzadeh, S.; Brown-Altvater, F.; Lee, K.; Hyldgaard, P.; Kronik, L.; Neaton, J. B. Structural and Excited-State Properties of Oligoacene Crystals from First Principles. *Phys. Rev. B* **2016**, *93* (11), 5206.

(38) Sharifzadeh, S.; Biller, A.; Kronik, L.; Neaton, J. B. Quasiparticle and Optical Spectroscopy of the Organic Semiconductors Pentacene and PTCDA from First Principles. *Phys. Rev. B* **2012**, *85* (12), 5307.

(39) Ambrosch-Draxl, C.; Nabok, D.; Puschnig, P.; Meisenbichler, C. The Role of Polymorphism in Organic Thin Films: Oligoacenes Investigated from First Principles. *New J. Phys.* **2009**, 11 (12), 5010.

(40) Nelson, S. F.; Lin, Y.-Y.; Gundlach, D. J.; Jackson, T. N. Temperature-Independent Transport in High-Mobility Pentacene Transistors. *Appl. Phys. Lett.* **1998**, *72* (15), 1854–1856.

(41) Lee, J. Y.; Roth, S.; Park, Y. W. Anisotropic Field Effect Mobility in Single Crystal Pentacene. *Appl. Phys. Lett.* **2006**, *88* (25), 2106.

(42) Takeya, J.; Yamagishi, M.; Tominari, Y.; Hirahara, R.; Nakazawa, Y.; Nishikawa, T.; Kawase, T.; Shimoda, T.; Ogawa, S. Very High-Mobility Organic Single-Crystal Transistors with in-Crystal Conduction Channels. *Appl. Phys. Lett.* **2007**, *90* (10), 2120.

(43) Dimitrakopoulos, C. D.; Brown, A. R.; Pomp, A. Molecular Beam Deposited Thin Films of Pentacene for Organic Field Effect Transistor Applications. *J. Appl. Phys.* **1996**, *80* (4), 2501–2508.

(44) Lin, Y.-Y.; Gundlach, D. I.; Nelson, S. F.; Jackson, T. N. Pentacene-Based Organic Thin-Film Transistors. *IEEE Trans. Electron Devices* **1997**, *44* (8), 1325–1331.

(45) Jin, Y.; Rang, Z.; Nathan, M. I.; Ruden, P. P.; Newman, C. R.; Frisbie, C. D. Pentacene Organic Field-Effect Transistor on Metal Substrate with Spin-Coated Smoothing Layer. *Appl. Phys. Lett.* **2004**, *85* (19), 4406–4408.

(46) Yang, S. Y.; Shin, K.; Park, C. E. The Effect of Gate-Dielectric Surface Energy on Pentacene Morphology and Organic Field-Effect Transistor Characteristics. *Adv. Funct. Mater. 15* (11), 1806–1814.

(47) Graz, I. M.; Lacour, S. P. Flexible Pentacene Organic Thin Film Transistor Circuits Fabricated Directly onto Elastic Silicone Membranes. *Appl. Phys. Lett.* **2009**, *95* (24), 3305.

(48) Varghese, S.; Das, S. Role of Molecular Packing in Determining Solid-State Optical Properties of π-Conjugated Materials. *J. Phys. Chem. Lett.* **2011**, *2* (8), 863–873.

(49) Köhler, A.; Wilson, J. S.; Friend, R. H. Fluorescence and Phosphorescence in Organic Materials. *Adv. Mater.* **2002**, *14* (10), 701–707.

(50) Benassi, E.; Corni, S. Exciton Transfer of Azobenzene Derivatives in Self-Assembled Monolayers. *J. Phys. Chem. C* **2013**, *117* (47), 25026–25041.

(51) Utecht, M.; Klamroth, T.; Saalfrank, P. Optical Absorption and Excitonic Coupling in Azobenzenes Forming Self-Assembled Monolayers: A Study Based on Density Functional Theory. *Phys. Chem. Chem. Phys.* **2011**, *13* (48), 21608–21614.

(52) Cocchi, C.; Moldt, T.; Gahl, C.; Weinelt, M.; Draxl, C. Optical Properties of Azobenzene-Functionalized Self-Assembled Monolayers: Intermolecular Coupling and Many-Body Interactions. *J. Chem. Phys.* **2016**, *145* (23), 1–12.

(53) Cocchi, C.; Draxl, C. Understanding the Effects of Packing and Chemical Terminations on the Optical Excitations of Azobenzene-Functionalized Self-Assembled Monolayers. *J. Phys. Condens. Matter* **2017**, *29* (39), 34005.

(54) Cocchi, C.; Draxl, C. Bound Excitons and Many-Body Effects in x-Ray Absorption Spectra of Azobenzene-Functionalized Self-Assembled Monolayers. *Phys. Rev. B* **2015**, *92* (20), 5105.

(55) Hohenberg, P.; Kohn, W. Inhomogeneous Electron Gas. *Phys. Rev.* **1964**, *136* (3B), B864--B871.

(56) Kohn, W.; Sham, L. J. Self-Consistent Equations Including Exchange and Correlation Effects. *Phys. Rev.* **1965**, *140* (4A), 133-138.

(57) Onida, G.; Reining, L.; Rubio, A. Electronic Excitations: Density-Functional versus Many-Body Green's-Function Approaches. *Rev. Mod. Phys.* **2002**, *74* (2), 601–659.

(58) Hedin, L. New Method for Calculating the One-Particle Green's Function with Application to the Electron-Gas-Problem. *Phys. Rev.* **1965**, *139* (3A), 796.

(59) Strinati, G. Application of the Green's Functions Method to the Study of the Optical Properties of Semiconductors. *La Riv. del Nuovo Cim.* **1988**, *11* (12), 1–86.

(60) Hybertsen, M. S.; Louie, S. G. Electron Correlation in Semiconductors and Insulators: Band Gaps and Quasiparticle Energies. *Phys. Rev. B* **1986**, *34* (8), 5390–5413.

(61) Hanke, W. Dielectric Theory of Elementary Excitations in Crystals. *Adv. Phys.* **1978**, *27* (2), 287–341.

(62) Frisch, M. J.; Trucks, G. W.; Schlegel, H. B.; Scuseria, G. E.; Robb, M. a.; Cheeseman, J. R.; Montgomery, J. a.; Vreven, T.; Kudin, K. N.; Burant, J. C.; et al. Gaussian 09W Tutorial. *an Introd. To Comput. Chem. Using G09W Avogadro Softw.* **2009**, 34.

(63) Yanai, T.; Tew, D. P.; Handy, N. C. A New Hybrid Exchange-Correlation Functional Using the Coulomb-Attenuating Method (CAM-B3LYP). *Chem. Phys. Lett.* **2004**, *393* (1–3), 51–57.

(64) Bruneval, F.; Rangel, T.; Hamed, S. M.; Shao, M.; Yang, C.; Neaton, J. B. Molgw 1: Many-Body Perturbation Theory Software for Atoms, Molecules, and Clusters. *Comput. Phys. Commun.* **2016**, 208, 149-161

(65) Giannozzi, P.; Baroni, S.; Bonini, N.; Calandra, M.; Car, R.; Cavazzoni, C.; Ceresoli, D.; Chiarotti, G. L.; Cococcioni, M.; Dabo, I.; et al. QUANTUM ESPRESSO: A Modular and Open-Source Software Project for Quantum Simulations of Materials. *J. Phys. Condens. Matter* **2009**, *21* (39), 5502.

(66) Perdew, J. P.; Burke, K.; Ernzerhof, M. Generalized Gradient Approximation Made Simple. *Phys. Rev. Lett.* **1996**, *77* (18), 3865–3868.

(67) Hamann, D. R. Optimized Norm-Conserving Vanderbilt Pseudopotentials. *Phys. Rev. B* **2013**, *88* (8), 5117.

(68) Marini, A.; Hogan, C.; Grüning, M.; Varsano, D. Yambo: An Ab Initio Tool for Excited State Calculations. *Comput. Phys. Commun.* **2009**, *180* (8), 1392–1403.

(69) Godby, R. W.; Needs, R. J. Metal-Insulator Transition in Kohn-Sham Theory and Quasiparticle Theory. *Phys. Rev. Lett.* **1989**, *62* (10), 1169–1172.

(70) van der Horst, J.; Bobbert, P.; de Jong, P.; Michels, M.; Brocks, G.; Kelly, P. Ab Initio Prediction of the Electronic and Optical Excitations in Polythiophene: Isolated Chains versus Bulk Polymer. *Phys. Rev. B - Condens. Matter Mater. Phys.* **2000**, *61* (23), 15817–15826.

(71) Cocchi, C.; Draxl, C. Optical Spectra from Molecules to Crystals: Insight from Many-Body Perturbation Theory. *Phys. Rev. B* **2015**, *92* (20), 5126.

(72) Alvarado, S. F.; Seidler, P. F.; Lidzey, D. G.; Bradley, D. D. C. Direct Determination of the Exciton Binding Energy of Conjugated Polymers Using a Scanning Tunneling Microscope. *Phys. Rev. Lett.* **1998**, *81* (5), 1082–1085.

(73) Campbell, I. H.; Hagler, T. W.; Smith, D. L.; Ferraris, J. P. Direct Measurement of Conjugated Polymer Electronic Excitation Energies Using Metal/Polymer/Metal Structures. *Phys. Rev. Lett.* **1996**, *76* (11), 1900–1903.

(74) Barth, S.; Bässler, H. Intrinsic Photoconduction in PPV-Type Conjugated Polymers. *Phys. Rev. Lett.* **1997**, *79* (22), 4445–4448.

(75) Varsano, D.; Marini, A.; Rubio, A. Optical Saturation Driven by Exciton Confinement in Molecular Chains: A Time-Dependent Density-Functional Theory Approach. *Phys. Rev. Lett.* **2008**, *101* (13), 3002.

(76) Cocchi, C.; Prezzi, D.; Ruini, A.; Caldas, M. J.; Molinari, E. Optical Properties and Charge-Transfer Excitations in Edge-Functionalized All-Graphene Nanojunctions. *J. Phys. Chem. Lett.* **2011**, *2* (11), 1315–1319.

(77) Ruini, A. Ab Initio Optical Absorption in Conjugated Polymers: The Role of Dimensionality. *Phys. Scr.* **2004**, *2004* (T109), 121.

(78) Barford, W. *Electronic and Optical Properties of Conjugated Polymers*; International Series of Monographs on Physics; OUP Oxford, 2005.

Appendix B – Supporting Information of: Interplay between intra- and inter-molecular charge transfer in the optical excitations of organic push-pull J-aggregates

3.2 Appendix B1 – MBPT theoretical framework and simulations workflow

We shall briefly present here the basic theory and simulation workflow procedures of a Many-Body perturbation theory (MBPT) calculation. The following procedure is the one we followed to simulate the electronic and the optical properties of the push-pull dye and its J-aggregate.

(1) DFT ground state calculation. The first step consists in a KS-DFT or g-KS (i.e., generalized Kohn-Sham[82,83,106,107]) ground state electronic structure calculation where one performs a starting point self-consistent (scf) calculation (using hybrid or non-hybrid xc-functionals) to evaluate independent single-particle energies $\varepsilon_{\tilde{n}}^{gKS}$ and KS orbitals $\psi_{\tilde{n}}^{gKS}(\boldsymbol{r})$ ($\tilde{n}$ in general being a multi index comprising band n and BZ k-point indices for Bloch states) obeying the usual generalized Kohn-Sham independent particle equation $\hat{h}_0(r)\psi_{\tilde{n}}^{gKS}(\boldsymbol{r}) + V_{xc}(r)\psi_{\tilde{n}}^{gKS}(\boldsymbol{r}) = \varepsilon_{\tilde{n}}^{gKS}\psi_{\tilde{n}}^{gKS}(\boldsymbol{r})$, where $\hat{h}_0 = -\frac{1}{2}\nabla^2 + V_H[n]$, $V_H[n] = \int \frac{n(\boldsymbol{r}')}{|\boldsymbol{r}-\boldsymbol{r}'|} d^3r'$ is the Hartree electrostatic potential, $\rho(\boldsymbol{r}) = \sum_{\tilde{n}} f_{\tilde{n}} \left|\psi_{\tilde{n}}^{gKS}(\boldsymbol{r})\right|^2$ the ground state charge density ($f_{\tilde{n}}$ occupation number for state $\tilde{n}$). The g-KS states $\psi_{\tilde{n}}^{gKS} = |\tilde{n}\rangle$, once calculated, are used as a basis and kept fixed in the successive steps;

(2) GW quasi-particle corrections. In the second step one performs a GW calculation[83,84,108–114] (with different possible flavors) which applies the quasi-particle corrections to the single particle energies. In our case both for the bulk crystal and for the isolated push-pull dye simulations, we have used a standard GW scheme[115,116] where one applies a first order perturbative correction to the KS energies $\varepsilon_{\tilde{n}}^{gKS}$ solving the non-linear quasi-particle equation

$$E_{\tilde{n}}^{QP} - \varepsilon_{\tilde{n}}^{gKS} = \left\langle \psi_{\tilde{n}}^{KS} \middle| \Sigma\left(E_{\tilde{n}}^{QP}\right) - V_{xc} \middle| \psi_{\tilde{n}}^{KS} \right\rangle \quad \text{B.1}$$

In the GW approach adopted by Yambo[96], which we used to simulate the bulk crystal, the self-energy $\hat{\Sigma}\left(E_{\tilde{n}}^{QP}\right)$ operator is separated into two components: a static term called *exchange self-energy* $\hat{\Sigma}_x$ and a dynamical (i.e., energy dependent) term called *correlation self-energy* $\hat{\Sigma}_c(\omega)$

$$\Sigma_{\tilde{n}}(\omega) = \left\langle \psi_{\tilde{n}}^{KS} \middle| \hat{\Sigma}(\omega) \middle| \psi_{\tilde{n}}^{KS} \right\rangle = \Sigma_{\tilde{n}}^{x} + \Sigma_{\tilde{n}}^{c}(\omega) \quad \text{B.2}$$

In this way one can treat the two terms separately. The exchange part contribution of the self-energy for a generic state in reciprocal space reads[96]

$$\Sigma^{x}_{nk} = \langle nk|\Sigma^{x}|nk\rangle = -\sum_m \int_{BZ} \frac{d\boldsymbol{q}}{(2\pi)^3} \sum_{\boldsymbol{G}} \frac{|\rho_{nm}(\boldsymbol{k},\boldsymbol{q},\boldsymbol{G})|^2}{|\boldsymbol{q}+\boldsymbol{G}|^2} f_{m(\boldsymbol{k}-\boldsymbol{q})} \quad \text{B.3}$$

As we can see, the exchange part depends only on the occupied states. On the other hand, the correlation part of the self-energy depends on both occupied and unoccupied states and is a dynamical quantity. In a plane wave representation it reads[96]

$$\Sigma^{c}_{nk}(\omega) = \langle nk|\Sigma^{c}(\omega)|nk\rangle = i\sum_m \int_{BZ} \frac{d\boldsymbol{q}}{(2\pi)^3} \sum_{\boldsymbol{G},\boldsymbol{G}'} \frac{4\pi}{|\boldsymbol{q}+\boldsymbol{G}|^2} \rho_{nm}(\boldsymbol{k},\boldsymbol{q},\boldsymbol{G}) \rho^{*}_{nm}(\boldsymbol{k},\boldsymbol{q},\boldsymbol{G}')\, \lambda_{m,GG'}(k,q,\omega) \quad \text{B.4}$$

$$\lambda_{m,GG'}(k,q,\omega) = \int d\omega' G^{0}_{m\boldsymbol{k}-\boldsymbol{q}}(\omega-\omega') \varepsilon^{-1}_{\boldsymbol{G},\boldsymbol{G}'}(\boldsymbol{q},\omega') \quad \text{B.5}$$

$$\rho_{nm}(\boldsymbol{k},\boldsymbol{q},\boldsymbol{G}) = \langle n\boldsymbol{k}|exp(i(\boldsymbol{q}+\boldsymbol{G})\cdot\boldsymbol{r})|m\boldsymbol{k}-\boldsymbol{q}\rangle \quad \text{B.6}$$

where $n, \boldsymbol{k}, \boldsymbol{G}$ are band index, *Brillouin Zone (BZ) k*-point and reciprocal wavevector, respectively; $G^{0}_{m\boldsymbol{k}-\boldsymbol{q}}(\omega) = \frac{f_{n\boldsymbol{k}-\boldsymbol{q}}}{\omega-\varepsilon^{gKS}_{m,\boldsymbol{k}-\boldsymbol{q}}-i0^{+}} + \frac{1-f_{n\boldsymbol{k}-\boldsymbol{q}}}{\omega+\varepsilon^{gKS}_{m,\boldsymbol{k}-\boldsymbol{q}}+i0^{-}}$ is the non-interacting Green's function in the KS basis and $\varepsilon^{-1}_{\boldsymbol{G},\boldsymbol{G}'}(\boldsymbol{q},\omega')$ the inverse microscopic dielectric function. The energy integral in Eq. (B.4) is the most demanding part of the GW calculation and it can be solved once the inverse dielectric function is known. The equation of motion of the latter follows from that of the reducible response function[108,117,118] χ as

$$\varepsilon^{-1}_{GG'}(q,\omega) = \delta_{GG'} + \frac{4\pi}{|q+G|^2}\chi_{GG'}(q,\omega) \quad \text{B.7}$$

The GW approximation for the self-energy is obtained when χ is calculated within the random phase approximation (RPA) [108,117,118]

$$\chi_{GG'}(q,\omega) = \left[\delta_{GG'} - \frac{4\pi}{|q+G''|^2}\chi^{0}_{GG''}(q,\omega)\right]^{-1} \chi^{0}_{G''G'}(q,\omega) \quad \text{B.8}$$

where the repeated reciprocal wavevector index is summed over. The non-interacting response function in (B.8) is

$$\chi^{0}_{GG'}(q,\omega) = 2\sum_{nn'} \int_{BZ} \frac{dk}{(2\pi)^3} \rho^{*}_{n'n}(k,q,G)\rho_{n'n}(k,q,G') f_{nk-q}(1-f_{n'k}) \varrho_{nn',kk-q}(\omega) \quad \text{B.9}$$

$$\varrho_{nn',kk-q}(\omega) = \left[\frac{1}{\omega+\varepsilon^{gKS}_{n,\boldsymbol{k}-\boldsymbol{q}}-\varepsilon^{gKS}_{n',\boldsymbol{k}}+i0^{+}} - \frac{1}{\omega+\varepsilon^{gKS}_{n',\boldsymbol{k}}-\varepsilon^{gKS}_{n,\boldsymbol{k}-\boldsymbol{q}}-i0^{+}}\right] \quad \text{B.10}$$

We have adopted the plasmon-pole approximation (PPA) for the GW self-energy in which the inverse dielectric function (B.7) is approximated with a single pole function[96].

In order to solve the quasi-particle equation (B.1) one needs to know the value of the self-energy at the quasi-particle energy value itself. There are in general two ways to solve (B.1): either updating only the energies $E_{\tilde{n}}^{QP}$ until self-consistency which is called eigenvalue-only self-consistent *GW* (i.e., *evscf-GW*), or solve the non-linear quasi-particle equation (B.1) at first order[119,120], by expanding the self-energy around the KS values in this way

$$E_{\tilde{n}}^{QP} - \epsilon_{\tilde{n}}^{gKS} \approx Z_{\tilde{n}} \langle \tilde{n} | \Sigma(\epsilon_{\tilde{n}}^{gKS}) - V_{xc} | \tilde{n} \rangle \qquad \text{B.11}$$

where the normalization factor $Z_{\tilde{n}} = \left[1 - \frac{d\Sigma_{\tilde{n}}(\omega)}{d\omega}\Big|_{\omega=\epsilon_{\tilde{n}}^{gKS}} \right]^{-1}$. The latter is usually called one-shot *GW* (i.e., *G0W0*).

(3) Bethe-Salpeter calculation: optical absorption spectrum. The final step consists in the evaluation, through the Bethe-Salpeter equation[83,121], of the macroscopic dielectric function[122] $\varepsilon_M(\omega) = \lim_{q\to 0} \frac{1}{\varepsilon_{00}^{-1}(q,\omega)}$. The optical absorption spectrum corresponds to taking the imaginary part of the latter quantity, i.e. $\Im\varepsilon_M(\omega)$. This step consists in solving a (pseudo)eigenvalue problem by building an effective two-particle Hamiltonian in the space of transitions (i.e. $|cvk\rangle = |ck\rangle|vk\rangle$ where indices *ck, vk* refer to unoccupied/occupied states, respectively) between valence and conduction states[83,96]. The two-particle effective Hamiltonian matrix elements are given by

$$H_{\substack{cv\boldsymbol{k} \\ v'c'\boldsymbol{k}'}} = (\epsilon_{ck} - \epsilon_{vk})\delta_{vv'}\delta_{cc'}\delta_{kk'} + (f_{ck} - f_{vk})\left[2\bar{V}_{\substack{vck \\ v'c'k}} - W_{\substack{vck \\ v'c'k'}} \right] \qquad \text{B.12}$$

Where (*vc**k***) indicates pair of quasi-particle states *v**k*** and *c**k***. The first term on the RHS of (B.12) contains the quasi-particle energy differences (diagonal part). The second term is the BSE kernel which is the sum of the electron-hole exchange part[95] *V* (which stems from the Hartree potential but without the long range contribution $\boldsymbol{G} = 0$ since we are dealing with transverse excitations[123–125]) and the electron-hole attraction part *W* (which stems from the screened exchange potential[108,119,123,126]). The kernel both shifts (diagonal contribution) and couples (off-diagonal contributions) the quasi-particle energy differences.

$$\bar{V}_{\substack{vc\boldsymbol{k} \\ v'c'\boldsymbol{k}'}} = \frac{1}{\Omega}\sum_{\boldsymbol{G}\neq 0} \frac{4\pi}{|\boldsymbol{G}|^2} \langle v'\boldsymbol{k}' | e^{-i\boldsymbol{G}\cdot\boldsymbol{r}} | c'\boldsymbol{k}' \rangle \langle c\boldsymbol{k} | e^{i\boldsymbol{G}\cdot\boldsymbol{r}} | v\boldsymbol{k} \rangle \qquad \text{B.13}$$

$$W_{\substack{vc\boldsymbol{k} \\ v'c'\boldsymbol{k}'}} = \frac{1}{\Omega}\sum_{\boldsymbol{G},\boldsymbol{G}'} \frac{4\pi}{|\boldsymbol{q}+\boldsymbol{G}'|^2} \varepsilon_{\boldsymbol{G},\boldsymbol{G}'}^{-1}(\boldsymbol{q},\omega=0) \langle v'\boldsymbol{k}' | e^{-i(\boldsymbol{q}+\boldsymbol{G}')\boldsymbol{r}} | v\boldsymbol{k} \rangle \langle c\boldsymbol{k} | e^{i(\boldsymbol{q}+\boldsymbol{G}')\boldsymbol{r}} | c'k' \rangle \delta_{\boldsymbol{q},\boldsymbol{k}-\boldsymbol{k}'} \qquad \text{B.14}$$

Where Ω is the unit cell volume and the screened exchange potential (B.14) is evaluated using the inverse microscopic dielectric function in the static limit (i.e., $\lim_{\omega\to 0} \varepsilon^{-1}_{\boldsymbol{G},\boldsymbol{G}'}(\boldsymbol{q},\omega)$). The Hamiltonian (B.12) is in general non Hermitian due to the couplings between positive energy (i.e., excitations) and negative energy (i.e., de-excitations) electron-hole (*eh*) transitions. In the following simulations we adopted the Tamm-Dancoff approximation[127,128] in which only positive *eh* transitions are considered and the Hamiltonian becomes Hermitian. At the end, the macroscopic dielectric function can be expressed in terms of the eigenstates $|\lambda\rangle$ and eigenvalues E_λ of (B.12)

$$\varepsilon_M(\omega) = 1 - \lim_{\boldsymbol{q}\to 0} \frac{8\pi}{|q|^2 \Omega N_q} \sum_{\substack{vck \\ vck'}} \rho^*_{cv\boldsymbol{k}}(\boldsymbol{q}, \boldsymbol{G}=0)\rho_{c'v'\boldsymbol{k}'}(\boldsymbol{q}, \boldsymbol{G}'=0) \times \sum_\lambda \frac{A^\lambda_{cv\boldsymbol{k}}\left(A^\lambda_{c'v'\boldsymbol{k}'}\right)^*}{\omega - E_\lambda - i0^+} \qquad \text{B.15}$$

With $A^\lambda_{cv\boldsymbol{k}} = \langle cv\boldsymbol{k}|\lambda\rangle$ the eigenvectors of *H*, N_q the number of BZ k-points. The absorption spectrum is thus

$$\Im\varepsilon_M(\omega) = \lim_{\boldsymbol{q}\to 0} \frac{8\pi}{q^2} \sum_\lambda \left|\sum_{cv\boldsymbol{k}} A^\lambda_{cv\boldsymbol{k}} \left\langle c\boldsymbol{k}+\boldsymbol{q}\middle|e^{-i\boldsymbol{q}\boldsymbol{r}}\middle|v\boldsymbol{k}\right\rangle\right|^2 \delta(\omega - E_\lambda) = \sum_\lambda \xi_\lambda \delta(\omega - E_\lambda) \qquad \text{B.16}$$

Where $\xi_\lambda = \lim_{q\to 0} \frac{8\pi}{q^2} \left|\sum_{cv\boldsymbol{k}} A^\lambda_{cv\boldsymbol{k}} \left\langle c\boldsymbol{k}+\boldsymbol{q}\middle|e^{-i\boldsymbol{q}\boldsymbol{r}}\middle|v\boldsymbol{k}\right\rangle\right|^2$ is the oscillator strength associated to the excited state λ. Furthermore, from the knowledge of the transition amplitudes A^λ_{cvk} in the KS basis one can also plot the exciton wavefunctions $\Psi_\lambda(r_e, r_h) = \sum_{cvk} A^\lambda_{cv\boldsymbol{k}} \varphi_{c\boldsymbol{k}}(r_e)\varphi^*_{v\boldsymbol{k}}(r_h)$ where r_e (r_h) refers to electron (hole) position.

3.3 Appendix B2 – MBPT simulations additional material

Isolated push-pull molecule

Table I.1 – Homo-Lumo gKS and GW corrected gaps for the isolated push-pull chromophore $C_{24}H_{19}F_4N$ using different starting point self-consistent schemes.

starting gKS scf	gKS H-L gap (eV)	G_0W_0 H-L gap (eV)	evscf-GW (eV)
PBE	2.05	5.19	6.4
PBE0	3.56	5.98	6.52
CAM-B3LYP	5.57	6.46	6.59
B3LYP	3.25	5.85	6.44
H-F	8.42	7.09	6.91

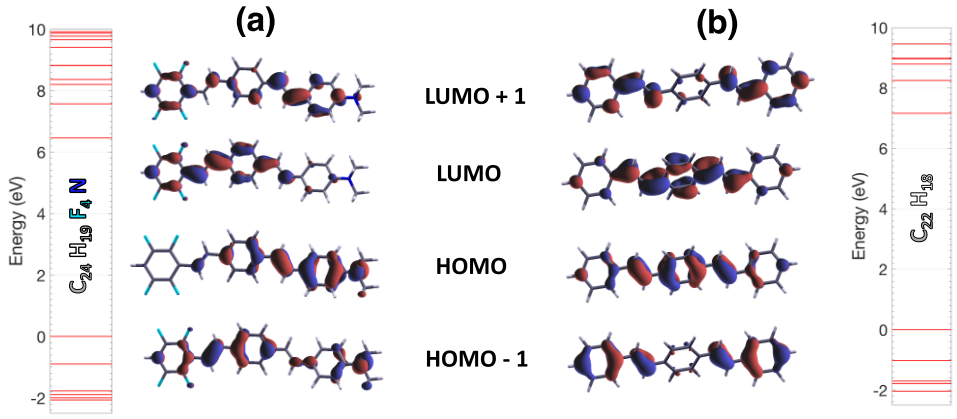

Figure B1 – (a) GW energy levels of isolated push-pull dye ($C_{24}H_{19}F_4N$) and (b) its counterpart without substituents ($C_{22}H_{18}$). HOMO levels of both systems have been put at 0 eV. We have reported also KS orbitals around H-G gap evaluated using cam-b3lyp xc-functional and cc-pVTZ localized basis. Isosurfaces fixed at 0.04 Bohr$^{-3/2}$.

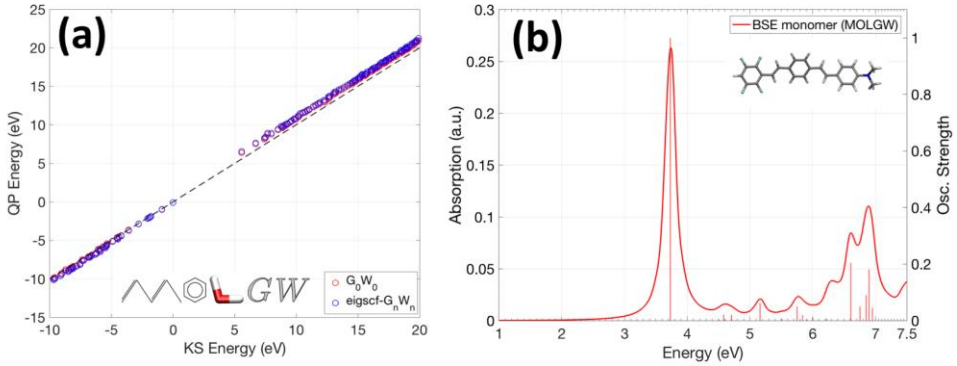

Figure B2 – Panel (a) GW Quasi-particle corrected energies for the push-pull monomer. In red are reported the corrected energies with one shot GW (i.e., G0W0) and in blue the corrected energies with eigenvalue only self-consistent GW (i.e., evscf-GW). In abscissa are reported the KS energies using the range separated cam-b3lyp xc-functional and zero value correspond to homo level. Dashed line is the bisector line. Panel (b) push-pull monomer BSE absorption spectrum where vertical bars represent the excited states whose heights are the oscillator strength normalized with respect to the maximum one. All the monomer simulations have been carried out with the localized basis code MOLGW[100].

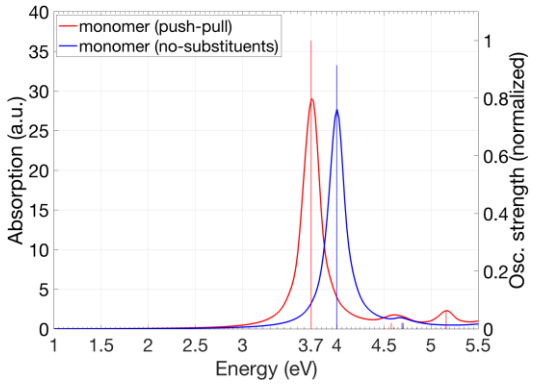

Figure B3 – optical absorption spectra of push-pull isolated organic dye (i.e., $C_{24}H_{19}F_4N$) and of its counterpart without substituents (i.e., $C_{22}H_{18}$)

Table B.1 – Energy decomposition of first seven excited states of push-pull dye $C_{24}H_{19}F_4N$. Energies expressed in eV. Only weights greater than 20% have been reported.

Excited state λ (eV)	**Osc. Stren.**	**Occupied level (v)**	**Unoccupied level (c)**	**Weight $\left\|A_{cv}^{\lambda}\right\|^2$**
3.73	2.44	H	L	0.76
4.50	0.01	H	L+3	0.40
4.58	0.05	H-2 H	L L+3	0.18 0.18
4.60	0.01	H-2	L	0.40
4.70	0.05	H-1	L	0.44
5.16	0.15	H-1 H	L L+1	0.20 0.40
5.51	0.02	H-3 H-1	L L+1	0.30 0.32

Table B.2 – Energy decomposition of non-polar molecule $C_{22}H_{18}$ first seven excited states. Energies expressed in eV. Only weights greater than 20% have been reported.

Excited state λ (eV)	**Osc. Stren.**	**Occupied level (v)**	**Unoccupied level (c)**	**Weight $\left\|A_{cv}^{\lambda}\right\|^2$**
4	2.23	H	L	0.90
4.69	0.05	H-4 H	L L+3	0.42 0.42
4.82	0	H-3 H	L L+4	0.20 0.20
4.85	0.01	H-3 H-2 H-1 H	L+1 L L+4 L+3	0.20 0.22 0.20 0.22
5.09	0	H-1 H	L L+1	0.48 0.32
5.49	0	H-1 H	L L+1	0.36 0.50
5.82	0.11	H-5 H-1	L L+1	0.22 0.20

J-aggregate bulk crystal

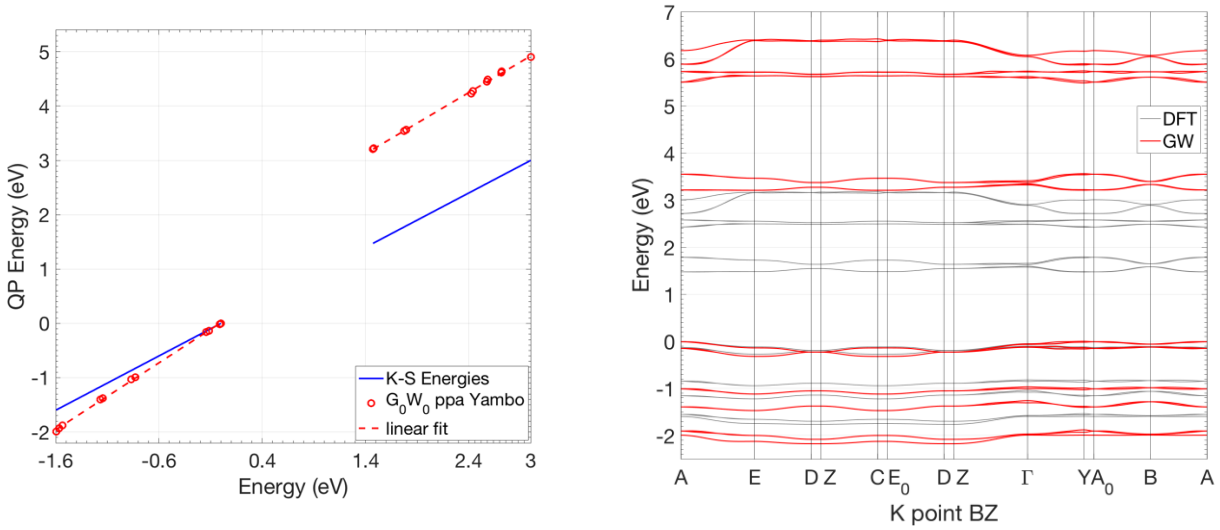

Figure B4 – Electronic band structure calculation for the bulk J-aggregate molecular crystal. (Left panel) quasiparticle G0W0 (using the plasmon-pole approximation) correction to KS single particle energies. The quasiparticle corrected values are measured with respect to the Homo corrected level (0 eV). The correction has been taken at the Y high symmetry point where the direct H-L gap is located and has been restricted to a symmetric window of 20 states around the H-L gap. In panel (b) we have reported the electronic DFT (gray) and GW (red) band structure.

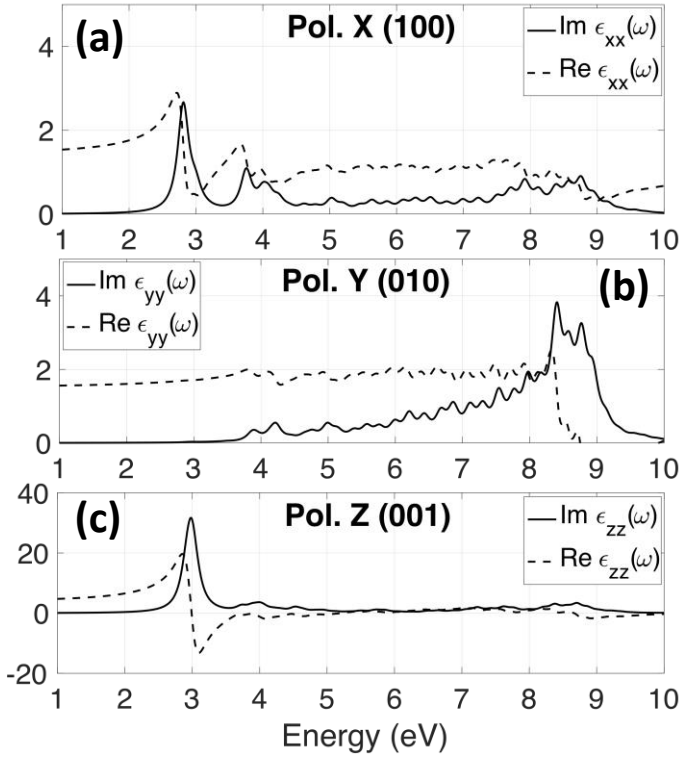

Figure B5 – Absorption optical spectra (solid line) of the push-pull J-aggregate, associated to three orthogonal exciting electric field polarizations: (a) along X (100), (b) along Y (010) and along Z (001); axes X, Y coincide with directions a, b of main text unit cell in Figure 1, while axis Z with the component of c perpendicular to a-b plane. We have reported as dashed lines the real parts of the macroscopic dielectric function for each polarization. The final absorption spectrum of the main text has been evaluated by taking the spatial average ($1/3\sum_{i=x,y,z}\varepsilon_{ii}(\omega)$) over these three absorption spectra.

Exciton, transition density plots and information of additional excited states

In the following we report some additional excited states of the J-aggregate with their associated exciton probability density (upper panel left) with fixed hole position in red dot, transition charge density plots (lower panel left) and information about the composition of the excited state (panel right). Excited states have been numbered in increasing energy order. In the tables, first and second columns report occupied and unoccupied KS orbitals involved in the excitation (VBM is valence band maximum, CBm conduction band minimum); third column reports the weight associated to the specific transition; fourth column the K-point in the BZ zone; last column the corresponding quasi-particle transition energy.

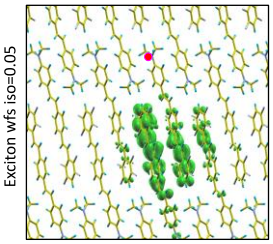

Excited state J_1 = 2.786 eV

Band occ	Band vir	Weight $\|A^{\lambda}_{cv}\|^2$ x10^{-1}	K-point BZ (rlu)	Energy (eV)
VBM	CBm+1	0.6349	(-0.4,0,0)	3.208
VBM	CBm+1	0.6343	(0.4,0,0)	3.208
VBM	CBm+1	0.6274	(0.4,0,-0.5)	3.210
VBM	CBm+1	0.6241	(-0.4,0,0.5)	3.210
VBM-1	CBm	0.5725	(-0.4,0,0.5)	3.213
VBM-1	CBm	0.5696	(0.4,0,-0.5)	3.213
VBM-1	CBm	0.5609	(-0.4,0,0)	3.217
VBM-1	CBm	0.5600	(0.4,0,0)	3.217
VBM-1	CBm	0.1483	(0.4,-0.33,-0.5)	3.298
VBM	CBm+1	0.1454	(0.2,0,0)	3.271
VBM	CBm+1	0.1454	(-0.2,0,0)	3.271
VBM	CBm	0.1413	(-0.4,0.33,0.5)	3.298
VBM	CBm+1	0.1374	(0.4,0.33,-0.5)	3.305
VBM-1	CBm	0.1351	(0.2,0,-0.5)	3.277
VBM-1	CBm	0.1344	(-0.2,0,0.5)	3.277
VBM-1	CBm+1	0.1195	(-0.4,-0.33,0.5)	3.305
VBM-1	CBm+1	0.1175	(-0.2,0,0.5)	3.277
VBM	CBm+1	0.1162	(0.2,0,-0.5)	3.277

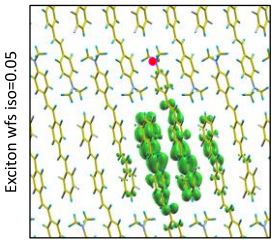

Excited state J_2 = 2.796 eV

Band occ	Band vir	Weight $\|A^{\lambda}_{cv}\|^2$ x10^{-1}	K-point BZ (rlu)	Energy (eV)
VBM	CBm+1	0.6349	(-0.4,0,0)	3.208
VBM	CBm+1	0.6343	(0.4,0,0)	3.208
VBM	CBm+1	0.6274	(0.4,0,-0.5)	3.210
VBM	CBm+1	0.6241	(-0.4,0,0.5)	3.210
VBM-1	CBm	0.5725	(-0.4,0,0.5)	3.213
VBM-1	CBm	0.5696	(0.4,0,-0.5)	3.213
VBM-1	CBm	0.5609	(-0.4,0,0)	3.217
VBM-1	CBm	0.5600	(0.4,0,0)	3.217
VBM	CBm	0.1483	(0.4,-0.33,-0.5)	3.298
VBM	CBm+1	0.1454	(0.2,0,0)	3.271
VBM	CBm+1	0.1454	(-0.2,0,0)	3.271
VBM	CBm	0.1413	(-0.4,0.33,0.5)	3.298
VBM-1	CBm+1	0.1374	(0.4,0.33,-0.5)	3.305
VBM-1	CBm	0.1351	(0.2,0,-0.5)	3.277
VBM-1	CBm	0.1344	(-0.2,0,0.5)	3.277
VBM-1	CBm+1	0.1195	(-0.4,-0.33,0.5)	3.305
VBM	CBm+1	0.1175	(-0.2,0,0.5)	3.277
VBM	CBm+1	0.1162	(0.2,0,-0.5)	3.277

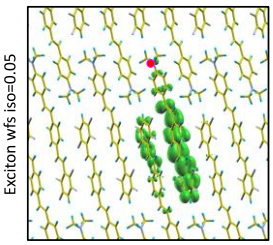

Excited state J_3 = 2.813 eV

Band occ	Band vir	Weight $\|A^{\lambda}_{cv}\|^2$ x10^{-1}	K-point BZ (rlu)	Energy (eV)
VBM-2	CBm+1	0.2404	(-0.4,0,0)	3.3190
VBM-2	CBm+1	0.2383	(-0.4,0,0.5)	3.3290
VBM-2	CBm+1	0.2304	(0.4,0,0)	3.3190
VBM-3	CBm	0.2248	(-0.4,0,0)	3.3410
VBM-3	CBm	0.2239	(0.4,0,-0.5)	3.3310
VBM-3	CBm	0.2224	(-0.4,0,0.5)	3.3310
VBM-2	CBm+1	0.2095	(0.4,0,-0.5)	3.3290
VBM-3	CBm	0.2060	(0.4,0,0)	3.3410
VBM-2	CBm+1	0.1803	(-0.2,0,0)	3.3430
VBM-3	CBm	0.1686	(-0.2,0,0)	3.3740
VBM-2	CBm+1	0.1678	(0.2,0,-0.5)	3.3570
VBM-3	CBm	0.1673	(-0.2,0,0.5)	3.3670
VBM-2	CBm+1	0.1648	(-0.2,0,0.5)	3.3570
VBM-3	CBm	0.1466	(0.2,0,0)	3.3740
VBM-1	CBm+1	0.1356	(0,0,0)	3.3810
VBM-2	CBm+1	0.1345	(0,2,0,0)	3.3430
VBM-3	CBm	0.1293	(0,0,0)	3.412
VBM-3	CBm	0.1227	(0.2,0,-0.5)	3.3670

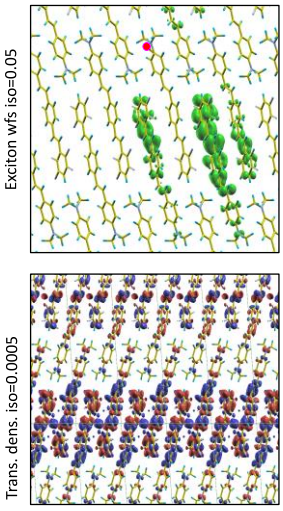

Excited state J_{16} = 2.986 eV

Band occ	Band vir	Weight $\|A^{\lambda}_{cv}\|^2$ x10^{-1}	K-point BZ (rlu)	Energy (eV)
VBM	CBm+1	0.5673	(0,0,0)	3.364
VBM-1	CBm+1C	0.4035	(0,0,-0.5)	3.361
VBM-2	Bm	0.3089	(0.2,0,-0.5)	3.350
VBM-2	CBm	0.2728	(-0.2,0,0.5)	3.350
VBM	CBm	0.2726	(0,0,-0.5)	3.360
VBM-2	CBm	0.2654	(0,0,0.5)	3.331
VBM-1	CBm	0.2523	(0.4,0,0)	3.217
VBM-2	CBm	0.2262	(0.2,0,0)	3.331
VBM-1	CBm	0.2223	(-0.4,0,0)	3.217
VBM-3	CBm+1	0.2196	(0.2,0,0)	3.386
VBM-2	CBm	0.2191	(0,0,0)	3.398
VBM	CBm+1	0.1905	(-0.2,0,0)	3.271
VBM-3	CBm+1	0.1771	(-0.2,0,0)	3.386
VBM	CBm+1	0.1620	(0.2,0,0)	3.271
VBM-3	CBm+1	0.1480	(0.2,0,-0.5)	3.375
VBM-1	CBm	0.1478	(-0.2,0,0.5)	3.277
VBM-3	CBm+1	0.1432	(-0.2,0,0.5)	3.375
VBM	CBm+1	0.1300	(0,0,-0.5)	3.360
VBM-1	CBm	0.1197	(0.2,0,-0.5)	3.277
VBM-3	CBm+1	0.1156	(-0.4,0,0.5)	3.332
VBM	CBm+1	0.1122	(0,-0.33,0)	3.440
VBM	CBm+1	0.1114	(0,0.33,0)	3.440
VBM-3	CBm+1	0.1095	(0.4,0,-0.5)	3.332

Exciton wfs iso=0.05

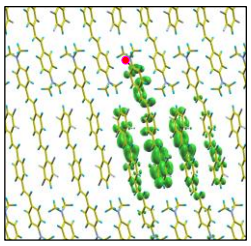

Trans. dens. iso=0.0005

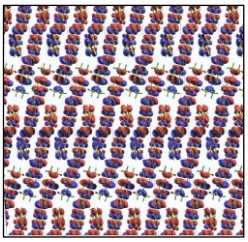

Excited state J_{483} = 3.752 eV

Band occ	Band vir	Weight $\lvert A^{\lambda}_{cv}\rvert^2 \times 10^{-1}$	K-point BZ (rlu)	Energy (eV)
VBM-4	CBm+1	0.2273	(0,0,0)	4.134
VBM-4	CBm	0.2252	(0.2,0,-0.5)	4.058
VBM-4	CBm	0.2242	(-0.2,0,0.5)	4.058
VBM-4	CBm	0.2102	(0.2,0,0)	4.069
VBM-4	CBm	0.2086	(-0.2,0,0)	4.069
VBM-5	CBm	0.2048	(0,0,0)	4.150
VBM-4	CBm	0.1901	(0,0,-0.5)	4.138
VBM-5	CBm+1	0.1895	(0,0,-0.5)	4.138
VBM-5	CBm+1	0.1797	(0.2,0,0)	4.092
VBM-5	CBm+1	0.1796	(-0.2,0,0)	4.092
VBM-4	CBm+1	0.1774	(0,0.33,0)	4.150
VBM-4	CBm+1	0.1774	(0,-0.33,0)	4.150
VBM-5	CBm	0.1705	(0,-0.33,0)	4.154
VBM-5	CBm	0.1705	(0,0.33,0)	4.154
VBM-5	CBm+1	0.1697	(0.2,0,-0-5)	4.104
VBM-5	CBm+1	0.1685	(-0.2,0,0.5)	4.104
VBM-4	CBm	0.1344	(-0.2,-0.33,0)	4.115
VBM-4	CBm	0.1337	(0.2,0.33,0)	4.115
VBM-4	CBm	0.1329	(0.2,0.33,0)	4.115
VBM-4	CBm	0.1319	(-0.2,0.33,0)	4.115

Exciton wfs iso=0.05

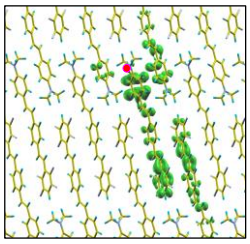

Trans. dens. iso=0.0005

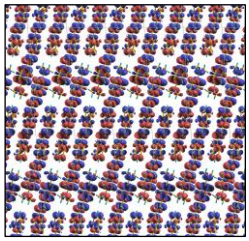

Excited state J_{505} = 4.03 eV

Band occ	Band vir	Weight $\lvert A^{\lambda}_{cv}\rvert^2 \times 10^{-1}$	K-point BZ (rlu)	Energy (eV)
VBM-4	CBm+1	0.4729	(0.4,0,-0.5)	4.041
VBM-4	CBm+1	0.3806	(-0.4,0,0.5)	4.041
VBM-5	CBm	0.1896	(0.4,0,-0.5)	4.054
VBM-1	CBm+5	0.1760	(0.4,0,0)	4.184
VBM-1	CBm+5	0.1717	(-0.4,0,0)	4.184
VBM	CBm+5	0.1461	(-0.4,0,0.5)	4.170
VBM-7	CBm	0.1400	(0.4,0,0)	4.352
VBM	CBm+5	0.1395	(0.4,0,-0.5)	4.170
VBM-7	CBm	0.1358	(-0.4,0,0)	4.352
VBM-7	CBm+1	0.1311	(-0.4,0,0.5)	4.356
VBM-4	CBm	0.1297	(-0.4,0,0.5)	4.054
VBM-7	CBm+1	0.1273	(0.4,0,0.5)	4.356

Chapter IV – Quantifying the plasmonic character of optical excitations in molecular crystals

While in the previous chapters we have discussed only in a qualitative way the character of the optical excitations in a push-pull molecular J-aggregate, in this part we shall give more a quantitative measure of them, focusing on the *J-band*. Since this is still an ongoing project and results are only partial thus far, we will concentrate the discussion only on the quantification of the collective *plasmonic character* of the optical excitations. We plan, in a future work, to quantify also the collective *excitonic character*. For "*plasmonic character*" of an excitation we mean a measure of the collective and coherent behavior of the electron motion which also relates to the ability to provide field enhancement[129–135].

The specific interest to investigate and quantify the plasmonic behavior in a molecular J-aggregate is principally driven by the question wheatear or not any strong absorption band such as the J-band with some sort of collective character in its microscopic origin, shares the status of plasmon.

In order to quantify the plasmonic behavior, we use as a metric the Generalized Plasmonicity Index (GPI) introduced recently by *Zhang et al*[136]. in the context of molecular and nanoplasmonics. This index is a frequency dependent function which, when evaluated at a specific resonance frequency corresponding to an electronic excitation of the system, is a measure of the quality factor and of the collective and coherent character of that excitation. This index represents a promising general way to define and quantify the plasmonic character of an electronic excitation both for an extended (e.g. molecular crystal, solid, etc.) and for a finite system (nanostructure, molecule, clusters, etc.).

By using a MBPT approach (from the results showed in the previous Chapter), we have evaluated the GPI for the lowest excited state of the single push-pull molecule and for some excited states within the J-band of the molecular J-aggregate. The results revealed that the excited states within the J-band have always lower GPIs with respect to the monomer. In order to rationalize this result, we have formulated a

simple theoretical analytical model of a one-dimensional linear J-aggregate which predicts that the J-band of the aggregate is always less plasmonic than the single monomer and that the negative plasmonic energy variation between the two exactly corresponds to the red-shift of the J-band with respect to the monomer first excited state.

With this study we demonstrate two facts: (1) the *J-band* of a molecular J-aggregate manifests always lower plasmonic character with respect to the single molecular unit it is composed of and (2) bright excitations in molecular systems, even when coming from a collective mechanism, may well have no relation with plasmons.

In the following we put the results in the form of a drafted paper that we submitted for publication in scientific international journal

4.1 Quantifying the plasmonic character of optical excitations in a molecular J-aggregate

Michele Guerrini[1,2], Arrigo Calzolari[2], Daniele Varsano[2] and Stefano Corni[2,3]*

[1]Dipartimento FIM, Università di Modena e Reggio Emilia, I-41125 Modena, Italy

[2]CNR Nano Istituto Nanoscienze, Centro S3, I-41125 Modena, Italy

[3]Dipartimento di Scienze Chimiche, Università di Padova, Italy

Keywords *– J-aggregates, push-pull dye, molecular plasmon, nanoplasmonics, many-body perturbation theory*

ABSTRACT: The definition of plasmon at the microscopic scale is far from being understood. Yet, it is very important to recognize plasmonic features in optical excitations, as they can inspire new application and trigger new discoveries by analogy with the rich phenomenology of metal nanoparticle plasmons, as exemplified by the recent discovery of plasmons in molecular systems. Recently, the concepts of plasmonicity index and the generalized plasmonicity index (GPI) have been devised as computational tools to quantify the plasmonic nature of optical excitations. The question may arise whether any strong absorption band, possibly with some sort of collective character in its microscopic origin, shares the status of plasmon. Here we demonstrate that this is not the case, by considering a well-known class of systems whose characteristic low-energy absorption band, although absorbing strongly and involving the collective excitation of many molecules, is recognized as not specifically plasmonic by the GPI. Such counterexample is represented by J-aggregates molecular crystals, characterized by the intense and narrow J-band. By means of first-principles simulations, based on a many-body perturbation theory formalism, we investigate the optical properties of a J-aggregate made of push-pull organic dyes and show that the effect of aggregation is to lower the GPI associated to the J-band with respect to the one associated to the isolated dye. In order to rationalize our finding, we then propose a simplified one-dimensional theoretical model of the J-aggregate. A useful microscopic picture of what discriminates a collective molecular crystal excitation from a plasmon is eventually obtained.

INTRODUCTION

The identification and quantification of plasmonic excitations in nano- and molecular systems is an important issue in the field of nanoplasmonics. In fact, the rich physics and technological potential of plasmonic metal nanoparticles has triggered the question whether other nanosystems also possess excitations with such plasmonic character, to some degree, and thus a similar phenomenology. Graphene and its nanoconfined structures (polycyclic aromatic hydrocarbons in the molecular limit) attracted a lot of attention in this respect.[1,2] This important motivation goes along with the goal of establishing the characters of localized surface plasmon excitations at a deeper microscopic level than the widespread treatment based on continuum electrodynamics. A relevant point to asses in this context is whether any strong absorption band with some sort of collective character in its microscopic origin, shares the status of plasmon or not. A positive answer (i.e., all strong excitations are plasmons) would in fact rather belittle the quest for plasmon-like excitations, and contradict the well-estabished physics of other collective excitations such as excitons.

Ideal systems to be investigated in this respect are J-aggregates. J-aggregates are a class of molecular crystals with special known optical properties as an intense, narrow absorption peak (known as J-band) that appears at low energy where the single isolated monomer unit has almost zero absorption[3] and the ability to give delocalize excitons.[4] These features have been thoroughly studied in the literature[4–7] and are the result of the (strong) intermolecular coupling, which causes delocalization of the electronic excitations of the single molecule over many sites of the aggregate[8,9]. Therefore, the J-band (i) is characterized by a strong absorption cross section, (ii) requires aggregation at the nanoscale, and (iii) has a microscopic origin rooted in a collective effect. In this light, J-band seems to bear a similarity with the localized surface plasmons in metallic nano-particles (i.e. high absorption cross section, a prominent role in nanoscopic systems and a collective origin)[10–15].

The focus of this work is specifically to quantify whether the J-band in the solid-state J-aggregate has a larger or smaller plasmonic character than its correspondig single isolated molecule. In doing this, we will respond to the underlying

question whether the J-band implies a plasmon-like response. To characterize the plasmonic character, we shall use the recently proposed generalized plasmonicity index[16] (GPI). The GPI is a frequency dependent adimensional function, that has been thoroughly tested in a wide range of nanostructures, including metallic nanoparticles, silicon clusters, graphene nanostructures, PAHs at various level of theory (classical electrodynamics, tight-binding, jellium and atomistic TDDFT)[16]. It improves over the plasmonicity index (PI) previously proposed by *Bursi at al.*[17] to quantify the difference between plasmonic and single-particle electronic transitions in finite structures. In the present work we not only exploit GPI, but we move one step further in two methodological aspects: on the one hand we shall use an alternative level of theory to TDDFT, namely many-body perturbation theory (MBPT), which is based on Green's function formalism and has a higher accuracy. On the other hand we shall compute the GPI also for a macroscopic extended system such as a molecular J-aggregate,[6,18,19] beside the single molecule it is composed of.

We focus in particular on a J-aggregate molecular crystal composed of the organic conjugated dye 4-(N,N-dimethyl-amino)-4-(2,3,5,6-tetra-fluorostyryl)-stilbene[20] (see Figure 1). This dye is a push-pull system[21,22] that possesses an intrinsic static electric dipole due to the presence of the dimethylamino group (push) and the fluorinated aromatic ring (pull) group. We have chosen to investigate this particular push-pull organic dye for several reasons: (i) the fact that it is a realistic complex system, yet not too demanding to be simulated by accurate computational techniques; (ii) the availability of its J-aggregate experimental X-ray crystal structure and of the optical absorption spectra[20]; (iii) its charge neutrality that makes it computationally convenient (no counter ions to simulate) but still electrostatically not trivial, due to its ground state static dipole moment.

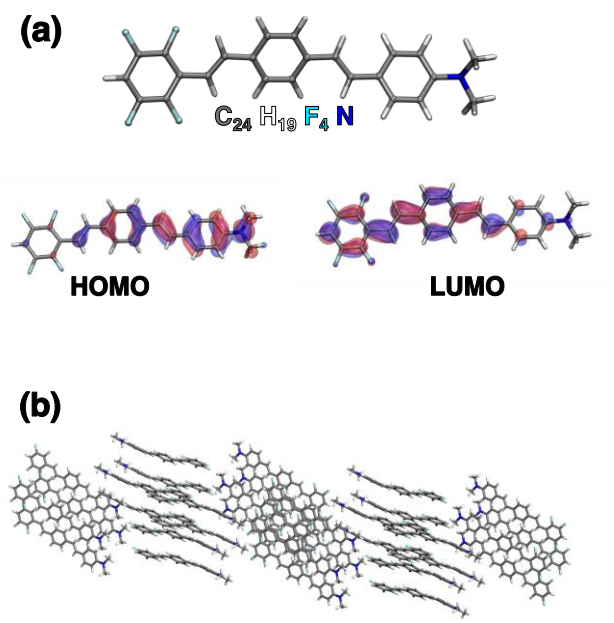

Figure 1 – Atomic structure of (a) 4-(N,N-dimethyl-amino)-4-(2,3,5,6-tetra-fluorostyryl)-stilbene push-pull single molecule and (b) partial 3D view of the J-aggregate molecular crystal composed of push-pull organic dyes investigated in this work. Insets in panel (a) show isosurface plots of the highest occupied (i.e., HOMO) and lowest unoccupied (i.e., LUMO) molecular orbitals of the single molecule evaluated at DFT level (cam-b3lyp xc-functional).

METHOD

GENERALIZED PLASMONICITY INDEX AT MBPT LEVEL The GPI[16] $\eta(\omega)$ is a functional of the induced charge density $\delta n(\mathrm{r},\omega)$ and of the external potential $v_{ext}(r',\omega)$ for a fixed excitation frequency ω. For convenience, we report here its formal expression

$$\eta(\omega) = \left|\frac{\int v^*_{ind}(r,\omega)\delta n(r,\omega)d^3r}{\int v^*_{ext}(r',\omega)\delta n(r',\omega)d^3r'}\right|, \quad (1)$$

where the induced Coulomb potential $v_{ind}(r,\omega)$ and the linear induced charge density $\delta n(\mathrm{r},\omega)$ are reported in Eq. (2)-(3), respectively

$$v_{ind}(r,\omega) = \int \frac{\delta n(r,\omega)}{|r-r'|}d^3r' \,, \quad (2)$$

$$\delta n(r,\omega) = \int \chi(r,r',\omega)v_{ext}(r',\omega)d^3r'. \quad (3)$$

The charge density variation at first order in Eq. (3) is obtained through the density-density correlation function causal kernel[23] $\chi(r,r',\omega)$. The poles of the latter (i.e., the resonance frequencies ω_ξ) give the electronic excitation energies $\hbar\omega_\xi$ of the system. When evaluated at a given resonance frequency ω_ξ , the GPI can be expressed as $\eta(\omega_\xi) \approx \Gamma^{-1}E^{plas}_\xi$, where Γ^{-1} is the excited state lifetime and E^{plas}_ξ is the plasmonic energy associated to the transition density $\rho_\xi(r)$, that represents the plasmonic contribution to the total excitation energy $\hbar\omega_\xi$

$$E^{plas}_\xi = \int \frac{\rho^*_\xi(r)\rho_\xi(r')}{|r-r'|}d^3rd^3r' = \sum_{ai}\left(C^\xi_{ai}\right)^* C^\xi_{a'i'}\int \frac{d^*_{ai}(r)d_{a'i'}(r')}{|r-r'|}d^3rd^3r' \quad (4)$$

$$\rho_\xi(r) = \langle\xi|\hat{\Psi}^\dagger(r)\hat{\Psi}(r)|0\rangle = \sum_{ai} C^\xi_{ai}d_{ai}(r) = \sum_{ai} C^\xi_{ai}\varphi^*_a(r)\varphi_i(r) \,, \quad (5)$$

$$\hat{\Psi}(\mathrm{r}) = \sum_n \varphi_n(r)\hat{c}_n \quad , \quad C^\xi_{ai} = \langle\xi|\hat{c}^\dagger_a\hat{c}_i|0\rangle \,. \quad (6)$$

Where in the second part of Eq. (4) we have re-expressed the transition density $\rho_\xi(r)$ as in Eq. (5) using an electron-hole space representation where index *a* (*i*) is associated to an empty (occupied) electronic state and C^ξ_{ai} is the amplitude coefficient associated to a transition from *i-th* to *a-th* electronic state.

In metal nanoparticles, the width of a plasmonic band (and thus Γ^{-1} in the GPI) is largely determined by the Landau damping mechanism[24], hallmark of the mixing of the plasmon with the continuum of single-particle excitations. Band broadening in molecules is instead dominated by inhomogeneous broadening plus vibronic effects, i.e., environmental and nuclei-related (not electron related) phenomena. Here we used a fixed Γ^{-1} value representative of electronic effects only.

In the present work we are calculating excitation energies, transition densities and consequently plasmonic energies starting from electronic structure simulation evaluated within the many-body perturbation theory (MBPT) framework. This assures an accurate treatment of excitations in molecular crystals, especially in the description of charge transfer effects[25,26]. Plasmonic energies are calculated as in Eq. (4), with transition densities coming from solution of the Bethe-Salpeter equation (BSE)[27].

RESULTS

DISCUSSION – Figure 2 shows the MBPT optical spectra of the single molecule and the bulk J-aggregate crystal (Figure 1). We observe the formation of the characteristic J-band that is red-shifted with respect to the isolated push-pull monomer principal peak *P*, in agreement with experimental and previous TDDFT results[20,28]. The red shifted J-band which dominates the absorption spectrum is composed not just of the principal bright transition J_1 at ~ 3 eV, but it gathers together many other optical transitions, with lower intensity. The inspection of the transition charge density (TCD) of the dominant excitation J_1 (inset of Figure 2(b)) indicates that the TCD is evidently displaced along linear molecular chains pointing along the longest axis of the crystal. Such inter-molecular head-to-tail dipolar arrangement is a typical manifestation of J-aggregate behavior[19] and results in a coherent alignment of each monomer transition dipole, giving the strong total oscillator strength of the main peak at ~3 eV.

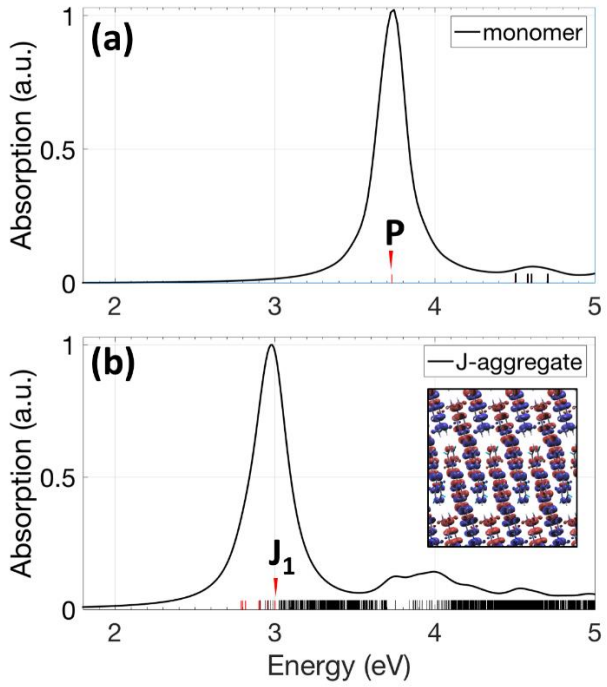

Figure 2 –Absorption optical spectra of (a) the single monomer and (b) its molecular J-aggregate. Spectra have been normalized with respect to the maximum value. The vertical bars indicate the position of the excited states (in red those that have been analyzed in the text). Specific excitations analyzed in the text are marked. Inset of panel (b) shows the isosurface plot of the transition charge density associated to excited state J_1 belonging to the dominant peak of the J-band; red (blue) is associated to positive (negative) charge.

TABLE I Selected excited states within J-band, their associated plasmonic energy, plasmonic energy variation $\Delta E_{\xi_k}^{plas} = E_{\xi_k}^{plas} - E_P^{plas}$ and GPI variation $\Delta\eta_{\xi_k} = \eta_{\xi_k} - \eta_P$ and ratio η_{ξ_k}/η_P with respect to monomer lowest energy optically active excited state P = 3.73 eV (linewidth fixed at Γ = 0.4 eV for all excited states; $E_P^{plas} = 0.68$ eV and $\eta_P = \Gamma^{-1}E_P^{plas} = 1.7$)

Excited state ξ_k	$E_{\xi_k}^{plas}$	$\Delta E_{\xi_k}^{plas}$	η_{ξ_k}	$\Delta\eta_{\xi_k}$	η_{ξ_k}/η_P
J_1 3 eV	0.072 eV	-0.608 eV	0.18	-1.52	0.1059
J_2 2.951 eV	0.008 eV	-0.672 eV	0.02	-1.68	0.0118
J_3 2.905 eV	0.020 eV	-0.66 eV	0.05	-1.65	0.0294
J_4 2.897 eV	0.011 eV	-0.833 eV	0.03	-1.67	0.0176
J_5 2.813 eV	0.349 eV	-0.331 eV	0.87	-0.83	0.5118
J_6 2.796 eV	0.111 eV	-0.57 eV	0.28	-1.42	0.1647
J_7 2.786 eV	0.116 eV	-0.56 eV	0.29	-1.41	0.1706

Furthermore, the constituent monomers manifest also a certain degree of intra-molecular charge transfer behavior, which is compatible with their push-pull character[22,29]. By inspection of Table I, we conclude that all the analyzed excited states within the J-band (i.e., $J_1 - J_7$), have always *lower* plasmonic energy and GPI values than those corresponding to the monomer lowest energy excited state *P* = 3.73 eV (panel a).

This is the key result of this work: GPI signals that the collective J-band of the molecular aggregate is *less* plasmonic than the single molecule, or in other terms, GPI identifies the J-band as non-plasmonic. This result is relevant also because it confirms the ability of the GPI to quantify the plasmonic character of excitations independently from their absorption intensity even for the molecular world (for nanoparticles it was already shown in Ref.[16]). In other words, the GPI do not simply remap strong absorption bands into plasmonic ones, but adds important independent information.

UNDERSTANDING THE GPI REDUCTION UPON AGGREGATION: A ONE-DIMENSIONAL MODEL BASED ON MOLECULAR EXCITON THEORY – In this section we present a simple theoretical model which turns out to be useful to rationalize and explain the reduction in the GPI values when moving from the single isolated molecule to the molecular aggregate, as observed in the previously presented numerical results. For the sake of simplicity we consider a one-dimensional aggregate (i.e., a 1D molecular chain) and we refer to its electronic excited state as *a molecular chain exciton, i.e.* an electronic excitation delocalized over several identical monomer units. Using a simple Frenkel Hamiltonian[6,19,30–33] model to describe the 1D aggregate, under periodic boundary conditions and for low lying excited states, the exciton eigenstates of an aggregate chain composed of *M* molecules have the following form[6,30,34]

$$|\xi_k\rangle = \frac{1}{\sqrt{M}}\sum_{m=1}^{M} e^{i\frac{2\pi}{M}km}|\lambda_m\rangle\,, \quad -M/2 \le k \le M/2 \qquad (7)$$

where $|\lambda_m\rangle = |\varphi_{exc}^m\rangle\prod_{n\neq m}|\varphi_{GS}^n\rangle$, $|\varphi_{exc}^m\rangle$ indicates the m-*th* monomer being in an electronic excited state and $|\varphi_{GS}^n\rangle$ the n-*th* monomer in the ground state. We have used Eq. (7), representing the molecular chain excited states, to derive the expression of the GPI within this model. In the GW/BSE simulations we assumed a fixed linewidth (damping) Γ. We can evaluate the molecular chain transition density (MCTD) $\rho_k^{pol}(\boldsymbol{r}) = \langle 0|\hat{\Psi}^\dagger(r)\hat{\Psi}(r)|\xi_k\rangle$ between the ground state $|0\rangle$ and a specific excited state $|\xi_k\rangle$ of the 1D aggregate, and then use it to obtain the resulting plasmonic energy [see Sec. I of Supporting Information (SI) for the derivation]

$$E_{\xi_k}^{plas} = \int \frac{\rho_k^{*pol}(\boldsymbol{r})\rho_k^{pol}(\boldsymbol{r'})}{|\boldsymbol{r}-\boldsymbol{r'}|}d\boldsymbol{r}d\boldsymbol{r'} = E_{exc}^{plas} + W(k), \qquad (8)$$

$$W(k) = \frac{1}{M}\sum_{m\neq m'} J_{mm'}e^{i\frac{2\pi}{M}(m-m')k}, \qquad (9)$$

where

$$\rho_k^{pol}(r) = = \frac{1}{\sqrt{M}}\sum_m e^{i\frac{2\pi}{M}km}\rho_{exc}^{mon}(r-R_m), \qquad (10)$$

$$\rho_{exc}^{mon}(r-R_m) = \langle\varphi_{GS}^m|\hat{\Psi}^\dagger(r)\hat{\Psi}(r)|\varphi_{exc}^m\rangle, \qquad (11)$$

$$J_{mm'} = \int \frac{\rho_{exc}^{*mon}(r-R_m)\rho_{exc}^{mon}(r'-R_{m'})}{|r-r'|}\mathrm{d}\boldsymbol{r}d\boldsymbol{r'}. \qquad (12)$$

Thus, by virtue of Eq. (8), the plasmonic energy associated to each excitonic level of the aggregate is given by the plasmonic energy of the monomer excited state plus a correction term $W(k) = \langle\xi_k|\hat{H}|\xi_k\rangle - \langle\lambda_m|\hat{H}|\lambda_m\rangle$, $\hat{H}$ being the molecular aggregate Hamiltonian operator, whose sign and magnitude depend on the interactions between the monomers transition densities $\rho_{exc}^{mon}(r'-R_{m'})$ composing the aggregate. The terms in (12) quantify the amount of inter-molecular coupling, i.e., the energy transfer rate between m-*th* and m'-*th* monomers through the interaction between their transition densities[30,35]. Within the point-dipole approximation, the coupling terms $J_{mm'}$ can be expressed as (see Sec. I of SI)

$$J_{mm'} = \frac{K_{mm'} - 3(\boldsymbol{\mu}_m^{mon}\cdot\bar{R})\left(\boldsymbol{\mu}_{m'}^{mon}\cdot\bar{R}\right)}{R_{mm'}^3}\,, \qquad (13)$$

where $K_{mm'} = \boldsymbol{\mu}_m^{mon}\cdot\boldsymbol{\mu}_{m'}^{mon}$, and $\boldsymbol{\mu}_m^{mon} = \langle\varphi_{GS}^m|\hat{\Psi}^\dagger(r)r\hat{\Psi}(r)|\varphi_{exc}^m\rangle$ is m-th monomer transition dipole; $R_{mm'} = |\vec{R}_m - \vec{R}_{m'}|$ is the distance between centers of m-th and m'-th monomers and $\bar{R}$ the associated unit vector. Assuming all equal transition dipoles and with the same relative orientation (i.e., $\boldsymbol{\mu}_m^{mon} = \boldsymbol{\mu}$ and $K_{mm'} = K$), one can demonstrate (see Sec. I of SI) that for a linear periodic chain aggregate there is a non-vanishing total transition dipole only for the excited state ξ_0 (i.e., $k = 0$), which in fact corresponds to the J-band of this simple 1D model.

We can now proceed to evaluate the GPI variation between the two states $|\xi_0\rangle$ and $|\varphi_{exc}\rangle$, which are the lowest energy excited states of the chain and the isolated monomer, respectively. For $|\xi_0\rangle$ the total transition dipole results as a coherent sum of the molecular transition dipoles, being all aligned and pointing in the same direction (the emission from this state to the ground state leads to superradiance[36]). As a rough approximation of the MCTD for $|\xi_0\rangle$, we assume a toy model composed of aligned finite-size dipoles of length *d*, arranged at a nearest neighbor distance $R = d + a$ as sketched in the inset of Figure 3(a). Here, we have assumed unitary charge and unit length dipoles (i.e. $d = 1$ nm)

and considered different inter-molecular distances by varying the parameter a . By virtue of Eq. (8), the energy shift term $W(k)$ physically represents the plasmonic energy variation between the monomer and the molecular chain aggregate. In turn, we can obtain the GPI variation from the single molecule excitation to the J-band as

$$\Delta\eta_{\xi_0} \approx \Gamma^{-1}\left(E_{\xi_0}^{plas,pol} - E_{exc}^{plas,mon}\right) = \Gamma^{-1}\Delta E_{\xi_0}^{plas} , \tag{14}$$

$$\Delta E_{\xi_0}^{plas} = \frac{1}{M}\sum_{m\neq m'} J_{|m-m'|} = \frac{2}{M}\sum_{n=1}^{M-1}(M-n)\tilde{J}_n < \\ < -\frac{4}{R}\left(\frac{M-1}{M}\right)(\gamma^2-1)^{-1} , \quad \gamma = \frac{R}{d} \tag{15}$$

$$J_{|m-m'|} = 2|D_{mm'}|^{-1} - |D_{mm'} + d|^{-1} - |D_{mm'} - d|^{-1} = \\ = \tilde{J}_{n=|m-m'|} \tag{16}$$

where $D_{mm'} = R_m - R_{m'} = (m-m')R$ is the distance between m-*th* and m'-*th* monomers within the molecular aggregate. The upper limit in Eq. (15) comes from the nearest-neighbors approximation, i.e. the sum in Eq. (15) is approximated by considering only those monomer indices for which $|m-m'| = 1$.

It is straightforward to verify that the coupling terms $\tilde{J}_n$ in Eq. (16) are always negative [for further details and derivations of Eqs. (15)-(16) consult Sec. II of SI].

Figure 3(a) shows GPI variation, i.e. Eq. (14), as a function of the total number of monomers and considering different nearest neighbor monomer separations R. GPI variation is always negative, which means that the main bright transition (i.e., the J-band) in this linear J-aggregate is always *less* plasmonic than that in the isolated monomer. The reason for this behavior resides into the intra-chain Coulomb couplings between monomers: when the transition dipoles of nearby molecules are parallelly aligned, the dipole-dipole interaction decreases the Coulomb energy needed to set up the overall transition density, and consequently the plasmonic energy. As demonstrated by the upper bound in (15), the closer the monomers (i.e., γ approaching 1) the more effective it is this effect.

To fully appreciate the difference with a clearly plasmonic transition, we compare the plasmonic energy for the lowest energy transition (i.e., k = 0) of this molecular aggregate 1D model with an equally schematic approach of a 1D quantum wire. To be comparable in terms of oscillator strength, the latter is characterized by a transition dipole as the one represented in the inset of Figure 3(b): two point-charges of opposite signs, with the same magnitude as the ones used for each molecule, but placed at the ends of the wire. In Figure 3(b) we reported the difference between the GPI of the lowest

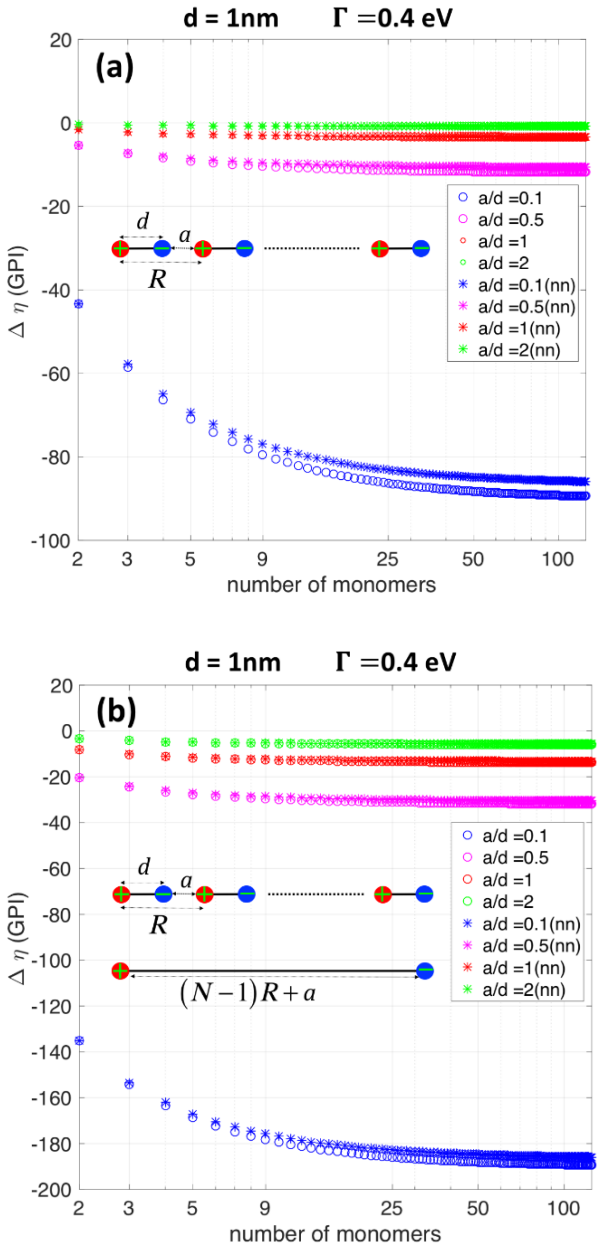

Figure 3 – Difference between GPI index of a linear 1D J-aggregate and of the single monomer unit (a) or a wire of same aggregate length (b), with respect to the total number of monomers in the molecular chain and by varying inter-molecular distances R. The GPI of the linear chain is associated to the lowest energy excited state (i.e. k = 0) where all monomer transition dipoles are aligned, while the GPI of the monomer to the excited state $|\varphi_{exc}\rangle$*. Plots with circles include all intersite molecular couplings, while those with asterisks have been analytically evaluated with nearest-neighbors (nn) approximation where every monomer interacts only with its two neighbors. Single monomers transition dipoles have been approximated as ideal dipoles of unit (1nm) length and unit charge.*

transition (i.e., ξ_0) of the molecular aggregate and the GPI of the plasmonic quantum wire for different aggregate and wire lengths. They are always negative, showing that indeed the J-band is far from being a plasmon.

The picture that emerges from this comparison is that two excitations with similar absorption spectrum (here the J-band and the plasmonic quantum wire ones) may have difference in their plasmonic character: even if the plus and minus poles internal to the medium cancel out in determining the oscillator strength of the J-band (see inset of Figure 3(b)), they do not for plasmonic energy and GPI.

CONCLUSIONS

In this work we have evaluated the generalized plasmonicity index of a push-pull organic dye and of its bulk J-aggregate molecular crystal, by using a many-body perturbation theory approach. Our results indicate that the electronic excitations within the characteristic red shifted J-band have a lower plasmonic character with respect to that of the single monomer. Despite the fact that the J-band is a collective excitation, it has not a plasmonic character. In order to explain and rationalize the MBPT result, we proposed a simple one-dimensional model to evaluate analytically the plasmonic energy of the extended molecular system. The model indeed is able to predict the lowering of the plasmonic energy as due to a globally negative interaction energy between monomers transition densities along the chain (i.e., intra-chain couplings), which is also the origin of the characteristic J-band red-shift.

In a more general perspective, we have clearly shown that a bright excitation in molecular systems, even when coming from a collective mechanism, may well have no relation with plasmons. This highlights the special status of molecular excitations that do present plasmon like excitations.[1,2,16,37–42]

COMPUTATIONAL DETAILS

Unit cell structure of bulk molecular J-aggregate has been taken from available X-ray diffraction measurements[20] (available in the *CCDC No.* 961738).

To simulate the isolated (i.e. in gas-phase) push-pull dye we extracted one monomer unit from the bulk J-aggregate crystal and then relaxed its structure with Gaussian[43] using cam-b3lyp xc-functional and fixing a force threshold of 10^{-5} Hartree / Bohr. Then, with MOLGW[44] code we performed a DFT ground state calculation using *cam-b3lyp* xc-functional and *cc-pVDZ* localized basis set with frozen core approximation, then we applied the quasi-particle corrections to the DFT energy levels by using an eigenvalue-only self-consistent GW[44] procedure and, at the end, we evaluated the BSE optical absorption spectrum using Tamm-Dancoff approximation.

To simulated the bulk molecular crystal, electronic and optical properties of the J-aggregate have been obtained by using the Quantum Espresso[45] (QE) package in conjunction with the pane wave MBPT code YAMBO[46]. Fixing PBE[47] xc-functional and norm-conserving pseudo-potentials[48], with QE we calculated the ground state DFT electronic structure of the aggregate. Then, with YAMBO we applied the GW quasi-particle correction to the DFT ground state energies using the plasmon pole approximation[49]. At the end, the J-aggregate optical absorption spectrum has been obtained through solution of the Bethe-Salpeter pseudo-eigenvalue equation[27,50,51] (BSE) in the Tamm-Dancoff approximation. Through direct diagonalization of the BSE Hamiltonian we have extracted, for each excited state $|\xi_k\rangle$, the transition coefficients $C_{ai}^{\xi_k}$ that enter in the expression of the transition density (Eq. 5) for each excited state and consequently of the plasmonic energy (Eq. 4) and GPI at resonance. In order to evaluate the plasmonic energy for each excited state, a specific post-processing routine has been implemented both in MOLGW and in Yambo.

Due to the strong anisotropy of the molecular bulk aggregate, the final optical absorption spectrum reported in Figure 2(b) has been evaluated by performing three independent simulations with three orthogonal external exciting field orientations and then taking the spatial average over the three obtained spectra, i.e. $\frac{1}{3}\cdot\Im Tr\left[\varepsilon_{M,ij}(\omega)\right]$, where $\Im$ stands for *imaginary part of* and $\varepsilon_{M,ij}(\omega)$ is the macroscopic, frequency dependent, dielectric tensor in the long wavelength limit.

ASSOCIATED CONTENT

Supporting Information

The Supporting Information is available free of charge on the ACS Publications website.

In Section I we have put the theoretical derivation of the polymer transition density together with the point-dipole approximation of the inter-molecular energy transfer integral (Eq. (10) and (12) of main text, respectively). In section II we derive the GPI variation from the single molecule to the one-dimensional J-aggregate model, i.e., Eqs. (14)-(16). In section III we show how one can extend the 1D linear chain model presented here to a more realistic 3D one by assuming to combine several linear chains to build the bulk crystal.

Funding Sources

This work was partially funded by the European 396 Union under the ERC grant TAME Plasmons (ERC-CoG-397681285).

ACKNOWLEDGMENT

The authors would like to thank Dr. Luca Bursi of Physics and Astronomy department at Rice University Houston (TX) for the useful discussions and the critical reading of the manuscript.

REFERENCES

(1) Chapkin, K. D.; Bursi, L.; Stec, G. J.; Lauchner, A.; Hogan, N. J.; Cui, Y.; Nordlander, P.; Halas, N. J. Lifetime Dynamics of Plasmons in the Few-Atom Limit. *Proc. Natl. Acad. Sci.* **2018**, 115 (37), 9134-9139

(2) Lauchner, A.; Schlather, A. E.; Manjavacas, A.; Cui, Y.; McClain, M. J.; Stec, G. J.; García De Abajo, F. J.; Nordlander, P.; Halas, N. J. Molecular Plasmonics. *Nano Lett.* **2015**, *15* (9), 6208–6214.

(3) Eisfeld, A.; Briggs, J. S. The \emph{J}-Band of Organic Dyes: Lineshape and Coherence Length. *Chem. Phys.* **2002**, *281* (1), 61–70.

(4) Frank, W.; E., K. T.; R., S.-M. C. J-Aggregates: From Serendipitous Discovery to Supramolecular Engineering of Functional Dye Materials. *Angew. Chemie Int. Ed. 50* (15), 3376–3410.

(5) Walczak, P. B.; Eisfeld, A.; Briggs, J. S. Exchange Narrowing of the J Band of Molecular Dye Aggregates. *J. Chem. Phys.* **2008**, *128* (4), 1–12.

(6) Egorov, V. V. Theory of the J-Band: From the Frenkel Exciton to Charge Transfer. *Phys. Procedia* **2009**, *2* (2), 223–326.

(7) Knapp, E. W. Lineshapes of Molecular Aggregates, Exchange Narrowing and Intersite Correlation. *Chem. Phys.* **1984**, *85* (1), 73–82.

(8) Van Burgel, M.; Wiersma, D. A.; Duppen, K. The Dynamics of One-Dimensional Excitons in Liquids. *J. Chem. Phys.* **1995**, *102* (1), 20–33.

(9) Tempelaar, R.; Stradomska, A.; Knoester, J.; Spano, F. C. Anatomy of an Exciton: Vibrational Distortion and Exciton Coherence in H- and J-Aggregates. *J. Phys. Chem. B* **2013**, *117* (1), 457–466.

(10) Tame, M. S.; McEnery, K. R.; Özdemir, Ş. K.; Lee, J.; Maier, S. A.; Kim, M. S. Quantum Plasmonics Review. *Nat Phys* **2013**, *9* (6), 329–340.

(11) Stiles, P. L.; Dieringer, J. A.; Shah, N. C.; Van Duyne, R. P. Surface-Enhanced Raman Spectroscopy. *Annu. Rev. Anal. Chem.* **2008**, *1* (1), 601–626.

(12) Archambault, A.; Marquier, F.; Greffet, J. J.; Arnold, C. Quantum Theory of Spontaneous and Stimulated Emission of Surface Plasmons. *Phys. Rev. B - Condens. Matter Mater. Phys.* **2010**, *82* (3), 1–10.

(13) Pitarke, J. M.; Silkin, V. M.; Chulkov, E. V; Echenique, P. M. Theory of Surface Plasmons and Surface-Plasmon Polaritons. *Rep. Prog. Phys.* **2007**, *70 (1)*, 1–87.

(14) Moradi, A. Surface and Bulk Plasmons of Electron-Hole Plasma in Semiconductor Nanowires. *Phys. Plasmas* **2016**, *23* (11), 4503.

(15) Novotny, L.; Hecht, B. Surface Plasmons. *Princ. Nano-Optics* **2014**, 407–450.

(16) Zhang, R.; Bursi, L.; Cox, J. D.; Cui, Y.; Krauter, C. M.; Alabastri, A.; Manjavacas, A.; Calzolari, A.; Corni, S.; Molinari, E.; et al. How to Identify Plasmons from the Optical Response of Nanostructures. *ACS Nano* **2017**, *11* (7), 7321–7335.

(17) Bursi, L.; Calzolari, A.; Corni, S.; Molinari, E. Quantifying the Plasmonic Character of Optical Excitations in Nanostructures. *ACS Photonics* **2016**, *3* (4), 520–525.

(18) Spano, F. C.; Silva, C. H- and J-Aggregate Behavior in Polymeric Semiconductors. *Annu. Rev. Phys. Chem.* **2014**, *65* (1), 477–500.

(19) Eisfeld, A.; Briggs, J. S. The J- and H-Bands of Organic Dye Aggregates. *Chem. Phys.* **2006**, *324* (2–3), 376–384.

(20) Botta, C.; Cariati, E.; Cavallo, G.; Dichiarante, V.; Forni, A.; Metrangolo, P.; Pilati, T.; Resnati, G.; Righetto, S.; Terraneo, G.; et al. Fluorine-Induced J-Aggregation Enhances Emissive Properties of a New NLO Push-Pull Chromophore. *J. Mater. Chem. C* **2014**, *2* (27), 5275–5279.

(21) Baumeier, B.; Rohlfing, M.; Andrienko, D. Electronic Excitations in Push-Pull Oligomers and Their Complexes with Fullerene from Many-Body Green's Functions Theory with Polarizable Embedding. *J. Chem. Theory Comput.* **2014**, *10* (8), 3104–3110.

(22) Panja, S. K.; Dwivedi, N.; Saha, S. Tuning the Intramolecular Charge Transfer (ICT) Process in Push–Pull Systems: Effect of Nitro Groups. *RSC Adv.* **2016**, *6* (107), 105786–105794.

(23) Alexander L. Fetter, John Dirk Walecka-Quantum Theory of Many-Particle Systems (2003).

(24) Li, X.; Xiao, D.; Zhang, Z. Landau Damping of Quantum Plasmons in Metal Nanostructures. *New J. Phys.* **2013**, *15 (2), 3011*.

(25) Baumeier, B.; Andrienko, D.; Rohlfing, M. Frenkel and Charge-Transfer Excitations in Donor–Acceptor Complexes from Many-Body Green's Functions Theory. *J. Chem. Theory Comput.* **2012**, *8* (8), 2790–2795.

(26) Blase, X.; Attaccalite, C. Charge-Transfer Excitations in Molecular Donor-Acceptor Complexes within the Many-Body Bethe-Salpeter Approach. *Appl. Phys. Lett.* **2011**, *99* (17), 1909.

(27) Onida, G.; Reining, L.; Rubio, A. Electronic Excitations: Density-Functional versus Many-Body Green's-Function Approaches. *Rev. Mod. Phys.* **2002**, *74* (2), 601–659.

(28) Guerrini, M.; Calzolari, A.; Corni, S. Solid-State Effects on the Optical Excitation of Push–Pull Molecular J-Aggregates by First-Principles Simulations. *ACS Omega* **2018**, *3* (9), 10481–10486.

(29) Huaning, Z.; Xian, W.; Renjun, M.; Zhuoran, K.; Qianjin, G.; Andong, X. Intramolecular Charge Transfer and Solvation of Photoactive Molecules with Conjugated Push–Pull Structures. *ChemPhysChem 17* (20), 3245–3251.

(30) Davydov, A. S. The Theory of Molecular Excitons (Translation). *Sov. Phys. Uspekhi* **1964**, *82* (3–4), 393–448.

(31) Barford, W.; Marcus, M. Theory of Optical Transitions in Conjugated Polymers. I. Ideal Systems. *J. Chem. Phys.* **2014**, *141* (16), 4101.

(32) Marcus, M.; Tozer, O. R.; Barford, W. Theory of Optical Transitions in Conjugated Polymers. II. Real Systems. *J. Chem. Phys.* **2014**, *141* (16), 4102.

(33) Eisfeld, A.; Briggs, J. S. The J-Band of Organic Dyes: Lineshape and Coherence Length. *Chem. Phys.* **2002**, *281* (1), 61–70.

(34) Kasha, M.; Rawls, H. R.; Ashraf El-Bayoumi, M. The Exciton Model in Molecular Spectroscopy. *Pure Appl. Chem.* **1965**, *11* (3–4), 371–392.

(35) Kasha, M. Energy Transfer Mechanisms and the Molecular Exciton Model for Molecular Aggregates. *Radiat. Res.* **1963**, *20* (1), 55–70.

(36) Spano, F. C.; Mukamel, S. Superradiance in Molecular Aggregates. *J. Chem. Phys.* **1989**, *91* (2), 683–700.

(37) Manjavacas, A.; Marchesin, F.; Thongrattanasiri, S.; Koval, P.; Nordlander, P.; Sánchez-Portal, D.; García De Abajo, F. J. Tunable Molecular Plasmons in Polycyclic Aromatic Hydrocarbons. *ACS Nano* **2013**, *7* (4), 3635–3643.

(38) Krauter, C. M.; Schirmer, J.; Jacob, C. R.; Pernpointner, M.; Dreuw, A. Plasmons in Molecules: Microscopic Characterization Based on Orbital Transitions and Momentum Conservation. *J. Chem. Phys.* **2014**, *141* (10), 4101.

(39) Bernadotte, S.; Evers, F.; Jacob, C. R. Plasmons in Molecules. *J. Phys. Chem. C* **2013**, *117* (4), 1863–1878.

(40) Guidez, E. B.; Aikens, C. M. Quantum Mechanical Origin of the Plasmon: From Molecular Systems to Nanoparticles. *Nanoscale* **2014**, *6* (20), 11512–11527.

(41) Bursi, L.; Calzolari, A.; Corni, S.; Molinari, E. Light-Induced Field Enhancement in Nanoscale Systems from First-Principles: The Case of Polyacenes. *ACS Photonics* **2014**, *1* (10), 1049–1058.

(42) Guidez, E. B.; Aikens, C. M. Origin and TDDFT Benchmarking of the Plasmon Resonance in Acenes. *J. Phys. Chem. C* **2013**, *117* (41), 21466–21475.

(43) Frisch, M. J.; Trucks, G. W.; Schlegel, H. B.; Scuseria, G. E.; Robb, M. a.; Cheeseman, J. R.; Montgomery, J. a.; Vreven, T.; Kudin, K. N.; Burant, J. C.; et al. Gaussian 09W Tutorial. *an Introd. To Comput. Chem. Using G09W Avogadro Softw.* **2009**, 34.

(44) Bruneval, F.; Rangel, T.; Hamed, S. M.; Shao, M.; Yang, C.; Neaton, J. B. Molgw 1: Many-Body Perturbation Theory Software for Atoms, Molecules, and Clusters. *Comput. Phys. Commun.* **2016**, *208*, 149–161.

(45) Giannozzi, P.; Baroni, S.; Bonini, N.; Calandra, M.; Car, R.; Cavazzoni, C.; Ceresoli, D.; Chiarotti, G. L.; Cococcioni, M.; Dabo, I.; et al. QUANTUM ESPRESSO: A Modular and Open-Source Software Project for Quantum Simulations of Materials. *J. Phys. Condens. Matter* **2009**, *21* (39), 5502.

(46) Marini, A.; Hogan, C.; Grüning, M.; Varsano, D. Yambo: An Ab Initio Tool for Excited State Calculations. *Comput. Phys. Commun.* **2009**, *180* (8), 1392–1403.

(47) Perdew, J. P.; Burke, K.; Ernzerhof, M. Generalized Gradient Approximation Made Simple. *Phys. Rev. Lett.* **1996**, *77* (18), 3865–3868.

(48) Hamann, D. R.; Schlüter, M.; Chiang, C. Norm-Conserving Pseudopotentials. *Phys. Rev. Lett.* **1979**, *43* (20), 1494–1497.

(49) Larson, P.; Dvorak, M.; Wu, Z. Role of the Plasmon-Pole Model in the GW Approximation. *Phys. Rev. B - Condens. Matter Mater. Phys.* **2013**, *88* (12), 42–46.

(50) Cudazzo, P.; Gatti, M.; Rubio, A. Excitons in Molecular Crystals from First-Principles Many-Body Perturbation Theory: Picene versus Pentacene. *Phys. Rev. B - Condens. Matter Mater. Phys.* **2012**, *86* (19), 1–8.

(51) Marques, M. A. L.; Ullrich, C. A.; Nogueira, F.; K., A. R.; Gross, E. K. U. *Time-Dependent Density Functional Theory*; 2006; Vol. 706.

Appendix C – Supporting Information of: Quantifying the plasmonic character of optical excitations in a molecular J-aggregate

4.2 Appendix C1 – Analytical derivation of 1D aggregate transition density

We give here the derivation of the transition density associated to a linear chain molecular aggregate (i.e., Eq. (7) of main text) by the knowledge on the single monomer transition density function. For low energy excitations, the polymer excited state can be expresses as

$$|\xi_k\rangle = \sum_n \varphi_{km}|m\rangle \qquad -M/2 \le k \le M/2 \qquad \text{C.1.1}$$

$$|\lambda_m\rangle = |\varphi_{exc}^m\rangle \prod_{n\neq m}|\varphi_{GS}^n\rangle \qquad m,n = 1,\dots,M \qquad \text{C.1.2}$$

Where M is the total number of molecules in the aggregate and it must be satisfied the completeness relation $\sum_m \varphi_{km}^* \varphi_{k'm} = \delta_{kk'}$. We now use one of the excited states (C.1.1) to evaluate the polymer transition density from molecular aggregate ground state $|0\rangle$ to excited state $|\xi_k\rangle$

$$\rho_{\xi_k}^{pol}(r) = \langle 0|\hat{\Psi}^\dagger(r)\hat{\Psi}(r)|\xi_k\rangle = \sum_{m=1}^{M} \varphi_{km}\langle GS_1,\dots,GS_i,\dots,GS_M|\sum_{i=1}^{M}\Psi_i^\dagger(r)\hat{\Psi}_i(r)\,|GS_1,\dots,exc_i,\dots,GS_M\rangle =$$

$$\sum_{m=1}^{M}\varphi_{km}\sum_{i\neq m}\langle GS_1|GS_1\rangle\dots\langle GS_i|\Psi_i^\dagger(r)\hat{\Psi}_i(r)|GS_i\rangle\dots\langle GS_m|exc_m\rangle\dots\langle GS_M|GS_M\rangle +$$

$$\sum_{m=1}^{M}\varphi_{km}\langle GS_1|GS_1\rangle\dots\langle GS_m|\Psi_m^\dagger(r)\hat{\Psi}_m(r)|exc_m\rangle\dots\langle GS_M|GS_M\rangle = \sum_{m=1}^{M}\varphi_{km}\rho_{exc,m}^{mon}(r) \qquad \text{C.1.3}$$

Where $|GS_i\rangle$ and $|exc_i\rangle$ are ground and excited state of *i-th* monomer in the aggregate, $\rho_m^{mon}(\boldsymbol{r}) = \langle GS_m|\hat{\Psi}^\dagger(r)\hat{\Psi}(r)|exc_m\rangle = \rho^{mon}(r-R_m)$ is the transition density of *m-th* monomer centered at position R_m in the aggregate. In the particular case in which the expansion coefficients φ_{kn} are discrete plane waves and all the monomers are equal with the same transition density, the expression of the polymer transition density becomes $\rho_{\xi_k}^{pol}(r) = \frac{1}{\sqrt{M}}\sum_m \exp\left(\frac{2\pi}{M}km\right)\rho_{exc,m}^{mon}(r)$.

Now we employ the general expression (C.1.3) of the molecular aggregate transition density to derive the energy transfer integral J_{mn}between monomers *m* and *n* (i.e., Eq. (13) of main text). This term is in general given by the Coulomb interaction energy between *m-th* an *n-th* monomers transition densities. Starting from Eq. (12) of the main text which gives the energy shift of polymer excited state $|\xi_k\rangle$ with respect to the monomer excited state $|exc\rangle$

$$W(k) = E_{\xi_k}^{plas} - E_{exc}^{plas} = \sum_{m\neq m'} \varphi_{km}^{*}\varphi_{km'} \int \frac{\rho_{exc}^{*mon}(r-R_m)\rho_{exc}^{mon}(r'-R_{m'})}{|r-r'|} drdr' \quad \text{C.1.4}$$

$$J_{mm'} = J_{m'm} = \int \frac{\rho_{exc}^{*mon}(r-R_m)\rho_{exc}^{mon}(r'-R_{m'})}{|r-r'|} drdr' \quad \text{C.1.5}$$

Since every transition density has no monopole term, in the first multipolar expansion it can be expanded as a point dipole and we can approximate the coupling integral J_{mn} in point dipole approximation which is the following

$$\hat{H}_{mm'}^{int} \approx \frac{\hat{\boldsymbol{\mu}}_m \cdot \hat{\boldsymbol{\mu}}_{m'} - 3(\hat{\boldsymbol{\mu}}_m \cdot \boldsymbol{R})(\hat{\boldsymbol{\mu}}_{m'} \cdot \boldsymbol{R})}{R_{mm'}^3} \quad \text{C.1.6}$$

Where $\hat{\boldsymbol{\mu}}_m$ is *m-th* monomer dipole moment (vector) operator, $R_{mm'}$ distance between *m-th* and *m'-th* monomers center of masses (CoM) and $\boldsymbol{R}$ the unit vector oriented from *m-th* to *m'-th* monomers CoM. Using the product state basis (C.1.2) the matrix elements of (C.1.6) can be evaluated and we get

$$J_{mm'} = \langle \lambda_m | \hat{H}_{mm'}^{int} | \lambda_{m'} \rangle \approx \frac{\boldsymbol{\mu}_m^{tr} \cdot \boldsymbol{\mu}_{m'}^{tr} - 3(\boldsymbol{\mu}_m^{tr} \cdot \boldsymbol{R})(\boldsymbol{\mu}_{m'}^{tr} \cdot \boldsymbol{R})}{R_{mm'}^3} \quad \text{C.1.7}$$

$$\langle \lambda_m | \hat{\boldsymbol{\mu}}_m \cdot \hat{\boldsymbol{\mu}}_{m'} | \lambda_{m'} \rangle = \langle GS_1 | GS_1 \rangle \dots \langle exc_m | \hat{\boldsymbol{\mu}}_m | GS_m \rangle \dots \langle GS_{m'} | \hat{\boldsymbol{\mu}}_{m'} | exc_{m'} \rangle \dots \langle GS_M | GS_M \rangle = \boldsymbol{\mu}_m^{tr} \cdot \boldsymbol{\mu}_{m'}^{tr}$$

$$\langle \lambda_m | (\hat{\boldsymbol{\mu}}_m \cdot \boldsymbol{R})(\hat{\boldsymbol{\mu}}_{m'} \cdot \boldsymbol{R}) | \lambda_{m'} \rangle = (\boldsymbol{\mu}_m^{tr} \cdot \boldsymbol{R}) \left(\boldsymbol{\mu}_{m'}^{tr} \cdot \boldsymbol{R} \right) \quad \text{C.1.8}$$

where $\boldsymbol{\mu}_m^{tr} = \langle exc_m | \Psi^{\dagger}(\boldsymbol{r}) \boldsymbol{r} \Psi(\boldsymbol{r}) | GS_m \rangle$ is transition dipole moment associated to *m-th* monomer unit.

4.3 Appendix C2 – Plasmonic Energy (GPI) variation between 1D aggregate and monomer excited states

We derive here Eq. (20) of main text which is an approximation for the variation of plasmonic energy between the molecular aggregate and single molecule lowest energy excited states.

Assuming to approximate monomer transition density at position $\boldsymbol{R}_m = m(\boldsymbol{d}+\boldsymbol{a})$ associated to state $|\varphi_{exc}\rangle$ with an extended dipole of length d of unit charge , i.e. $\rho^{mom}_{exc,m}(r) \approx \delta(\boldsymbol{r}-\boldsymbol{R}_m) - \delta(\boldsymbol{r}-\boldsymbol{R}_m-\boldsymbol{d})$ and polymer (composed on *M* aligned monomers) transition density associated to its lowest excited state $|\xi_0\rangle$ as $\rho^{pol}_{\xi_0}(r) \approx \frac{1}{\sqrt{M}}\sum_m \delta(\boldsymbol{r}-\boldsymbol{R}_m) - \delta(\boldsymbol{r}-\boldsymbol{R}_m-\boldsymbol{d})$, one can approximate the plasmonic energy difference between polymer and monomer lowest energy excited states (Eq. (20) of main text)

$$\Delta E^{plas}_{\xi_0} = E^{plas,pol}_{\xi_0} - E^{plas,mon}_{exc} = \int \frac{\rho^{pol}_{\xi_0}(\boldsymbol{r})\rho^{pol}_{\xi_0}(\boldsymbol{r}')}{|\boldsymbol{r}-\boldsymbol{r}'|}d\boldsymbol{r}d\boldsymbol{r}' - \int \frac{\rho^{mon}_{exc}(\boldsymbol{r})\rho^{mon}_{exc}(\boldsymbol{r}')}{|\boldsymbol{r}-\boldsymbol{r}'|}d\boldsymbol{r}d\boldsymbol{r}' \approx$$

$$\approx \frac{1}{M}\sum_{m,m'=1}^{M}\int \frac{[\delta(\boldsymbol{r}-\boldsymbol{R}_m)-\delta(\boldsymbol{r}-\boldsymbol{R}_m-\boldsymbol{d})][\delta(\boldsymbol{r}-\boldsymbol{R}_{m'})-\delta(\boldsymbol{r}-\boldsymbol{R}_{m'}-\boldsymbol{d})]}{|\boldsymbol{r}-\boldsymbol{r}'|}d\boldsymbol{r}d\boldsymbol{r}' - \int \frac{[\delta(\boldsymbol{r})-\delta(\boldsymbol{r}-\boldsymbol{d})][\delta(\boldsymbol{r}')-\delta(\boldsymbol{r}'-\boldsymbol{d})]}{|\boldsymbol{r}-\boldsymbol{r}'|}d\boldsymbol{r}d\boldsymbol{r}' =$$

$$\left[E^{plas,mon}_{exc} + \frac{1}{M}\sum_{m\neq m'} 2|R_m - R_{m'}|^{-1} - |R_m - R_{m'}+d|^{-1} - |R_{m'}-R_m+d|^{-1}\right] - E^{plas,mon}_{exc} =$$

$$\frac{1}{M}\sum_{m\neq m'} 2|R_m - R_{m'}|^{-1} - |R_m - R_{m'}+d|^{-1} - |R_{m'}-R_m+d|^{-1} \qquad \text{C.2.1}$$

The effects of intra-chain couplings are even more pronounced if we consider the variation of plasmonic energy between a linear chain and an extended dipole of the same length which roughly simulates a quantum wire where electronic states are completely delocalized as in an electron gas. In this case Eq. (C.2.1) must be simply shifted by the constant (negative) term $\Delta P = -\frac{2}{a}\left(\frac{\sigma}{\sigma+1}\right)$, where $\sigma = (N-1)\frac{R}{a}$. Eq. (C.2.1) and related GPI with the correction term ΔP is what we have reported in Figure 3(b) of the main text where one can observe a stronger negative variation when monomers are closer due to ΔP.

4.4 Appendix C3 – Extension of 1D aggregate to a 3D aggregate model

In this section we extend our one-dimensional molecular aggregate model to a three-dimensional one. In simple terms, one can imagine the bulk crystal we have simulated as formed by aggregating N_C linear chains in three dimensions with parallel orientations. Just as we have done for the linear chain, at first order approximation, one can express the bulk crystal excited state $|\xi_\nu\rangle$ as a linear combination of N_C polymer states (C.1.1) each one in an excited state k

$$|\xi_\nu^{bulk}\rangle \approx \sum_{ck} \alpha_{\nu k}^{(c)} |\xi_k^{(c)}\rangle = \sum_{ckm} \alpha_{\nu k}^{(c)} \varphi_{km} |\lambda_m^{(c)}\rangle \qquad \text{C.3.1}$$

where $\nu = 0, \dots, N_C - 1$ ($M_{tot} = MN_C$ is total number of monomers within the bulk crystal and M total number of monomers per chain) $-\frac{M}{2} < k \leq \frac{M}{2}$ $k \in \mathbb{Z}$, $n = 1, \dots, M$ $n \in \mathbb{N}$ and $c = 1, \dots, N_C$ and we have the orthonormalization conditions for the coefficients, i.e. $\sum_{\substack{kk' \\ cc'}} \alpha_{\nu k}^{*(c)} \alpha_{\nu k'}^{(c')} = \delta_{kk'}\delta_{cc'}$ and $\sum_{nn'} \varphi_{kn}^* \varphi_{k'n'} = \delta_{nn'}\delta_{kk'}$. From Eq. (C.3.1) we can derive bulk transition density associated to excited state ν and the energy shift (i.e., Eq. (11) in the main text) due to both intra- and inter-chain couplings

$$\rho_{\xi_\nu}^{bulk}(r) = \langle 0|\hat{\Psi}^\dagger(\boldsymbol{r})\hat{\Psi}(\boldsymbol{r})|\xi_\nu^{bulk}\rangle = \sum_{ck} \alpha_{\nu k}^{(c)} \rho_k^{pol}(\boldsymbol{r} - \boldsymbol{R}_c) = \sum_{ckm} \alpha_{\nu k}^{(c)} \varphi_{km} \rho_{exc}^{mon}(\boldsymbol{r} - \boldsymbol{R}_{c,m}) \qquad \text{C.3.2}$$

$$E_{\xi_\nu}^{plas,bulk} = \sum_{cc'} \sum_{kk'} \left(\alpha_{\nu k}^{(c)}\right)^* \alpha_{\nu k'}^{(c')} \int \frac{\rho_k^{pol}(\boldsymbol{r} - \boldsymbol{R}_c)\rho_{k'}^{pol}(\boldsymbol{r}' - \boldsymbol{R}_{c'})}{|\boldsymbol{r} - \boldsymbol{r}'|} d\boldsymbol{r} d\boldsymbol{r}' =$$

$$\sum_{ck} \left|\alpha_{\nu k}^{(c)}\right|^2 E_{\xi_k^{(c)}}^{plas,pol} + \sum_{c(k \neq k')} \left(\alpha_{\nu k}^{(c)}\right)^* \alpha_{\nu k'}^{(c')} W_{cc}(k,k') + \sum_{(c \neq c')k} \left(\alpha_{\nu k}^{(c)}\right)^* \alpha_{\nu k'}^{(c')} W_{cc'}(k,k) + \sum_{\substack{(c \neq c') \\ (k \neq k')}} \left(\alpha_{\nu k}^{(c)}\right)^* \alpha_{\nu k'}^{(c')} W_{cc'}(k,k') =$$

$$E_{exc}^{plas,mon} + \sum_{ck} \left|\alpha_{\nu k}^{(c)}\right|^2 W_{cc}(k,k) + \sum_{c(k \neq k')} \left(\alpha_{\nu k}^{(c)}\right)^* \alpha_{\nu k'}^{(c')} W_{cc}(k,k') + \sum_{(c \neq c')k} \left(\alpha_{\nu k}^{(c)}\right)^* \alpha_{\nu k'}^{(c')} W_{cc'}(k,k) + \sum_{\substack{(c \neq c') \\ (k \neq k')}} \left(\alpha_{\nu k}^{(c)}\right)^* \alpha_{\nu k'}^{(c')} W_{cc'}(k,k') \qquad \text{C.3.3}$$

$$W_{cc'}(k,k') = \int \frac{\rho_k^{pol}(\boldsymbol{r})\rho_{k'}^{pol}(\boldsymbol{r}')}{|\boldsymbol{r} - \boldsymbol{r}'|} d\boldsymbol{r} d\boldsymbol{r}' \qquad \text{C.3.4}$$

Where R_c indicates center-of-mass location of *c-th* polymer chain.

The terms (C.3.4) generally indicate the coupling between *c-th* polymer chain transition density in excited state $|\xi_k^{pol}\rangle$ and *c'-th* polymer chain transition density in excited state $|\xi_{k'}^{pol}\rangle$. We can see that when one makes different polymer chains to interact, there is: an energy level shift due to an average of intra-chain couplings for each polymer excited state $|\xi_k^{pol}\rangle$ (second term of (C.3.3)); intra-chain mixing between different polymer excited states of same chain (third term in (C.3.3)); inter-chain mixing between different chains in the same polymer excited state k (fourth term of (C.3.3)) or both of the last two simultaneously (fifth term of (C.3.3)). The weighted sum of all these terms through the coefficients $\alpha_{\upsilon k}^{(c)}$ contributes to the energy level shift of the bulk excited states $|\xi_\upsilon^{bulk}\rangle$ with respect to the single monomer excited state $|exc\rangle$. If we assume only the polymer chain lowest excited state (i.e. *k*=0) Eq. (C.3.3) is simplified and we can express energy shift of bulk excited state $|\xi_\upsilon^{bulk}\rangle$ with respect to the polymer lowest excited state as

$$\Delta E_{\xi_\nu}^{plas,bulk} = E_{\xi_\nu}^{plas,bulk} - E_{\xi_0}^{plas,pol} = W(\nu) = \sum_{c\neq c'}\left(\alpha_{\nu 0}^{(c)}\right)^* \alpha_{\nu 0}^{(c')} \int \frac{\rho_{\xi_0}^{*pol}(\boldsymbol{r}-\boldsymbol{R}_c)\rho_{\xi_0}^{pol}\left(\boldsymbol{r}'-\boldsymbol{R}_{c'}\right)}{|\boldsymbol{r}-\boldsymbol{r}'|} d\boldsymbol{r} d\boldsymbol{r}' \qquad \text{C.3.5}$$

$$\approx \frac{1}{N_C}\sum_{c\neq c'} e^{i\frac{2\pi}{N_C}\nu(c'-c)}\left(\frac{\boldsymbol{\mu}_{\xi_0,pol}^{(c)}\cdot\boldsymbol{\mu}_{\xi_0,pol}^{(c')} - 3\left(\boldsymbol{\mu}_{\xi_0,pol}^{(c)}\cdot\boldsymbol{R}_{cc'}\right)\left(\boldsymbol{\mu}_{\xi_0,pol}^{(c')}\cdot\boldsymbol{R}_{cc'}\right)}{R_{cc'}^3}\right) \qquad \text{C.3.6}$$

$$= \frac{1}{N_C}\sum_{c\neq c'} e^{i\frac{2\pi}{N_C}\nu(c'-c)}\frac{|\boldsymbol{\mu}_{\xi_0,pol}|^2(1-3cos^2\theta)}{R_{cc'}^3} = \frac{|\boldsymbol{\mu}_{\xi_0,pol}|^2(1-3cos^2\theta)}{N_C}\sum_{c\neq c'}\frac{cos^2\left(\frac{2\pi}{N_C}\nu(c-c')\right)}{R_{cc'}^3} \qquad \text{C.3.7}$$

$$\approx \left|\boldsymbol{\mu}_{\xi_0,pol}\right|^2(1-3cos^2\theta)\frac{2(N_C-1)}{N_C}\frac{cos^2\left(\frac{2\pi}{N_C}\nu\right)}{\Delta R^3} \qquad \text{C.3.8}$$

where we have indicated with $\boldsymbol{\mu}_{0,pol}^{(c)} = \left\langle 0^{(c)}\middle|\Psi^\dagger(\boldsymbol{r})\boldsymbol{r}\Psi(\boldsymbol{r})\middle|\xi_0^{(c)}\right\rangle$ the transition dipole of *c-th* polymer chain, $\widehat{\boldsymbol{R}}_{cc'}$ the unit vector pointing from center-of-masses (CoM) of *c-th* to *c'-th* polymer chain; $R_{cc'} = (c-c')\Delta R$ the distance between CoM of *c-th* and *c'-th* polymer chains and in (C.3.6) we have used a point-dipole approximation and assumed plane wave expansion coefficients $\alpha_{\nu 0}^{(c)} = \frac{1}{\sqrt{N_C}} exp\left(i\frac{2\pi}{N_C}\nu c\right)$, θ (< 90°) is the slip angle between line joining centers of polymer chains and direction of polymer transition density (see Figure S.1). In (C.3.7) we assumed all polymer chains transition dipoles are equal and pointing in the same direction.

We can see that Eq. (C.3.5) has the same form of Eq. (12) of main text. If the slip angle θ = 54,73°, there is no energy shift with respect to the polymer chain since Eq. (S.3.10) is identically zero. This same effect

happens when $\nu = \frac{N_C}{4}$. If we consider Eq. (C.3.8) which assumes nearest neighbor approximation, when $\theta > 54{,}73°$ the energy shift ΔE^{plas} is never negative (positive) when $|\nu| < \frac{N_C}{4}$ ($\frac{N_C}{4} < |\nu| < \frac{N_C}{2}$) and the bulk excited states must have always higher (lower) energy with respect to the polymer lowest excited state. When $\theta < 54{,}73°$ the situation is reversed. When bulk excited state index is $\nu = 0$ and $\theta > 54{,}73°$ one should expect to have a big energy blue-shift since there is maximum *H*-aggregate behavior with respect to the single polymer chain lowest excited state (i.e. *H*-aggregate polymers arranged as in Figure C3(b)). In this case all transition dipoles of the polymers are aligned and coherently summed and there is an enhancement of the total transition dipole (see formula C.3.9). Instead, when $\theta > 54{,}73°$ and the bulk excited states assume the extrema values $\nu = \pm\frac{N_C}{2}$ there is maximum J-aggregate behavior (see Figure C1(a)) since energy shift (C.3.8) assumes the most negative value with respect to the polymer lowest excited state but the state is dark since total transition dipole is very low (i.e. J-aggregate polymers arranged as in Figure C1(a)). The other bulk excited states shall assume an energy shift with respect to the polymer chain lowest excited state in the window

$$\pm\left|\boldsymbol{\mu}_{\xi_0,pol}\right|^2 \frac{\left(1-3cos^2\theta\right)}{\Delta R^3} \frac{2(N_C-1)}{N_C} \qquad \text{C.3.9}$$

Figure C3 - extended dipole model for linear chain 2D aggregate model in J- (a) and H- (b) aggregate arrangement. Extension to the 3D model is straightforward by just vertically stacking the 2D aggregate.

From the expression of bulk transition density (C.3.2) one can also obtain the bulk total transition dipole for generic excited state $|\xi_\upsilon^{bulk}\rangle$ and get all selection rules for the bulk crystal visible excited states, namely

$$\left|\mu_{\xi_\nu}^{bulk}\right|^2 = \boldsymbol{\mu}_{\xi_\nu}^{bulk} \cdot \boldsymbol{\mu}_{\xi_\nu}^{bulk} = \int \boldsymbol{r}\cdot\boldsymbol{r}'\rho_{\xi_\nu}^{bulk}(\boldsymbol{r})\rho_{\xi_\nu}^{bulk}(\boldsymbol{r}')d\boldsymbol{r}d\boldsymbol{r}'$$

$$= \sum_{\substack{cc'\\kk'}}\left(\alpha_{\nu k}^{(c)}\right)^* \alpha_{\nu k'}^{(c')} \int \boldsymbol{r}\,\rho_{\xi_k}^{pol}(\boldsymbol{r}-\boldsymbol{R}_c)d\boldsymbol{r}\cdot\int \boldsymbol{r}'\rho_{\xi_{k'}}^{pol}(\boldsymbol{r}'-\boldsymbol{R}_{c'})d\boldsymbol{r}' = \sum_{\substack{cc'\\kk'}}\left(\alpha_{\nu k}^{(c)}\right)^* \alpha_{\nu k'}^{(c')}\boldsymbol{\mu}_{\xi_k}^{(c),pol}\cdot\boldsymbol{\mu}_{\xi_{k'}}^{(c'),pol}$$

$$= \sum_{\substack{cc' \\ kk'}} \left(\alpha_{vk}^{(c)}\right)^* \alpha_{vk'}^{(c')} \varphi_{km}^* \varphi_{k'm'} \boldsymbol{\mu}_m^{(c),mon} \cdot \boldsymbol{\mu}_{m'}^{(c'),mon} = \sum_{ck} \left|\alpha_{vk}^{(c)}\right|^2 \sum_{mm'} \varphi_{km}^* \varphi_{km'} M_{mm'}^{(c,c),mon} +$$

$$\sum_{c(k\neq k')} \left(\alpha_{vk}^{(c)}\right)^* \alpha_{vk'}^{(c)} \sum_{mm'} \varphi_{km}^* \varphi_{k'm'} M_{mm'}^{(c,c),mon} + \sum_{(c\neq c')k} \left(\alpha_{vk}^{(c)}\right)^* \alpha_{vk}^{(c')} \sum_{mm'} \varphi_{km}^* \varphi_{km'} M_{mm'}^{(c,c'),mon} +$$

$$\sum_{\substack{(c\neq c') \\ (k\neq k')}} \left(\alpha_{vk}^{(c)}\right)^* \alpha_{vk'}^{(c')} \sum_{mm'} \varphi_{km}^* \varphi_{k'm'} M_{mm'}^{(c,c'),mon} \qquad \text{C.3.10}$$

$$M_{mm'}^{(c,c'),mon} = \boldsymbol{\mu}_m^{(c),mon} \cdot \boldsymbol{\mu}_m^{(c'),mon} \qquad \text{C.3.11}$$

Where (C.3.11) indicates inner product between transition dipole of *m-th* monomer in *c-th* chain with transition dipole of *m'-th* monomer in *c'-th* chain.

4.5 Appendix C4 – Frenkel Hamiltonian from molecular exciton theory

Following the molecular exciton theory of Davydov[49], the total energy operator of a molecular crystal can be modeled with the so called Frenkel effective Hamiltonian

$$\hat{H} = \sum_m \epsilon_{exc}^m \hat{a}_m^\dagger \hat{a}_m + \sum_{m\neq m'} J_{mm'} \hat{a}_m^\dagger \hat{a}_{m'} \qquad \text{C.4.1}$$

where we have fixed to zero total energy of the entire aggregate ground state $|0\rangle$, $a_m^\dagger = |\lambda_m\rangle\langle 0|$ ($\hat{a}_m = |0\rangle\langle\lambda_m|$) is molecular exciton creation (annihilation) operator at *n*-th molecular site and where

$$|0\rangle = \prod_{i=1}^M |\varphi_{GS}^i\rangle \qquad |\lambda_m\rangle = |\varphi_{exc}^m\rangle \prod_{i\neq m} |\varphi_{GS}^i\rangle \qquad \text{i =1,…,}M \qquad \text{C.4.2}$$

$$J_{nm} = \int \varphi_{exc}^{*n} \varphi_{GS}^m V_{nm} \varphi_{GS}^n \varphi_{exc}^{*m} d\tau_n d\tau_m \qquad \text{C.4.3}$$

$$\epsilon_{exc}^m = E_{exc} - E_{GS} + \Delta D_{exc}^m \qquad \text{C.4.4}$$

$$\Delta D_{exc}^m = \sum_{i\neq m} \int (|\varphi_{exc}^m|^2 - |\varphi_{GS}^m|^2) V_{mi} \left|\varphi_{GS}^i\right|^2 d\tau_m d\tau_i \qquad \text{C.4.5}$$

$|0\rangle$ is the total molecular aggregate ground state, $|\lambda_m\rangle$ is a direct product of M molecular states in which $M-1$ molecules are in the ground state $|\varphi_{GS}\rangle$ of energy E_{GS} and the *n*-th one in the excited state $|\varphi_{exc}\rangle$

of energy E_{exc}. For a simple model we shall assume excitation energies (3.4) all equal for each molecular site (i.e. no disorder) so that there is no dependence on monomer index m; $V_{nm} = V_{mn} = \sum_{i \neq j} 1/\left|r_{n_i} - r_{m_j}\right|$ is the Coulomb coupling operator between n-th and m-th monomers (here indices i,j run over all electrons of n-th and m-th monomers, respectively, and $d\tau_n = dr_{n_1} \ldots dr_{n_L}$ where L is total number of electron per molecule); $J_{nm} = J_{mn}$ are coupling integrals due to exciton exchange interaction and account for inter-molecular energy transfer rate and their magnitude is proportional to the inverse transfer time of excitation from n-th to m-th monomer[49]. For J-(H-) aggregate configurations $J_{nm} < 0$ ($J_{nm} > 0$)[24] ; Eq. (C.4.5) is a negative energy shift term (i.e. red-shift) and is related to the variation of van der Waals interaction energy[49,53] between states $|\lambda_m\rangle$ and $|0\rangle$. It physically represents the change in the interaction energy of a single molecule with all the others upon transition to excited state $|\varphi_{exc}\rangle$[49,53] (or else, it is the shift of the excitation energy level of the molecule due to aggregation – the excitonic shift, for short). Equation (C.4.1) is a simplified model of the more general Frenkel-Holstein one[19] that includes also exciton-phonon coupling. Since we are not interested in describing the latter effect as it does not play role in the J-band[27,28,137], we shall assume Born-Oppenheimer approximation, valid in the regime where the nuclear dynamics are slow compared to the excitonic dynamics. We shall consider the following approximations for our one-dimensional polymer model: (i) small electronic neutral excitations (only single exciton states); (ii) neglect the overlap between neighboring molecular wavefunctions (i.e. tight binding approximation valid for loose aggregates[27] describing Frenkel type excitons in which the electron-hole pair stays localized within each molecule[29]), thus avoiding to include exchange anti-symmetry between electrons of different molecules (taking into account electron exchange effects gives rise to an admixture of charge-separated states, corresponding to Wannier-Mott excitons[29]); (iii) assume a two-state model (i.e., $|\varphi_{GS}\rangle$ and $|\varphi_{exc}\rangle$) for the single monomer; (iv) periodic boundary conditions (PBC) to avoid edge effects and (v) infinite exciton coherence length (delocalization length), i.e., the electronic excitations are coherently delocalized over the entire aggregate, leading to a broad (i.e. constant envelope) spatial coherence function[35,138] $C(r) = \langle \xi_k | \sum_n \hat{a}^\dagger_{n+r} \hat{a}_n | \xi_k \rangle$, where $|\xi_k\rangle$ is the molecular exciton wavefunction associated to k-th excited state. The latter condition happens when the inter-molecular energy transfer rate J is so fast that it never decoheres with the molecular vibrational modes (i.e. free exciton model), this is a valid assumption when $\lambda^2 \omega_0 / |J| \ll 1$ where ω_0 is the molecular vibrational quantum and λ^2 the Huang-Rhys (H-R) factor that quantifies the shift between ground and excited state PES minima[24]. The latter condition implies also the Born-Oppenheimer (BO) regime. Within these assumptions the general molecular exciton eigenstate of Eq. (C.4.1) is described by a

coherent superposition of product states (i.e. an entangled state) in which only one monomer carries the electronic excitation[21,22,27]

$$|\xi_k\rangle = \sum_{m=1}^{M} \psi_{km} |\lambda_m\rangle \qquad \text{s.t.} \quad \langle \xi_{k'} | \hat{H} | \xi_k \rangle = E_k \delta_{kk'} \tag{C.4.6}$$

$$E_k = \epsilon_{exc} + \sum_{i \neq j} \psi_{ik}^* \psi_{jk} J_{ij} = E_{exc} - E_{GS} + \Delta D_{exc} + L(k) \tag{C.4.7}$$

the coefficients ψ_{nk} must be chosen in order to satisfy the conditions

$$\sum_{i \neq j} \psi_{ik'}^* \psi_{jk} J_{ij} = \delta_{kk'} L(k) \qquad \text{s.t.} \ \sum_i \psi_{ik'}^* \psi_{ik} = \delta_{kk'} \tag{C.4.8}$$

With PBC and no disorder (i.e. all monomers have equal excitation energies), by virtue of translational symmetry, the energy eigenstates coefficients of (C.4.6) are discrete plane waves[29]

$$|\xi_k\rangle = \frac{1}{\sqrt{M}} \sum_{m=1}^{M} e^{i\frac{2\pi}{M}km} |\lambda_m\rangle \qquad -M/2 \leq k \leq M/2 \tag{C.4.9}$$

where M is total number of monomers. Without inter molecular interactions the excited states (C.4.9) are M-fold degenerate with respect to the wave vector index k. This degeneracy is removed when we take into account the inter molecular interactions V_{nm}. In molecular crystals the latter is usually small[49,53] and one can assume weak coupling regime (i.e. $|J| \ll E_{exc} - E_{GS}$). Hence, in the first order perturbation theory, the excitation energies are[49]

$$\langle \xi_k | \hat{H} | \xi_k \rangle = E(k) = \langle \lambda_{\bar{m}} | \hat{H} | \lambda_{\bar{m}} \rangle + L(k) = \Delta\epsilon_{exc} + \Delta D_{exc} + L(k) \tag{C.4.10}$$

where

$$\Delta\epsilon_{exc} = E_{exc} - E_{GS} \tag{C.4.11}$$

$$L(k) = \frac{1}{M} \sum_{m \neq m'} J_{mm'} e^{i\frac{2\pi}{M}k(m-m')} = \frac{1}{M} \sum_{m \neq m'} J_{mm'} cos\left(\frac{2\pi}{M} k(m-m')\right) =$$

$$\frac{2}{M} \sum_{\tilde{m}=1}^{M-1} (M - \tilde{m}) J_{\tilde{m}} cos\left(\frac{2\pi}{M} k\tilde{m}\right) \tag{C.4.12}$$

Where $\bar{m}$ indicate a certain fixed monomer in the aggregate. Eq. (C.4.11) gives the isolated monomer transition energy; Eq. (C.4.12) is an exciton splitting term[49,53] , usually called zonal component[29], related

to monomer excited state delocalization via the inter-molecular couplings J_{nm}. Last relation in (C.4.12) is valid whenever $J_{mm'} = J_{\tilde{m}=|m-m'|}$, i.e. for translational invariant couplings as for the Coulomb interaction. In the dimer case (i.e., *N*=2) Eq. (C.4.12) gives the known Davydov exciton splitting term and represents an interaction energy due to exchange of excitation energy between the two molecules[53]. With increasing number of monomers, a quasi-continuum band of *N* molecular excited states forms as the result of the delocalization of the single monomer excited state due to inter molecular coupling and is expressed by the energy dispersion relation (C.4.10); if one assumes only nearest neighbors coupling J, the value of $W = 4|J|$ is a measure of exciton bandwidth[24]. By relation (C.4.12) one can also evaluate a group velocity as $v_g(k) \equiv \frac{R}{\hbar}\frac{\partial E(k)}{\partial k} = -\frac{2JR}{\hbar}\frac{N-1}{N} sin(k)$ and an exciton effective mass[19] $m^*(k) \equiv \left(\frac{R}{\hbar}\frac{\partial v_g}{\partial k}\right)^{-1} = -\frac{\hbar^2}{2JR^2}\frac{N}{N-1}\frac{1}{cos(k)}$, where R is neighboring monomers distance. We can see that, when the coupling is weak, like in molecular crystals, dispersion is small and negligible. The wavevector index k is associated to the number of nodes of the molecular exciton wave-function (C.4.9). In molecular exciton wave-functions, the nodes correspond to a change in the phase relation between transition dipoles[53], so for a 1D aggregate only the node-less (i.e. $k = 0$) excited state is optically allowed from the ground state[24,35].

4.6 Appendix C5 – 1D aggregate energy dispersion from intra-chain molecular couplings

If we consider the higher energy polymer excited states ($k \neq 0$) of the same band associated to the monomer excited state $|\varphi_{exc}\rangle$, one gets

$$\Delta\eta_{\xi_k} \approx \Gamma^{-1}\left(E_{\xi_k}^{plas,pol} - E_{exc}^{plas,mon}\right) = \Gamma^{-1}\Delta E_{\xi_k}^{plas} \qquad \text{C.5.1}$$

$$\Delta E_{\xi_k}^{plas} = \frac{1}{M}\sum_{m\neq m'} J_{|m-m'|} cos\left(\frac{2\pi}{M}k(m-m')\right) = \frac{2}{M}\sum_{\tilde{m}=1}^{M-1}\tilde{J}_{\tilde{m}}(M-\tilde{m})cos\left(\frac{2\pi}{M}k\tilde{m}\right) \qquad \text{C.5.2}$$

$$\tilde{J}_{\tilde{m}} = 2(\tilde{m}R)^{-1} - (\tilde{m}R + d)^{-1} - (\tilde{m}R - d)^{-1} \qquad \text{C.5.3}$$

Where $-M/2 \leq k \leq M/2$. In Figure C.5(a)-(d) we have reported Eq. (C.5.2) as a function of polymer excited state (wavevector) index k considering a progressively increasing total number of monomers *M*

starting from at least M = 2. One can see how a quasi continuous band of electronic excited states forms as the number of monomers increases. Energy dispersion is more pronounced for closer inter molecular distances R, since Coulomb coupling terms $\tilde{J}_{\tilde{m}}$ are stronger. We can observe also that the nearest neighbors approximation is quite good even for closer inter monomer distances and can be straightforwardly used instead of considering all the inter molecular couplings.

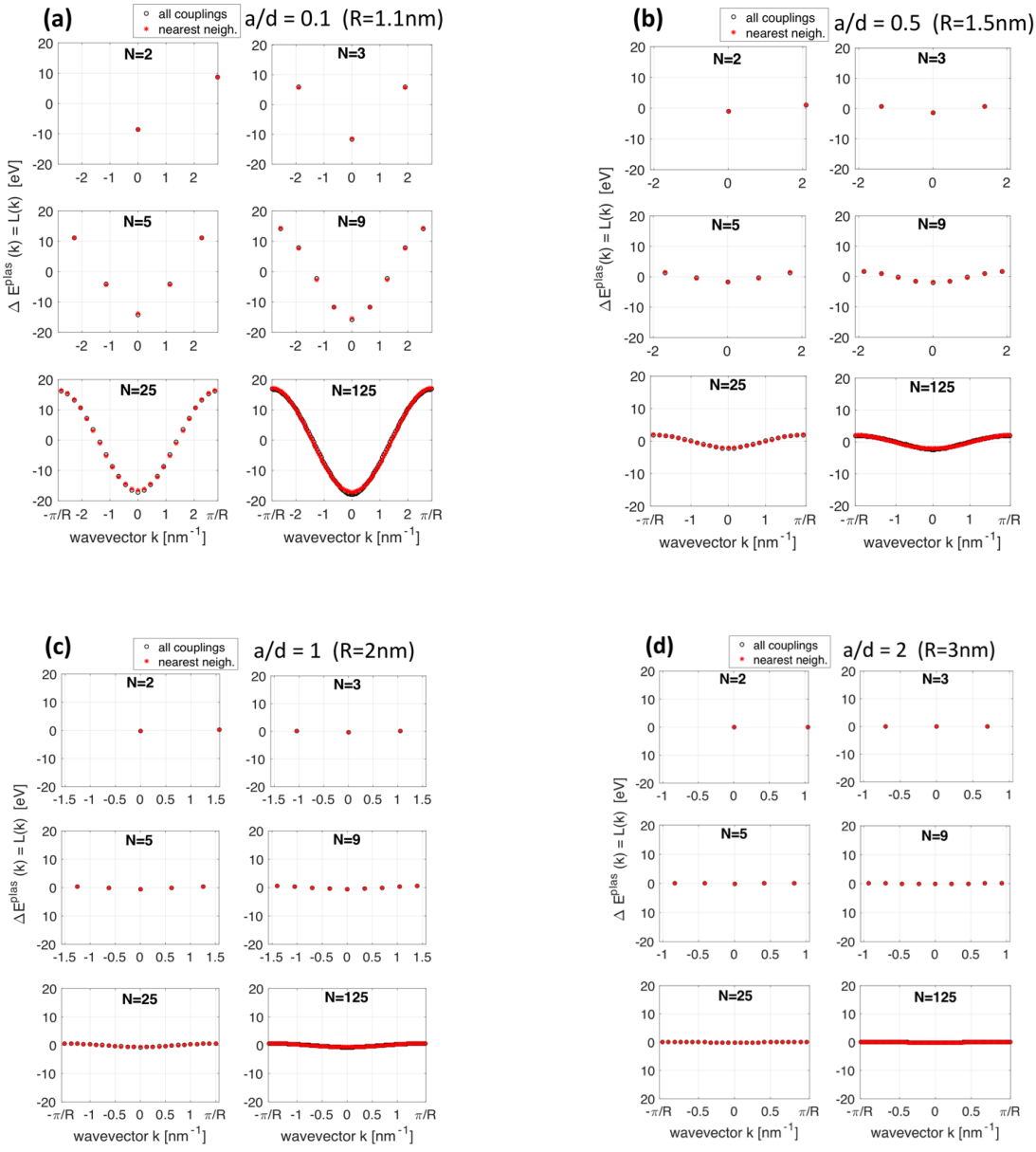

Figure C.5 –Exciton energy splitting vs excited state index k (i.e, dispersion relation) for a one-dimensional chain J-aggregate considering different inter monomer distances R = a + d (d is the single monomer length and distance a permits to vary inter-monomer distance by keeping d fixed) and by varying total number of monomers M.

Conclusions

The original contribution of this PhD activity is the ab-initio investigation of the electronic and optical properties of a J-aggregate composed of push-pull organic dyes, that represents a realistic prototype for the study of the microscopic understanding of the optical excitations in complex molecular crystals with enhanced light-matter interaction, beyond the most often studied case of *oligo-acenes* or *polithiopenes* aggregates. We can summarize the main outcomes and conclusions of this PhD activity as follows:

(1) In the first part dedicated to the TDDFT first principles results, we showed that the *J-band*, i.e., the intense peak dominating the absorption onset of the molecular aggregate, results from a collective molecular behavior coming from solid-state effects (i.e. inter-molecular Coulomb couplings) and its red-shift with respect to the single molecule absorption onset cannot be fully explained by considering separated portions of the aggregate. Since the overall red-shift of that narrow band results from competing microscopic coupling mechanisms, the only way is to take into account all the inter-molecular interactions in the first-principles simulation.

(2) In the second part, we adopted a framework alternative to TDDFT, namely MBPT. The description of correlated many-body effects, coming from two-particle interactions (i.e., electron-hole interaction), proper of the MBPT approach, clearly showed a further advancement in the characterization of the optical spectra of J-aggregates and of the corresponding electronic excitations. Specifically, we found that the *J-band* is formed by a several number of excitations the most intense of which, responsible for the strong optical absorption, exhibits a combination of inter- and intra-molecular charge-transfer (CT) behavior where there is coexistence between inter and intra-molecular interactions. This mixed character results from the dense molecular packing which favors electron delocalization around neighboring molecules and the push-pull nature of the constituting molecules and cannot be caught by the TDDFT approach used in the first part. In the specific system under investigation, the push-pull mechanism of the single monomers determines a significantly different optical behavior from that found for low lying excited states in oligoacenes[95,139] (e.g. pentacene[95]) where basically the constituent molecular units, not being polar, do not manifest any intra-molecular CT character. Excitations within the J-band with very weak intensity and pronounced intermolecular CT character have been also found.

In summary, the MBPT approach improved the TDDFT one as it showed a better description of CT states which comes out from using a non local screened exchange interaction with the correct long range Coulomb-like behavior[102,104], missing in TDDFT with standard (semi)local xc kernel (e.g. LDA, PBE), and also it included BZ k-points other than Γ (while in the TDDFT framework we worked strictly at Γ). Nevertheless, the TDDFT results remain still valid for what concerns the description of those excited states with no (or very low) inter-molecule CT character, i.e., those in which there is no inter-molecular electron transfer and each molecule stays charge neutral.

(3) In the last part of this work we showed the non-plasmonic behavior of the *J-band* that results from the microscopic polarization mechanisms inside the crystal and is physical explained in terms of the couplings between the molecular transition densities. Specifically, we demonstrated that a bright excitation in a molecular system such as the *J-band* of J-aggregates, even when coming from a collective mechanism which manifests a strong absorption, may have no relation with plasmonic behavior. In fact, excitations with similar absorption spectrum (e.g. a linear molecular aggregate vs a quantum wire with same total oscillator strengths) may have difference in their plasmonic character since the latter strictly depends on the Coulomb interaction between the molecular transition dipoles formed within the medium. The presence or not of an equal amount of positive and negative displaced charges internal to the medium, while makes no difference for the total oscillator strength, it does for the plasmonic behavior. With this result, we respond to the surrounding question whether or not any strong absorption band, with some sort of collective character in its microscopic origin, shares the status of plasmon.

The overall picture that emerges from this study is that the optical character of the *J-band* in a J-aggregate results from a complex interplay between collective crystal-like interactions and intra-molecular interactions. The usual textbook picture of the optical properties of J-aggregates (specifically the *J-band*) is based on the excitonic delocalization on several molecules of a neutral molecular excitation. Such excitation may or may not have an intra-molecular CT character depending on the molecular features, but no *inter-molecular* CT character is involved. Our rigorous first-principles results showed that reality is more complex than that. We find that the *J-band* clearly mixes with inter-molecular CT excitations not accounted for by the standard picture. One can also relate the inter- and intra-molecular CT behavior with the non-plasmonic character of the excitations within the *J-band*: the presence of both intra- and inter-molecular CT effects within the *J-band* favors localized electronic states and makes the induced charge density not-homogeneous within the unit cell, thus deviating from the ideal electron gas behavior

(i.e., completely delocalized states) which is the reference point for plasmonic-like systems. This fact directly reflects on the non-plasmonic character of the J-band.

Our results showed also the need to use a numerical first-principles approach to overcome the limits of the simplified theoretical analytical models used so far to describe extended molecular aggregates since the latter are not able to: (i) account for ground state variation of the molecules in aggregate phase due to solid-state effects (e.g., van der Waals interactions); (ii) account for exchange of electrons between different molecules which is non-negligible when there is molecular wavefunctions overlap in densely packed aggregates; (iii) simulate complex realistic crystal morphologies beyond the simple 1D chain model; (iv) describe the presence of multiple excited states within the J-band, including those with pure charge transfer character (i.e. dark excited states) that would not be possible to detect with conventional absorption experiments; (v) represent microscopic physical quantities (e.g., induce charge densities, exciton joint probability density functions, etc.) that help to analyze the character of the optical excitations.

With these findings and their interpretation, on the one hand we have contributed to clarify the character of excitations in organic semiconductors; on the other hand we have contributed to a better understanding of the optical properties of J-aggregate molecular crystals that have been also analyzed through the unconventional perspective of molecular plasmonics materials. In a more general way, we have also demonstrated the power of first-principles methods to study nanomaterials.

In the future, we are planning to quantify, in addition to the plasmonic character, also the excitonic character of the optical excitations in the single push-pull dye and J-aggregate. This will proceed through the definition and application of an *excitonic index*, on top of the plasmonic one (i.e., GPI) used in this work. Through the *excitonic index* we shall provide a measure of the electron-hole interaction strength associated to an optical excitation in a molecular-like system or nanostructure.

BIBLIOGRAPHY

(1) JELLEY, E. E. Spectral Absorption and Fluorescence of Dyes in the Molecular State. *Nature* **1936**, *138*, 1009-1010.

(2) JELLEY, E. E. Molecular, Nematic and Crystal States of I: I-Diethyl--Cyanine Chloride. *Nature* **1937**, *139*, 631.

(3) Scheibe, G. Über Die Veränderlichkeit Der Absorptionsspektren in Lösungen Und Die Nebenvalenzen Als Ihre Ursache. *Angew. Chem.* **2006**, *50 (11)*, 212–219.

(4) Franck, J.; Teller, E. Migration and Photochemical Action of Excitation Energy in Crystals. *J. Chem. Phys.* **1938**, *6* (12), 861–872.

(5) Prokhorov, V. V.; Pozin, S. I.; Lypenko, D. A.; Perelygina, O. M.; Mal'tsev, E. I.; Vannikov, A. V. Molecular Arrangements in Two-Dimensional J-Aggregate Monolayers of Cyanine Dyes. *Macroheterocycles* **2012**, *5* (4–5), 371–376.

(6) Prokhorov, V. V; Pozin, S. I.; Perelygina, O. M.; Zolotarevskii, V. I.; Mal'tsev, E. I.; Vannikov, A. V. Polymorphism of 2D Monolayer J-Aggregates of Cyanine Dyes. *Inorg. Mater. Appl. Res.* **2017**, *8* (4), 494–501.

(7) Prokhorov, V. V.; Perelygina, O. M.; Mal'tsev, E. I.; Vannikov, A. V. Crystalline Structure of Two-Dimensional Cyanine Dye J-Aggregates. *Crystallogr. Rep.* **2014**, *59* (6), 896–899.

(8) Yao, H.; Kitamura, S.; Kimura, K. Morphology Transformation of Mesoscopic Supramolecular J Aggregates in Solution. *Phys. Chem. Chem. Phys.* **2001**, *3* (20), 4560–4565.

(9) Shapiro, B. I.; Manulik, E. V.; Prokhorov, V. V. Multilayer J-Aggregates of Cyanine Dyes. *Nanotechnologies Russ.* **2016**, *11* (5–6), 265–272.

(10) von Berlepsch, H.; Böttcher, C.; Ouart, A.; Burger, C.; Dähne, S.; Kirstein, S. Supramolecular Structures of *J* -Aggregates of Carbocyanine Dyes in Solution. *J. Phys. Chem. B* **2000**, *104* (22), 5255–5262.

(11) von Berlepsch, H.; Böttcher, C.; Dähne, L. Structure of J-Aggregates of Pseudoisocyanine Dye in Aqueous Solution. *J. Phys. Chem. B* **2000**, *104* (37), 8792–8799.

(12) von Berlepsch, H.; Kirstein, S.; Hania, R.; Pugžlys, A.; Böttcher, C. Modification of the Nanoscale Structure of the J-Aggregate of a Sulfonate-Substituted Amphiphilic Carbocyanine Dye through Incorporation of Surface-Active Additives. *J. Phys. Chem. B* **2007**, *111* (7), 1701–1711.

(13) Kirstein, S.; Daehne, S. J-Aggregates of Amphiphilic Cyanine Dyes: Self-Organization of Artificial Light Harvesting Complexes. *Int. J. Photoenergy* **2006**, *2006*, 1–21.

(14) Yao, H. 5 Morphology Transformations in Solutions: Dynamic Supramolecular Aggregates. *Annu. Rep. Prog. Chem., Sect. C: Phys. Chem.* **2004**, *100* (0), 99–148.

(15) Prokhorov, V. V.; Perelygina, O. M.; Pozin, S. I.; Mal'tsev, E. I.; Vannikov, A. V.; Tsivadze, A. Y. Tubular Structure of J-Aggregates of Cyanine Dye. *Dokl. Chem.* **2015**, *460* (1), 1–4.

(16) Prokhorov, V. V.; Mal'tsev, E. I.; Perelygina, O. M.; Lypenko, D. A.; Pozin, S. I.; Vannikov, A. V. High Precision Nanoscale AFM Height Measurements of J-Aggregates. *Nanotechnologies Russ.* **2011**, *6* (5–6), 286–297.

(17) Rösch, U.; Yao, S.; Wortmann, R.; Würthner, F. Fluorescent H-Aggregates of Merocyanine Dyes. *Angew. Chem. Int. Ed. 45* (42), 7026–7030.

(18) Petrova, M. G.; Prokhorov, V. V.; Pozin, S. I.; Kovaleva, N. N.; Demikhov, E. I. Atomic Force and Scanning Near-Field Optical Microscopy Study of Carbocyanine Dye J-Aggregates. *Bull. Russ. Acad. Sci. Phys.* **2014**, *78* (12), 1362–1366.

(19) Holstein, T. Studies of Polaron Motion: Part I. The Molecular-Crystal Model. *Ann. Phys. (N. Y).* **2000**, *281* (1–2), 706–724.

(20) Tozer, O. R.; Barford, W. Localization of Large Polarons in the Disordered Holstein Model. *Phys. Rev. B - Condens. Matter Mater. Phys.* **2014**, *89* (15), 1–7.

(21) Barford, W.; Marcus, M. Theory of Optical Transitions in Conjugated Polymers. I. Ideal Systems. *J. Chem. Phys.* **2014**, *141* (16), 4101.

(22) Marcus, M.; Tozer, O. R.; Barford, W. Theory of Optical Transitions in Conjugated Polymers. II. Real Systems. *J. Chem. Phys.* **2014**, *141* (16), 4102.

(23) Spano, F. C.; Yamagata, H. Vibronic Coupling in J-Aggregates and Beyond : A Direct Means of Determining the Exciton Coherence Length from the Photoluminescence Spectrum. **2011**, 115 (18), 5133–5143.

(24) Spano, F. C. The Spectral Signatures of Frenkel Polarons in H-and J-Aggregates. *Acc. Chem. Res.* **2009**, *43* (3), 429–439.

(25) Yamagata, H.; Spano, F. C. Strong Photophysical Similarities between Conjugated Polymers and J-Aggregates. *J. Phys. Chem. Lett.* **2014**, *5* (3), 622–632.

(26) Paquin, F.; Yamagata, H.; Hestand, N.; Sakowicz, M.; Bérubé, N.; Côté, M.; X. Reynolds, L.; A. Haque, S.; Stingelin, N.; Spano, F.; et al. Two-Dimensional Spatial Coherence of Excitons in Semicrystalline Polymeric Semiconductors: Effect of Molecular Weight. *Phys. Rev. B* **2013**, *88 (15), 5202*.

(27) Eisfeld, A.; Briggs, J. S. The J- and H-Bands of Organic Dye Aggregates. *Chem. Phys.* **2006**, *324* (2–3), 376–384.

(28) Walczak, P. B.; Eisfeld, A.; Briggs, J. S. Exchange Narrowing of the J Band of Molecular Dye Aggregates. *J. Chem. Phys.* **2008**, *128* (4), 1–12.

(29) Egorov, V. V. Theory of the J-Band: From the Frenkel Exciton to Charge Transfer. *Phys. Procedia* **2009**, *2* (2), 223–326.

(30) Engelhard, S.; Faisal, F. H. M. Quantum Mechanical Study of Time-Dependent Energy Transfer Between perturbers in a Scheibe Aggregate. *J. Chem. Phys.* **1999**, *110 (7)*, 3596-3605.

(31) Bartnik, E. A.; Blinowska, K. J. Efficient Energy Transfer in Langmuir-Blodgett Monolayers by Optimized Quantum Capture. *Phys. Lett. A* **1989**, *134* (7), 448–450.

(32) Eisfeld, A.; Briggs, J. S. The J-Band of Organic Dyes: Lineshape and Coherence Length. *Chem. Phys.* **2002**, *281* (1), 61–70.

(33) Prokhorov, V. V; Perelygina, O. M.; Pozin, S. I.; Mal'tsev, E. I.; Vannikov, A. V. Polymorphism of Two-Dimensional Cyanine Dye J-Aggregates and Its Genesis: Fluorescence Microscopy and Atomic Force Microscopy Study. *J. Phys. Chem. B* **2015**, *119* (48), 15046–15053.

(34) Frank, W.; E., K. T.; R., S.-M. C. J-Aggregates: From Serendipitous Discovery to Supramolecular Engineering of Functional Dye Materials. *Angew. Chem. Int. Ed. 50* (15), 3376–3410.

(35) Spano, F. C.; Silva, C. H- and J-Aggregate Behavior in Polymeric Semiconductors. *Annu. Rev. Phys. Chem.* **2014**, *65* (1), 477–500.

(36) Bricks, J. L.; Slominskii, Y. L.; Panas, I. D.; Demchenko, A. P. Fluorescent J-Aggregates of Cyanine Dyes: Basic Research and Applications Review. *Methods Appl. Fluoresc.* **2017**, *6* (1), 2001.

(37) Thilagam, a. Entanglement Dynamics of J-Aggregate Systems. *J. Phys. A Math. Theor.* **2011**, *44* (13), 5306.

(38) Scheblykin, I. G.; Drobizhev, M. A.; Varnavsky, O. P.; der Auweraer, M. Van; Vitukhnovsky, A. G. Reorientation of Transition Dipoles during Exciton Relaxation in J-Aggregates Probed by Flourescence Anisotropy. *Chem. Phys. Lett.* **1996**, *261* (1), 181–190.

(39) Belfield, K. D.; Bondar, M. V; Hernandez, F. E.; Przhonska, O. V; Yao, S. Two-Photon Absorption of a Supramolecular Pseudoisocyanine J-Aggregate Assembly. *Chem. Phys.* **2006**, *320* (2), 118–124.

(40) Yao, H.; Domoto, K.; Isohashi, T.; Kimura, K. In Situ Detection of Birefringent Mesoscopic H and J Aggregates of Thiacarbocyanine Dye in Solution. *Langmuir* **2005**, *21* (3), 1067–1073.

(41) Misawa, K.; Ono, H.; Minoshima, K.; Kobayashi, T. New Fabrication Method for Highly Oriented J Aggregates

Dispersed in Polymer Films. *Appl. Phys. Lett.* **1993**, *63* (5), 577–579.

(42) Knoester, J. Modeling the Optical Properties of Excitons in Linear and Tubular J-Aggregates. *Int. J. Photoenergy* **2006**, *2006 (1)*, 61364.

(43) Eisfeld, A.; Briggs, J. S. The Shape of the J-Band of Pseudoisocyanine. *Chem. Phys. Lett.* **2007**, *446* (4), 354–358.

(44) Obara, Y.; Saitoh, K.; Oda, M.; Tani, T. Room-Temperature Fluorescence Lifetime of Pseudoisocyanine (PIC) J Excitons with Various Aggregate Morphologies in Relation to Microcavity Polariton Formation. *Int. J. Mol. Sci.* **2012**, *13* (5), 5851–5865.

(45) Fidder, H.; Knoester, J.; Wiersma, D. A. Superradiant Emission and Optical Dephasing in J-Aggregates. *Chem. Phys. Lett.* **1990**, *171* (5–6), 529–536.

(46) Chen, Z.; Liu, Y.; Wagner, W.; Stepanenko, V.; Ren, X.; Ogi, S.; Würthner, F. Near-IR Absorbing J-Aggregate of an Amphiphilic BF2-Azadipyrromethene Dye by Kinetic Cooperative Self-Assembly. *Angew. Chemie Int. Ed. 56* (21), 5729–5733.

(47) Ginzburg, V. L. On Crystal Optics with Spatial Dispersion. *Phys. Rep.* **1990**, *194* (5), 245–251.

(48) Abramavicius, D.; Palmieri, B.; Voronine, D. V; Frantisek, S.; Mukamel, S. Coherent Multidimensional Optical Spectroscopy of Excitons in Molecular Aggregates ; Quasiparticle versus Supermolecule Perspectives. **2009**, *109* (6), 2350–2408.

(49) Davydov, A. S. The Theory of Molecular Excitons (Translation). *Sov. Phys. Uspekhi* **1964**, *82* (3–4), 393–448.

(50) Van Burgel, M.; Wiersma, D. A.; Duppen, K. The Dynamics of One-Dimensional Excitons in Liquids. *J. Chem. Phys.* **1995**, *102* (1), 20–33.

(51) Shapiro, B. I. Molecular Assemblies of Polymethine Dyes. *Russ. Chem. Rev.* **2006**, *75* (5), 433-456.

(52) Möbius, D. Scheibe Aggregates. *Adv. Mater.* **1995**, *7* (5), 437–444.

(53) Kasha, M.; Rawls, H. R.; Ashraf El-Bayoumi, M. The Exciton Model in Molecular Spectroscopy. *Pure Appl. Chem.* **1965**, *11* (3–4), 371–392.

(54) Kasha, M. Energy Transfer Mechanisms and the Molecular Exciton Model for Molecular Aggregates. *Radiat. Res.* **1963**, *20* (1), 55–70.

(55) Czikkely, V.; Försterling, H. D.; Kuhn, H. Light Absorption and Structure of Aggregates of Dye Molecules. *Chem. Phys. Lett.* **1970**, *6* (1), 11–14.

(56) Czikklely, V.; Forsterling, H. D.; Kuhn, H. Extended Dipole Model for Aggregates of Dye Molecules. *Chem. Phys. Lett.* **1970**, *6* (3), 207–210.

(57) Hestand, N. J.; Spano, F. C. Molecular Aggregate Photophysics beyond the Kasha Model: Novel Design Principles for Organic Materials. *Acc. Chem. Res.* **2017**, *50* (2), 341–350.

(58) Petrenko, A.; Stein, M. Molecular Reorganization Energy as a Key Determinant of J-Band Formation in J-Aggregates of Polymethine Dyes. *J. Phys. Chem. A* **2015**, *119* (26), 6773–6780.

(59) Knapp, E. W. Lineshapes of Molecular Aggregates, Exchange Narrowing and Intersite Correlation. *Chem. Phys.* **1984**, *85* (1), 73–82.

(60) Knapp, E. W.; Scherer, P. O. J.; Fischer, S. F. On the Lineshapes of Vibronically Resolved Molecular Aggregate Spectra. Application to Pseudoisocyanin (PIC). *Chem. Phys. Lett.* **1984**, *111* (4–5), 481–486.

(61) Scherer, P. O. J.; Fischer, S. F. On the Theory of Vibronic Structure of Linear Aggregates. Application to Pseudoisocyanin (PIC). *Chem. Phys.* **1984**, *86* (3), 269–283.

(62) Egorov, V. V. Nature of the Narrow Optical Band in H-Aggregates: Dozy-Chaos-Exciton Coupling. *AIP Adv.* **2014**, *4* (7), 7111.

(63) Egorov, V. V. Nature of the Optical Transition in Polymethine Dyes and J-Aggregates. *J. Chem. Phys.* **2002**, *116* (7), 3090–3103.

(64) Novotny, L.; Hecht, B. *Principles of Nano-Optics*; Cambridge University Press, 2006.

(65) Lim, I.-I. S.; Goroleski, F.; Mott, D.; Kariuki, N.; Ip, W.; Luo, J.; Zhong, C.-J. Adsorption of Cyanine Dyes on Gold Nanoparticles and Formation of J-Aggregates in the Nanoparticle Assembly. *J. Phys. Chem. B* **2006**, *110* (13), 6673–6682.

(66) Kelley, A. M. A Molecular Spectroscopic Description of Optical Spectra of J-Aggregated Dyes on Gold Nanoparticles. *Nano Lett.* **2007**, *7* (10), 3235–3240.

(67) Yoshida, A.; Kometani, N. Effect of the Interaction between Molecular Exciton and Localized Surface Plasmon on the Spectroscopic Properties of Silver Nanoparticles Coated with Cyanine Dye J-Aggregates. *J. Phys. Chem. C* **2010**, *114* (7), 2867–2872.

(68) DeLacy, B. G.; Qiu, W.; Soljačić, M.; Hsu, C. W.; Miller, O. D.; Johnson, S. G.; Joannopoulos, J. D. Layer-by-Layer Self-Assembly of Plexcitonic Nanoparticles. *Opt. Express* **2013**, *21* (16), 19103–19112.

(69) Sorokin, A. V; Zabolotskii, A. A.; Pereverzev, N. V; Yefimova, S. L.; Malyukin, Y. V; Plekhanov, A. I. Plasmon Controlled Exciton Fluorescence of Molecular Aggregates. *J. Phys. Chem. C* **2014**, *118* (14), 7599–7605.

(70) Wiederrecht, G. P.; Wurtz, G. A.; Hranisavljevic, J. Coherent Coupling of Molecular Excitons to Electronic Polarizations of Noble Metal Nanoparticles. *Nano Lett.* **2004**, *4* (11), 2121–2125.

(71) Fofang, N. T.; Park, T.-H.; Neumann, O.; Mirin, N. A.; Nordlander, P.; Halas, N. J. Plexcitonic Nanoparticles: Plasmon−Exciton Coupling in Nanoshell−J-Aggregate Complexes. *Nano Lett.* **2008**, *8* (10), 3481–3487.

(72) Zengin, G.; Johansson, G.; Johansson, P.; Antosiewicz, T. J.; Käll, M.; Shegai, T. Approaching the Strong Coupling Limit in Single Plasmonic Nanorods Interacting with J-Aggregates. *Sci. Rep.* **2013**, 3, 3074.

(73) Wurtz, G. A.; Evans, P. R.; Hendren, W.; Atkinson, R.; Dickson, W.; Pollard, R. J.; Zayats, A. V; Harrison, W.; Bower, C. Molecular Plasmonics with Tunable Exciton−Plasmon Coupling Strength in J-Aggregate Hybridized Au Nanorod Assemblies. *Nano Lett.* **2007**, *7* (5), 1297–1303.

(74) Yoshida, A.; Uchida, N.; Kometani, N. Synthesis and Spectroscopic Studies of Composite Gold Nanorods with a Double-Shell Structure Composed of Spacer and Cyanine Dye J-Aggregate Layers. *Langmuir* **2009**, *25* (19), 11802–11807.

(75) Melnikau, D.; Savateeva, D.; Susha, A. S.; Rogach, A. L.; Rakovich, Y. P. Strong Plasmon-Exciton Coupling in a Hybrid System of Gold Nanostars and J-Aggregates. *Nanoscale Res. Lett.*; **2013**, *8* (1), 134.

(76) Zheng, Y. B.; Juluri, B. K.; Lin Jensen, L.; Ahmed, D.; Lu, M.; Jensen, L.; Huang, T. J. Dynamic Tuning of Plasmon–Exciton Coupling in Arrays of Nanodisk–J-Aggregate Complexes. *Adv. Mater.* *22* (32), 3603–3607.

(77) Balci, S. Ultrastrong Plasmon-Exciton Coupling in Metal Nanoprisms with J-Aggregates. *Opt. Lett.* **2013**, *38* (21), 4498–4501.

(78) Saikin, S. K.; Eisfeld, A.; Valleau, S.; Aspuru-Guzik, A. Photonics Meets Excitonics: Natural and Artificial Molecular Aggregates. *Nanophotonics* **2013**, *2* (1), 21-38.

(79) Lebedev, V. S.; Medvedev, A. S. Plasmon — Exciton Coupling Effects in Light Absorption and Scattering by Metal/J-Aggregate Bilayer Nanoparticles. *Quantum Electron.* **2012**, *42* (8), 701.

(80) Shapiro, B. I.; Tyshkunova, E. S.; Kondorskiy, A. D.; Lebedev, V. S. Light Absorption and Plasmon – Exciton Interaction in Three-Layer Nanorods with a Gold Core and Outer Shell Composed of Molecular J- and H-Aggregates of Dyes. *Quantum Electron.* **2015**, *45* (12), 1153.

(81) Laban, B.; Vodnik, V.; Dramićanin, M.; Novaković, M.; Bibić, N.; Sovilj, S. P.; Vasić, V. M. Mechanism and Kinetics of J-Aggregation of Thiacyanine Dye in the Presence of Silver Nanoparticles. *J. Phys. Chem. C* **2014**, *118* (40), 23393–23401.

(82) Marques, M. A. L.; Ullrich, C. A.; Nogueira, F.; Burke, K.; Gross, E. K. U. *Time-Dependent Density Functional Theory*; 2006; Vol. 706.

(83) Onida, G.; Reining, L.; Rubio, A. Electronic Excitations: Density-Functional versus Many-Body Green's-Function Approaches. *Rev. Mod. Phys.* **2002**, *74* (2), 601–659.

(84) Friedrich, C.; Schindlmayr, A. Many-Body Perturbation Theory : The GW Approximation. *Computational Nanoscience: Do It Yourself!* **2006**, 31, 335–355.

(85) Lani, G.; Romaniello, P.; Reining, L. Approximations for Many-Body Green's Functions: Insights from the Fundamental Equations. *New J. Phys.* **2012**, *14* (3), 1–17.

(86) Barford, W.; Marcus, M. Theory of Optical Transitions in Conjugated Polymers. I. Ideal Systems. *J. Chem. Phys.* **2014**, *141* (16).

(87) Haverkort, F.; Stradomska, A.; Knoester, J. First-Principles Simulations of the Initial Phase of Self-Aggregation of a Cyanine Dye: Structure and Optical Spectra. *J. Phys. Chem. B* **2014**, *118* (29), 8877–8890.

(88) Haverkort, F.; Stradomska, A.; de Vries, A. H.; Knoester, J. First-Principles Calculation of the Optical Properties of an Amphiphilic Cyanine Dye Aggregate. *J. Phys. Chem. A* **2014**, *118* (6), 1012–1023.

(89) Törmö, P.; Barnes, W. L. Strong Coupling between Surface Plasmon Polaritons and Emitters: A Review. *Reports Prog. Phys.* **2015**, *78* (1), 2901-2934.

(90) Wang, H.; Toma, A.; Wang, H.-Y.; Bozzola, A.; Miele, E.; Haddadpour, A.; Veronis, G.; De Angelis, F.; Wang, L.; Chen, Q.-D.; et al. The Role of Rabi Splitting Tuning in the Dynamics of Strongly Coupled J-Aggregates and Surface Plasmon Polaritons in Nanohole Arrays. *Nanoscale* **2016**, *8* (27), 13445–13453.

(91) Bonnand, C.; Bellessa, J.; Plenet, J. C. Properties of Surface Plasmons Strongly Coupled to Excitons in an Organic Semiconductor near a Metallic Surface. *Phys. Rev. B* **2006**, *73* (24), 5330.

(92) Tame, M. S.; McEnery, K. R.; Özdemir, Ş. K.; Lee, J.; Maier, S. A.; Kim, M. S. Quantum Plasmonics Review. *Nat. Phys.* **2013**, *9* (6), 329–340.

(93) Pirotta, S.; Patrini, M.; Liscidini, M.; Galli, M.; Dacarro, G.; Canazza, G.; Guizzetti, G.; Comoretto, D.; Bajoni, D. Strong Coupling between Excitons in Organic Semiconductors and Bloch Surface Waves. *Appl. Phys. Lett.* **2014**, *104* (5), 1111.

(94) Todisco, F.; Agostino, S. D.; Esposito, M.; Ferna, A. I.; Giorgi, M. De; Ballarini, D.; Dominici, L.; Tarantini, I.; Cuscuna, M.; Sala, F. Della; et al. Exciton-Plasmon Coupling Enhancement via Metal Oxidation. *ACS Nano* **2015**, *9* (10), 9691–9699.

(95) Cudazzo, P.; Gatti, M.; Rubio, A. Excitons in Molecular Crystals from First-Principles Many-Body Perturbation Theory: Picene versus Pentacene. *Phys. Rev. B - Condens. Matter Mater. Phys.* **2012**, *86* (19), 1–8.

(96) Marini, A.; Hogan, C.; Grüning, M.; Varsano, D. Yambo: An Ab Initio Tool for Excited State Calculations. *Comput. Phys. Commun.* **2009**, *180* (8), 1392–1403.

(97) Botta, C.; Cariati, E.; Cavallo, G.; Dichiarante, V.; Forni, A.; Metrangolo, P.; Pilati, T.; Resnati, G.; Righetto, S. Fluorine-Induced J -Aggregation Enhances Emissive Properties of a New NLO Push-Pull Chromophore. *J. Mat. Chem. C* **2014**, *2* (27), 5275-5279.

(98) Giannozzi, P.; Baroni, S.; Bonini, N.; Calandra, M.; Car, R.; Cavazzoni, C.; Ceresoli, D.; Chiarotti, G. L.; Cococcioni, M.; Dabo, I.; et al. QUANTUM ESPRESSO: A Modular and Open-Source Software Project for Quantum Simulations of Materials. *J. Phys. Condens. Matter* **2009**, *21* (39), 5502.

(99) Malcioğlu, O. B.; Gebauer, R.; Rocca, D.; Baroni, S. TurboTDDFT - A Code for the Simulation of Molecular Spectra Using the Liouville-Lanczos Approach to Time-Dependent Density-Functional Perturbation Theory. *Comput. Phys. Commun.* **2011**, *182* (8), 1744–1754.

(100) Bruneval, F.; Rangel, T.; Hamed, S. M.; Shao, M.; Yang, C.; Neaton, J. B. Molgw 1: Many-Body Perturbation Theory Software for Atoms, Molecules, and Clusters. *Comput. Phys. Comm.* **2016**, 208, 149-161.

(101) Perdew, J. P.; Burke, K.; Ernzerhof, M. Generalized Gradient Approximation Made Simple. *Phys. Rev. Lett.* **1996**, *77* (18), 3865–3868.

(102) Dreuw, A.; Dreuw, A.; Head-gordon, M.; Head-gordon, M. Single-Reference Ab Initio Methods for the Calculation of Excited States of Large Molecules. *Sci. York* **2005**, *105* (11), 4009–4037.

(103) Sottile, F.; Bruneval, F.; Marinopoulos, A. G.; Dash, L. K.; Botti, S.; Olevano, V.; Vast, N.; Rubio, A.; Reining, L. TDDFT from Molecules to Solids: The Role of Long-Range Interactions. *Int. J. Quantum Chem.* **2005**, *102* 684–

701.

(104) Dreuw, A.; Weisman, J. L.; Head-Gordon, M. Long-Range Charge-Transfer Excited States in Time-Dependent Density Functional Theory Require Non-Local Exchange. **2003**, *119* (6), *2943-2946*.

(105) Botti, S.; Sottile, F.; Vast, N.; Olevano, V.; Reining, L.; Weissker, H. C.; Rubio, A.; Onida, G.; Del Sole, R.; Godby, R. W. Long-Range Contribution to the Exchange-Correlation Kernel of Time-Dependent Density Functional Theory. *Phys. Rev. B - Condens. Matter Mater. Phys.* **2004**, *69* (15), 1–14.

(106) Seidl, A.; Görling, A.; Vogl, P.; Majewski, J.; Levy, M. Generalized Kohn-Sham Schemes and the Band-Gap Problem. *Phys. Rev. B - Condens. Matter Mater. Phys.* **1996**, *53* (7), 3764–3774.

(107) Perdew, J. P.; Yang, W.; Burke, K.; Yang, Z.; Gross, E. K. U.; Scheffler, M.; Scuseria, G. E.; Henderson, T. M.; Zhang, I. Y.; Ruzsinszky, A.; et al. Understanding Band Gaps of Solids in Generalized Kohn–Sham Theory. *Proc. Natl. Acad. Sci.* **2017**, *114* (11), 2801–2806.

(108) Hedin, L. New Method for Calculating the One-Particle Green's Function with Application to the Electron-Gas-Problem. *Phys. Rev.* **1965**, *139* (3A), 796.

(109) Bruneval, F. GW Approximation of the Many-Body Problem and Changes in the Particle Number. *Phys. Rev. Lett.* **2009**, *103* (17), 1–4.

(110) Larson, P.; Dvorak, M.; Wu, Z. Role of the Plasmon-Pole Model in the GW Approximation. *Phys. Rev. B - Condens. Matter Mater. Phys.* **2013**, *88* (12), 42–46.

(111) Koval, P.; Foerster, D.; Daniel, S.; Koval, P.; Foerster, D.; Daniel, S. Fully Self-Consistent GW and Quasi-Particle Self-Consistent GW for Molecules. *Phys. Rev. B* **2014**, *89* (15), 5417

(112) Hüser, F.; Olsen, T.; Thygesen, K. S. Quasiparticle GW Calculations for Solids, Molecules, and Two-Dimensional Materials. *Phys. Rev. B - Condens. Matter Mater. Phys.* **2013**, *87* (23), 1–14.

(113) Gatti, M. The One-Particle Green's Function and the GW Approximation. *TDDFT School - Benasque* **2012**.

(114) Aryasetiawan, F.; Gunnarsson, O. The GW Method. *Reports Prog. Phys.* **1998**, *61* (3), 237–312.

(115) Jain, M.; Deslippe, J.; Samsonidze, G.; Cohen, M. L.; Chelikowsky, J. R.; Louie, S. G. Improved Quasiparticle Wave Functions and Mean Field for G_0W_0 Calculations: Initialization with the COHSEX Operator. *Phys. Rev. B - Condens. Matter Mater. Phys.* **2014**, *90* (11), 1–9.

(116) Li, X. Z.; Gómez-Abal, R.; Jiang, H.; Ambrosch-Draxl, C.; Scheffler, M. Impact of Widely Used Approximations to the G_0W_0 method: An All-Electron Perspective. *New J. Phys.* **2012**, *14* (2), 3006.

(117) Ehrenreich, H.; Cohen, M. H. Self-Consistent Field Approach to the Many-Electron Problem. *Phys. Rev.* **1959**, *115* (4), 786–790.

(118) Rohl, M.; Louie, S. G. Electron-Hole Excitations and Optical Spectra from Rst Principles. *Phys. Rev. B* **2000**, *62* (8), 4927–4944.

(119) Hybertsen, M. S.; Louie, S. G. Electron Correlation in Semiconductors and Insulators: Band Gaps and Quasiparticle Energies. *Phys. Rev. B* **1986**, *34* (8), 5390–5413.

(120) Morris, A. J.; Stankovski, M.; Delaney, K. T.; Rinke, P.; García-González, P.; Godby, R. W. Vertex Corrections in Localized and Extended Systems. *Phys. Rev. B - Condens. Matter Mater. Phys.* **2007**, *76* (15), 1–9.

(121) Reining, L. Linear Response and More : The Bethe-Salpeter Equation. *Quantum Mater. Exp. Theory* **2016**, *6* (10).

(122) Adler, S. L. Quantum Theory of the Dielectric Constant in Real Solids. *Phys. Rev.* **1962**, *126* (2), 413–420.

(123) Hanke, W.; Sham, L. J. Many-Particle Effects in the Optical Spectrum of a Semiconductor. *Phys. Rev. B* **1980**, *21* (10), 4656–4673.

(124) Hanke, W.; Sham, L. J. Local-Field and Excitonic Effects in the Optical Spectrum of a Covalent Crystal. *Phys. Rev. B* **1975**, *12* (10), 4501–4511.

(125) Del Sole, R.; Fiorino, E. Macroscopic Dielectric Tensor at Crystal Surfaces. *Phys. Rev. B* **1984**, *29* (8), 4631–4645.

(126) Faber, C.; Boulanger, P.; Duchemin, I.; Attaccalite, C.; Blase, X. Many-Body Green's Function GW and Bethe-Salpeter Study of the Optical Excitations in a Paradigmatic Model Dipeptide. *J. Chem. Phys.* **2013**, *139* (19), 1–25.

(127) Sander, T.; Maggio, E.; Kresse, G. Beyond the Tamm-Dancoff Approximation for Extended Systems Using Exact Diagonalization. *Phys. Rev. B* **2015**, *92* (4), 045209.

(128) Grüning, M.; Marini, A.; Gonze, X. Exciton-Plasmon States in Nanoscale Materials: Breakdown of the Tamm-Dancoff Approximation. *Nano Lett.* **2009**, *9* (8), 2820–2824.

(129) Bohm, D.; Pines, D. Collective Description of Electron Interactions. I. Magnetic Interactions **1951**, *82* (5) , 625-634.

(130) Bohm, D.; Pines, D. A Collective Description of Electron Interactions: II. Collective vs Individual Particle Aspects of the Interactions. *Phys. Rev.* **1952**, *85* (2), 338–353.

(131) Bohm, D.; Pines, D. A Collective Description Of-Electron Interactions: III. Coulomb Interactions. **1953**, *92* (3), 609–625.

(132) Stiles, P. L.; Dieringer, J. A.; Shah, N. C.; Van Duyne, R. P. Surface-Enhanced Raman Spectroscopy. *Annu. Rev. Anal. Chem.* **2008**, *1* (1), 601–626.

(133) Long, D. A. *The Raman Effect*; **2002**; Vol. 8.

(134) Della Sala, F.; D'Agostino, S. *Handbook of Molecular Plasmonics* **2013**.

(135) Höppener, C. Exploiting the Light Matter Interaction for Bio-Applications Nano- Raman Ion Microscopy. *School of Photonics - Cortona* **2016**.

(136) Zhang, R.; Bursi, L.; Cox, J. D.; Cui, Y.; Krauter, C. M.; Alabastri, A.; Manjavacas, A.; Calzolari, A.; Corni, S.; Molinari, E.; et al. How to Identify Plasmons from the Optical Response of Nanostructures. *ACS Nano* **2017**, *11* (7), 7321–7335.

(137) Eisfeld, A.; Briggs, J. S. The J-Band of Organic Dyes: Lineshape and Coherence Length. *Chem. Phys.* **2002**, *281* (1), 61–70.

(138) Tempelaar, R.; Stradomska, A.; Knoester, J.; Spano, F. C. Anatomy of an Exciton: Vibrational Distortion and Exciton Coherence in H- and J-Aggregates. *J. Phys. Chem. B* **2013**, *117* (1), 457–466.

(139) Hummer, K.; Ambrosch-Draxl, C. Oligoacene Exciton Binding Energies: Their Dependence on Molecular Size. *Phys. Rev. B - Condens. Matter Mater. Phys.* **2005**, *71* (8), 1–4.

AKNOWLEDGMENTS

These three PhD years have represented for me a unique opportunity not only to strengthen and improve my knowledge but also to meet and collaborate with wonderful and very professional people. Among these, I feel very grateful and thankful to my personal supervisors Stefano and Arrigo, and to my co-tutors Daniele and Caterina from whom I have learned many things in these three years through useful discussions and advices. A special thank also to Prof. Elisa Molinari which, when I moved to Modena in November 2016 to begin the PhD program in Physics and Nanoscience, gave to me the opportunity to begin to work with my supervisors Stefano and Arrigo.

I want also to thank my colleagues of the XXXIst PhD cycle that have shared with me this beautiful journey: Celeste, Michael, Matteo, Nicola, Giulia and Jacopo. A special thank goes also to Luca Bursi who helped me a lot during the first year of my PhD to learn how to use Quantum Espresso and also many other stuffs.

And most of all I want to thank my family which always supported and helped me during these years, I will always be grateful to you.